MIT Libraries | DSpace@MIT

MIT Open Access Articles

Butyl Acetate Pyrolysis and Combustion Chemistry: Mechanism Generation and Shock Tube Experiments

The MIT Faculty has made this article openly available. ***Please share*** how this access benefits you. Your story matters.

Citation: Dong, X.; Pio, G.; Arafin, F.; Laich, A.; Baker, J.; Ninnemann, E.; Vasu, S. S.; Green, W. H. Butyl Acetate Pyrolysis and Combustion Chemistry: Mechanism Generation and Shock Tube Experiments. J. Phys. Chem. A 2023, 127, 3231– 3245.

As Published: 10.1021/acs.jpca.2c07545

Publisher: American Chemical Society (ACS)

Persistent URL: https://hdl.handle.net/1721.1/153214

Version: Author's final manuscript: final author's manuscript post peer review, without publisher's formatting or copy editing

Terms of use: Creative Commons Attribution-Noncommercial-Share Alike

Massachusetts Institute of Technology

Butyl Acetate Pyrolysis and Combustion Chemistry: Mechanism Generation and Shock Tube Experiments

Xiaorui Dong[a], Gianmaria Pio[b], Farhan Arafin[c], Andrew Laich[c], Jessica Baker[c], Erik Ninnemann[c], Subith S. Vasu[c], and William H. Green[a*]

[a] *Department of Chemical Engineering, Massachusetts Institute of Technology, Cambridge, MA, 02139, USA*
[b] *Department of Civil, Chemical, Environmental, and Materials Engineering (DICAM), Alma Mater Studiorum, University of Bologna, Bologna, 40126, Italy*
[c] *Center for Advanced Turbomachinery and Energy Research (CATER), Mechanical and Aerospace Engineering, University of Central Florida, Orlando, FL, 32816, USA*

* Corresponding author. *Email address*: whgreen@mit.edu (W. H. Green).

Abstract

The combustion and pyrolysis behavior of light esters and fatty acid methyl esters have been widely studied due to their relevance as biofuel and fuel additives. However, a knowledge gap exists for mid-size alkyl acetates, especially ones with long alkoxyl groups. Butyl acetate, in particular, is a promising biofuel with its economic and robust production possibilities and ability to enhance blendstock performance and reduce soot formation. However, it is little studied from both experimental and modeling aspects. This work created detailed oxidation mechanisms for the four butyl acetate isomers (normal-, sec-, tert-, and iso-butyl acetate) at temperatures varying from 650 K to 2000 K and pressures up to 100 atm using the Reaction Mechanism Generator. About 60% of species in each model have thermochemical parameters from published data or in-house quantum calculations, including fuel molecules and intermediate combustion products. Kinetics of essential primary reactions, retro-ene and hydrogen atom abstraction by OH or HO_2, governing the fuel oxidation pathways, were also calculated quantum-mechanically. Simulation of the developed mechanisms indicates that the majority of the fuel will decompose into acetic acid and relevant butenes at elevated temperatures, making their ignition behaviors similar to butenes. The adaptability of the developed models to high-temperature pyrolysis systems was tested against newly collected high-pressure shock experiments; the simulated CO mole fraction time histories have a reasonable agreement with the laser measurement in the shock tube. This work reveals the high-temperature oxidation chemistry of butyl acetates and demonstrates the validity of predictive models for biofuel chemistry established on accurate thermochemical and kinetic parameters.

Keywords:
Butyl acetate; Pyrolysis; Combustion chemistry; Reaction mechanism; Shock tube; Biofuels.

1 Introduction

In the last decades, the increased utilization of oxygenated biofuels for the energy supply has promoted the development of comprehensive kinetic mechanisms suitable for accurately representing their combustion chemistry.[1] Numerous studies have been performed to unravel the chemistry of long-chain methyl esters (i.e., fatty acid methyl esters or FAMEs).[2,3] In contrast, the importance of small-chain esters only gained interest recently, incentivizing accurate analysis of

their combustion and pyrolysis behaviors.[4] Indeed, carbon/oxygen bonds in the small-chain esters intrinsically diminish soot formation.[5] Recently, several studies investigated the oxidation chemistry of methyl formate, methyl acetate, methyl propanoate, and methyl butanoate, either experimentally or computationally.[6–11] However, the chemistry of the homologous mid-size alkyl acetate (i.e., propyl acetate and butyl acetate) has been poorly studied so far, despite their promising properties for energy supply purposes.[12] In this regard, butyl acetate (BA) has been recognized for its great potential as a sustainable biofuel additive because of its low freezing point, higher flash point, and limited impacts on the cetane number and heat of combustion of the resulting mixture.[13] Conventionally, a heterogeneous catalyzed reactive distillation of acetic acid with butanol was adopted to produce BA.[14,15] However, the use of strong acids as catalysts strongly limits this route due to the significant impact on environmental-related key performance indicators of the whole process.[16] In this perspective, alternative bioprocesses based on fermentation have been extensively investigated and successfully tested for environmentally and economically sustainable production of BA.[17] A recent investigation by Wang et al. has characterized the burning properties of droplets of BA.[18] However, to our knowledge, a detailed kinetic mechanism reproducing its chemistry in an oxidative system is still missing, highlighting the need for accurate models to characterize its combustion behavior. In addition, all four isomeric structures of BA (i.e., normal-, sec-, tert-, and iso-butyl acetate, or nBA, sBA, tBA, and iBA) should be considered, as each may be ruled by different chemistry and overall reactivity. Hence, these structures should be distinguished to properly account for the chemistry of this species.[19] For clarity, Figure 1 shows their molecular structures and nomenclature considered in this work to distinguish different carbon atoms on the molecule.

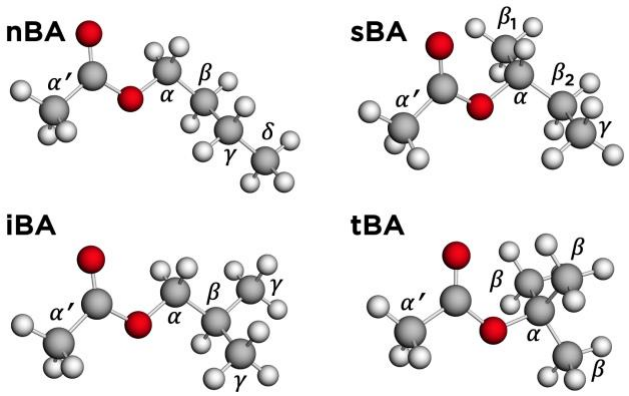

Figure 1. Molecule structures of butyl acetate isomers with carbons adjacent to the ester group labeled by the Greek letters.

Understanding the governing reactions is the key to correctly modeling the chemistry of BA isomers. Regardless of the investigated chemical structure, hydrogen atom abstraction reactions by small radicals (e.g., H, OH, and HO_2) play significant roles in combustion chemistry.[20] More specifically, the hydrogen atom abstractions from the α and α' positions of an ester group have been reported as dominant primary reactions at low- and intermediate temperatures.[21–23] Further, recent studies on ethyl acetate showed the dominance of unimolecular decomposition (i.e., retro-ene reaction) at high temperatures.[3,8] The retro-ene reaction is a concerted pericyclic reaction that involves an intra-molecular hydrogen transfer, a bond break, and a double bond formation via a six-membered ring transition state.[24] Undoubtedly, accurate kinetics of the reactions mentioned above is the prerequisite for quantitatively modeling relevant systems. However, the kinetic data

for BA-involved reactions are missing in both cases and can only be inferred from the rate rules.[25] To overcome this problem and increase the accuracy of the resulting model, deriving the kinetics from the *ab initio* calculations is highly desirable.[26] This approach has been extensively adopted for estimating the kinetic parameters of elementary reactions,[27–37] allowing for forming an inclusive and robust kinetic database suitable for sub-mechanisms. Besides, theoretical calculations based on the molecular structure are also useful for obtaining thermochemical data that is usually helpful for inferring reaction reverse rates.[38] Among other quantum chemistry methods, the composite method CBS-QB3 developed by Montgomery et al. (1999)[39] has been largely suggested for relevant purposes because of its accuracy attested as within ~ 1 kcal/mol of the experimental values and the limited computational costs required.[40,41]

Historically, detailed kinetic models were built in a postdictive manner. A model was usually generated hierarchically, from small intermediate species to the actual fuel-size molecules, according to expert chemistry knowledge. It usually needed to be fit to experimental data to fill the gap caused by missing reactions, inaccurate thermochemical and kinetic parameters, or other issues. However, to our knowledge, BA chemistry cannot be modeled in such a way due to missing data suitable for model validation. Instead, a predictive modeling approach that is embedded in the Reaction Mechanism Generator (RMG) has the potential to generate effective models.[42,43] RMG creates a mechanism based on accurate thermochemical and kinetic parameters.[44–46] Starting from a seed mechanism, it makes reasonable estimations for required parameters, uses those parameters to simulate the systems at the conditions of interest, and picks up the significant species and reactions according to their fluxes to enlarge the model. One of our recent studies also shows that once the most sensitive parameters are refined, the RMG-generated model can even outperform models that are fitted to the experiments.[47] Therefore, RMG is ideal for modeling BA chemistry.

This work was devoted to developing butyl acetate predictive kinetic models for each butyl acetate isomer, which help predict combustion behaviors. A significant amount of theoretical-sound thermochemical and kinetic data was collected from the literature and calculated in-house to enhance the model fidelity. The generated models were used to study the combustion chemistry and predict combustion behaviors at engine-relevant conditions. The adaptability of the produced mechanisms to pyrolysis systems was assessed by validating them with high-pressure shock tube (HPST) experiments collected in this study.

2 Computational Methods

In this work, detailed kinetic mechanisms were generated from the first principles for butyl acetate isomers using RMG[44–46], simulated using various chemical kinetics simulation software[48,49], and validated against measurements collected in pyrolysis conditions through a shock tube. The applied schematic of the model construction is similar to the one reported in our previous work,[47] where mechanisms have been developed and improved iteratively. The kinetics of the primary reaction and potential sub-mechanisms in the oxidation mechanism were calculated using the quantum chemistry approach and collected from the literature, respectively. Additional details on the procedures are provided in the following sections.

2.1 Quantum chemistry calculation

Quantum chemistry calculations were done on species thermochemical properties and primary reaction kinetics under rigid rotor harmonic oscillator (RRHO) approximation with a 1D hindered rotor correction and transition state theory.[50] A schematic representation of the procedure, facilitated by using Gaussian[51,52], ARC[53], and Arkane[54], is given in Figure 2.

Firstly, a rough guess of the species and transition states (TSs) 3D geometry is generated according to the following approach:

- Species geometries were first created from the ETKDG[55] algorithm and then optimized by MMFF94s force field;[56,57] conformers are explored by a torsion mapping algorithm[53,58].
- TSs geometries were manually created, whereas up to five conformers were tried based on the lowest energy reactant and product conformers to account for different conformation.

Quantum chemical calculations at the CBS-QB3 level of theory were then applied to the resultant geometries–geometry optimization, harmonic frequencies calculation, and torsional scan were done using the density functional theory at B3LYP/CBSB7, and single point energy was calculated at CBS-QB3 as suggested by Montgomery et al.[39] As indicated in Figure 2, several troubleshooting strategies were implemented to monitor the quality of the calculation job and ensure reasonable results. Eventually, the quantum chemistry results were utilized by the software Arkane and converted to thermochemical and kinetic parameters used in the mechanism.

Details about the calculation environment, quantum chemistry calculation schemes, utilization of bond additivity correction, etc., can be found in Section 1 of SI.

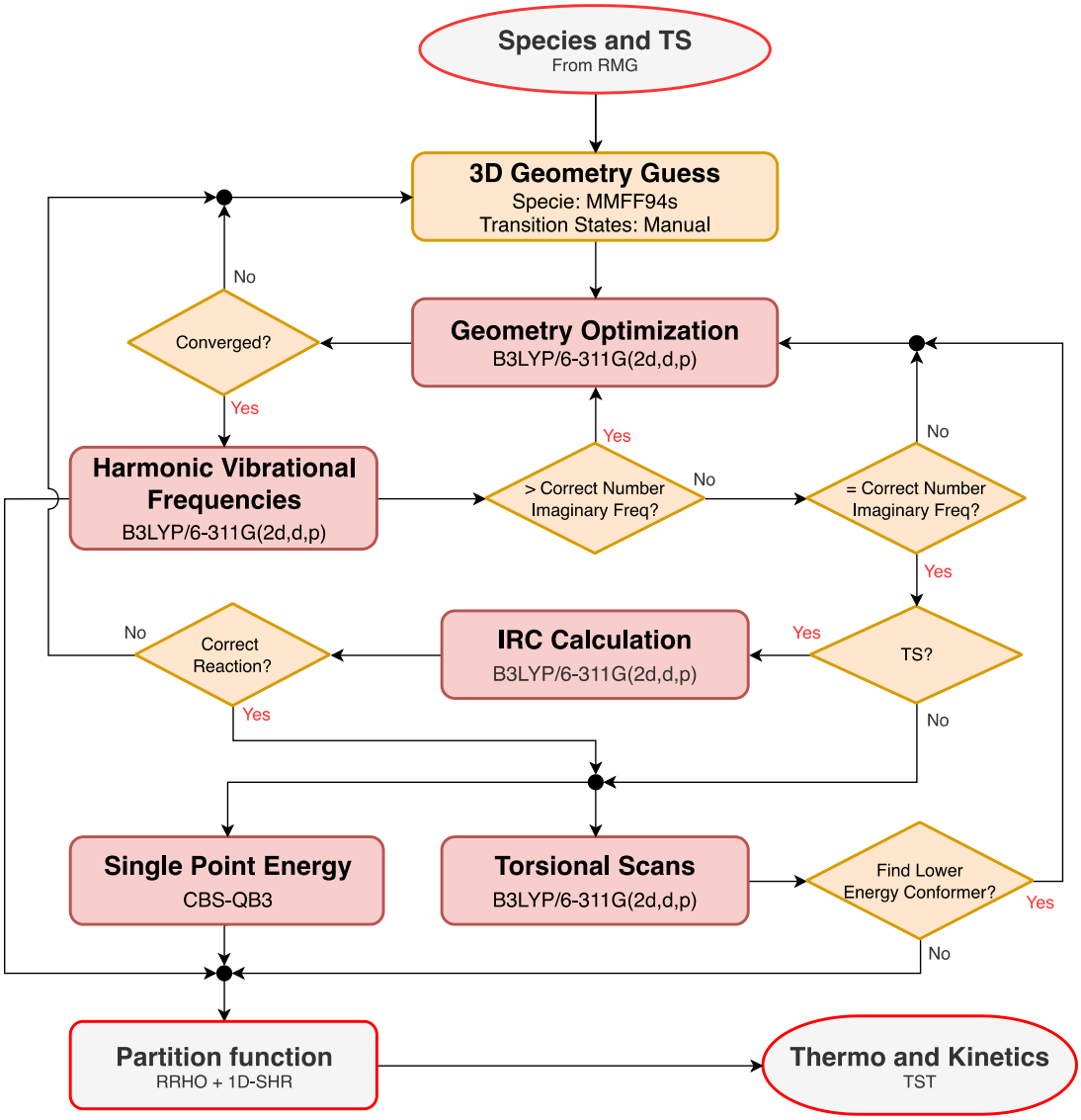

Figure 2. Schematic representation of the workflow used for thermochemical and kinetic properties calculation. Please consider that each color of the nodes corresponds to a different software program applied. Grey boxes: RMG[44–46] and Arkane[54]; Orange boxes: ARC[53]; Red boxes: Gaussian 09[51] or Gaussian 16[52].

2.2 Relevant kinetic data

Although kinetic data is missing for BA-involved reactions, quantum-mechanically calculated kinetic data for smaller esters or potential intermediates are available, helpful in creating sub-mechanism and improving RMG built-in rate rules. Potentially important reactions are inferred from disconnecting the BA molecules (Figure 3), motivated by the important beta-scission and bond-fission reactions at elevated temperatures. The disconnection analysis reveals that oxidation chemistry involving acetic acid, light alkenes (C_2-C_4), smaller formate/acetate, and C_4

alcohol/aldehyde/ketone are potentially significant. In this regard, rate constants for the following reactions are eventually collected from the literature:

- H-atom abstraction by OH[23], HO_2[21] from various esters
- H-atom abstraction by OH[59], HO_2[60] from butanols
- H-atom abstraction by OH, HO_2, and CH_3 from aldehydes and acids[31]
- Acetic acid H-atom abstraction and decomposition[29]
- Methyl acetate H-atom abstraction[61] and decomposition[33]
- Decomposition of methyl formate[36]
- H[62], OH[63] and HO_2[64] radical addition to light alkenes
- QOOH decompositions to HO_2 and light alkenes[64]

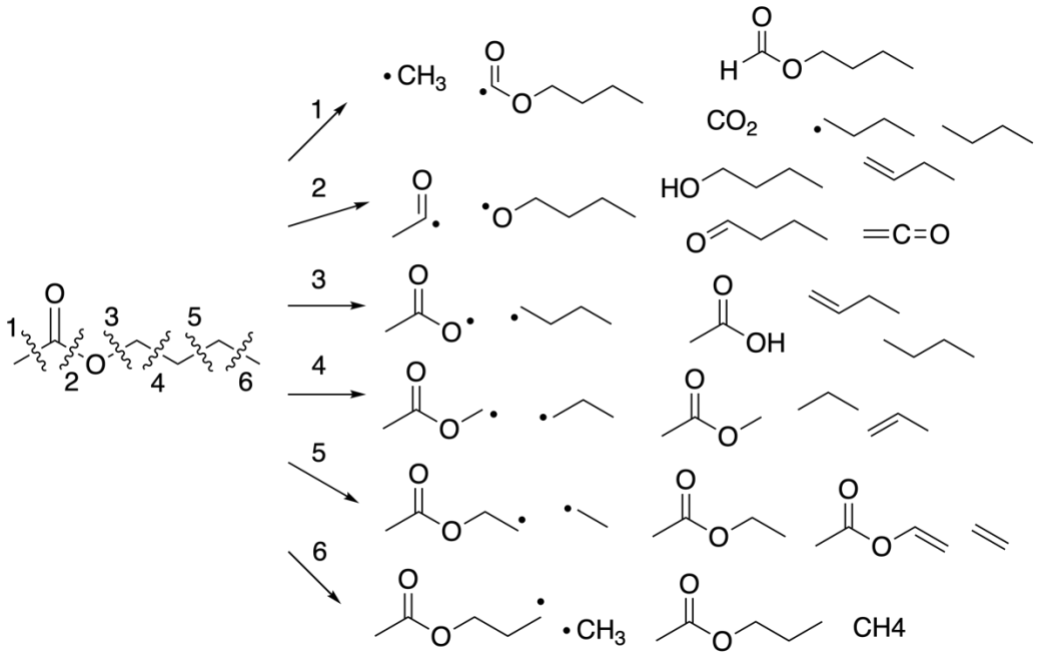

Figure 3. An illustration of disconnecting butyl acetate molecules. nBA is used as an example.

Besides, the thermochemistry of species in the C_2-C_4 alkene oxidation sub-mechanisms was extensively refined in our previous work[47], and the corresponding data were also used when building the kinetic model.

2.3 Mechanism generation

A rate-based method software, above-mentioned as RMG, was implemented for the automatic generation of reaction mechanisms for the investigated fuels. Details about the network generation and expansion algorithm can be found in Liu et al.[44] and Gao et al.[45], and the choice of parameter libraries[41,65–69] and algorithm setup was similar to the light alkene modeling by Pio et al.[47] Mechanisms were built for each isomer respectively. Considering the molecular structure of the investigated species, the maximum number of carbon and oxygen atoms allowed in a single molecule was limited to 15 and 8, respectively. Mono- and bi-radicals, together with the singlet configuration for oxygen, were permitted. For the sake of simplicity, nitrogen was assumed as an inert species, and nitrogen oxidation chemistry was neglected. Calculated and collected thermochemical and kinetic parameters were stored in the RMG database and retrieved whenever

needed. Other parameters were estimated through a linear combination of known sub-molecular fragments, following Benson's group additivity method[70] for the thermochemistry or rate rules based on decision trees distinguishing reaction families for the kinetics.[46]

The mechanism refinement was based on identifying the most influential species and reactions to the selected measurable properties via sensitivity and reaction flux analyses (introduced in Section 2.4). The impact of a given perturbation of enthalpy of formation H_{f298} on the outcomes of mole fraction of reactants and hydroxyl radicals was evaluated and considered as a sorting score. The ones estimated from the group additivity approach and with the highest scores were refined using the approach described in section 2.1. The later obtained refinements were then introduced into the RMG database, and a new model was generated with the updates. The database update allows RMG to estimate reaction fluxes more accurately and make better judgments on selecting essential pathways in the following iteration. A more detailed discussion about mechanism changes across iterations can be found in Section 2.5 of SI. The iterative procedure implemented in this work for the generation and refinement of detailed kinetic mechanisms, as described so far, was schematized in Figure 4.

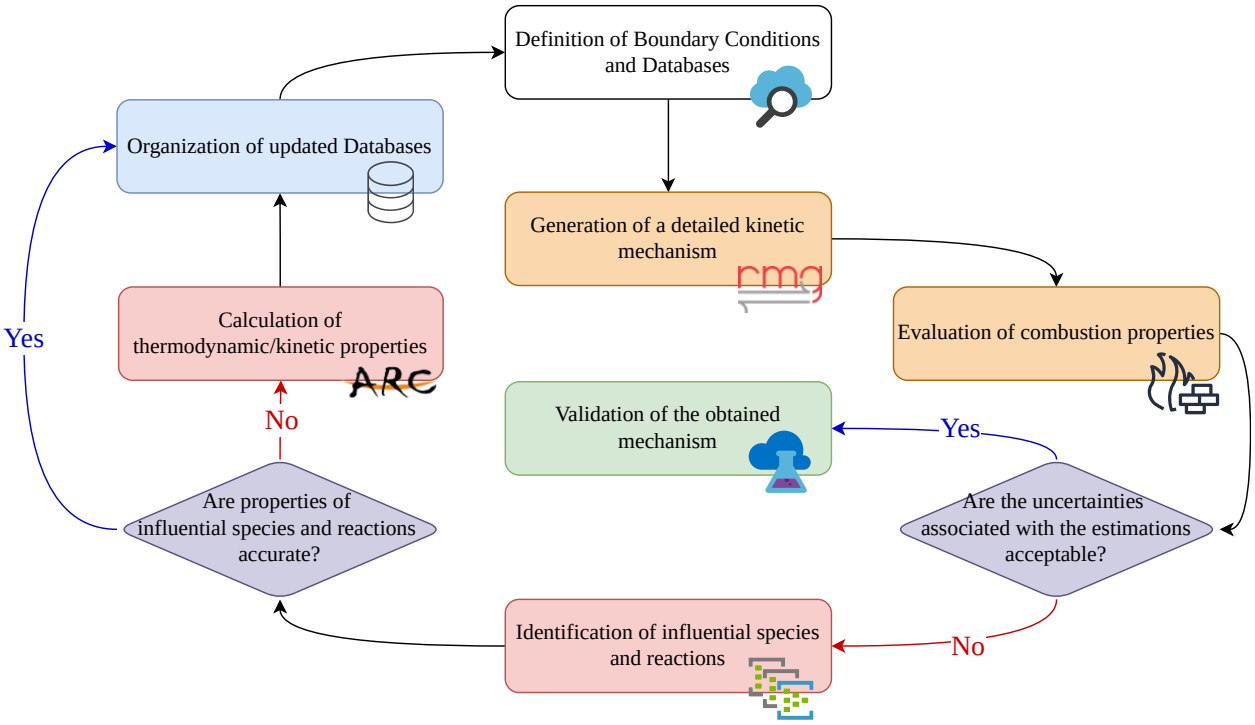

Figure 4. Schematic representation of the workflow used for the generation and refinement of detailed kinetic mechanisms.

2.4 Reactor model simulation

The produced mechanisms were utilized to estimate the ignition delay time (IDT) and generate flux diagrams and sensitivities using the Chemkin[71] and Reaction Mechanism Simulator (RMS)[49,72] software packages. The time evolution of pressure, temperature, and composition was estimated assuming a closed, isochoric, and adiabatic vessel. The initial temperature and pressure of the simulation were varied within 850 – 1500 K and 5 and 10 atm, respectively. The IDT was

identified by the peak of OH concentration time history. The flux diagrams were generated once at 20% and 50% of the IDTs, where time was selected to balance information reported in terms of decomposition and oxidation pathways. Temperature sensitivities were calculated at the ignition delay time defined by the peak of dT/dt, providing good estimates of relative IDT sensitivities as suggested by Ji et al.[73] To validate the BA pyrolysis in the HPST, a 0-D reactor under isochoric and adiabatic conditions was modeled to mimic the experimental system adopted in this work. The temperature and the pressure behind the reflected shock (T_5 and P_5) were used as the initial conditions of the simulation. The resulting carbon monoxide (CO) time histories were compared with measurements at first. RMS was also used to analyze the rate of production (ROP) of important intermediates and estimate the branching ratio under combustion-relevant conditions.

3 Experiments

3.1 Shock Tube Facility

Pyrolysis experiments of 4 different isomers of butyl acetate were performed in a stainless-steel, heated shock tube of 14.17 cm inner diameter located at the University of Central Florida. Specific details of the shock tube facility can be found in our previous works[74–76]. Five piezoelectric pressure transducers, spaced along the last 1.4 m of the shock tube and connected to four time-interval counters, were used to measure the incident shock velocities and the reflected shock pressure. The measured incident shock velocities were linearly extrapolated to obtain the reflected shock velocity at the end wall. Using the measured shock velocity, thermodynamic data of the mixture, and pre-shock temperature and pressure (T_1, P_1) in normal-shock relations, pressure and temperature behind reflected shock wave (P_5 and T_5) were calculated with the shock condition calculator FROSH[77]. P_5 was also monitored with a Kistler-type 603B1 sensor.

3.2 Mixture preparation

BA mixtures were prepared manometrically with two Baratrons from MKS instruments: a 10,000 Torr (628D, accuracy of 0.25% of reading) and a 100 Torr (E27D, accuracy of 0.12% of reading). Each isomer of butyl acetate has very low vapor pressure (~1.5-2.5 kPa at room temperature). So, the entire facility, including the mixing tank, filling line, manifold, and shock tube, was heated at 80°C to prevent fuel condensation. Also, while preparing the mixture, the partial pressure of the fuel was kept < 75% of the vapor pressure at 80°C to further ensure the gaseous phase of the fuel. Mixtures were prepared with 0.5% fuel loading (research graded, purity > 99%) in an argon bath (> 99.999% purity; nexAir) and were mixed in a 33 L mixing tank. Before starting experiments, each mixture was kept at rest overnight to get homogeneous.

3.3 Carbon monoxide (CO) absorbance

Two optical ports, at 2 cm away from the end wall and around the circumference of the tube, were used for the spectroscopic measurements. CO concentrations formed during BA pyrolysis were measured using a continuous-wave distributed feedback quantum cascade laser from Alpes Lasers (TO3-L-50) centered at 2046.277 cm^{-1}. A Bristol 771 Spectrum Analyzer was used to check the wavenumber of the laser beam before each experiment.
The concentration of CO was calculated through the Beer-Lambert Law:

$$X = \frac{\alpha RT}{\sigma PL} \quad (1)$$

where α is the measured absorbance from the laser, P is the time-varying reflected shock pressure of the gas mixture (Pa) found from the Kistler pressure transducer, T is the time-varying temperature of the mixture (K) estimated assuming isentropic condition, L is the path length of the absorbing species (m), R is the universal gas constant $\left(\frac{J}{mol.K}\right)$, and σ is the absorption cross-section of CO $\left(\frac{m^2}{mol}\right)$. The time-varying CO cross-section at T_5, P_5, and specified wavenumber were taken from the HITEMP database[78] assuming self-broadening with Voight profile. The relative uncertainty in the measured concentrations of CO was calculated as a time-varying quantity by the root mean square of the relative uncertainties of the absorbance, pressure, and temperature in Beer's Law (1), which is < 10% for all cases.

4 Results and Discussion

4.1 Quantum chemistry calculation

Quantum chemistry calculations conducted in this work include thermochemistry of important fuel, intermediates, and products and rate constants of BA retro-ene reactions and H-atom abstraction reactions. The differences in enthalpy and entropy of formation at 298 K (H_{f298} and S_{f298}) between the group additivity values (GAV) and values from quantum chemistry calculation (QM) (Figure 5) stress the importance of refining these parameters. Eventually, we refined the thermochemistry for around 60% of the species in the final models of this work, and a more detailed analysis can be found in Sections 1.5 and 2.4 of SI.

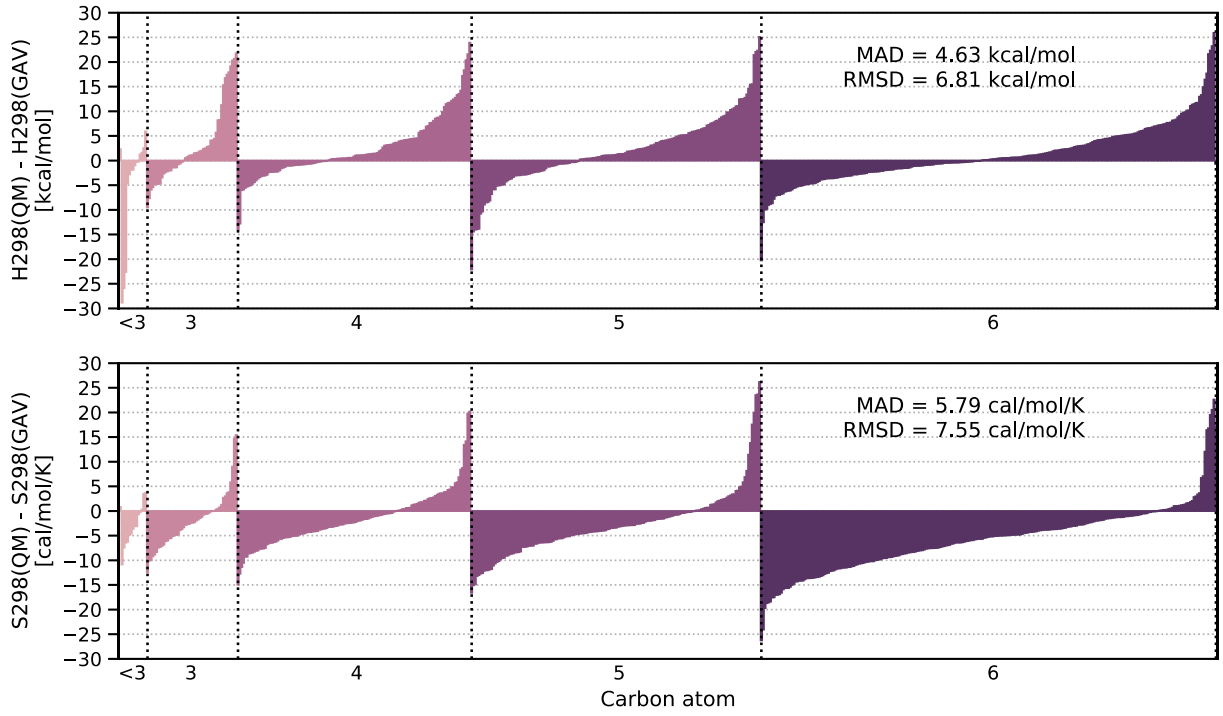

Figure 5. H_{f298} (upper) and S_{f298} (lower) differences between GAV and QM for each species calculated in this work. For better visualization, molecules are grouped by the number of carbon atoms and sorted by the deviations in each group. Note, the molecule sequence in the two subplots is different.

The kinetics of BA retro-ene reactions were calculated in this study. These reactions convert one BA molecule into an acetic acid and a corresponding butene. Considering the different chemical environments of the β-H atoms (the migrating atom) on BA molecules, a single reaction path was identified for nBA, iBA, and tBA, respectively, and three reaction paths were found for sBA. The transition state geometries (of their lowest energy conformer) and calculated rate constants are shown in Figure 6 and Table 1, respectively. Due to the p-π conjugation in the ester functional group, the reaction center in the transition states is nearly planar, contrasting with the geometry in alkene retro-ene transition states. When combining our calculation with published rate constants of ethyl, n-propyl, and iso-propyl acetate (i.e., EA[9], nPA[79], and iPA[10]), we found that a higher degree of substitution at the α-carbon or a lower degree at the β-carbon results in a higher rate constant (Figure 7A). The observation coincides with chemical intuition. More alkyl groups at the α-carbon weaken the C-O bond that is to break in the reaction, while more alkyl groups at the β-carbon introduce a stronger steric hindrance. The rate rules of acetate retro-ene reactions were summarized in Table 2. Besides, the degeneracy varies significantly among BA molecules: tBA has nine accessible β-H atoms, while iBA only has one. Differences in both reactivity and degeneracy of BA molecules accumulate into orders of magnitude differences in retro-ene rate constants of different BAs (Figure 7B), potentially affecting the branching in the oxidation.

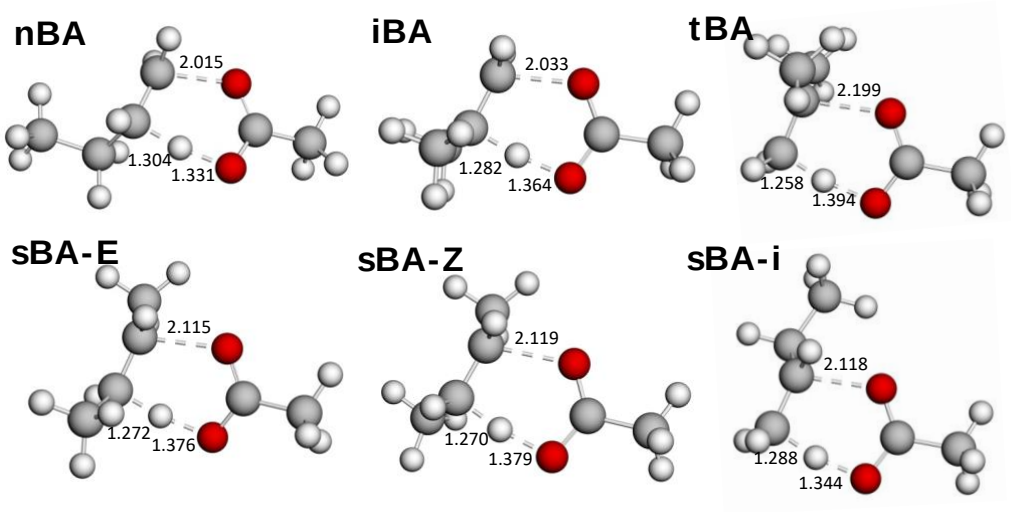

Figure 6. Transition states of butyl acetate retro-ene reactions calculated in this work. The distances of bonds that are formed or broken during the reaction are noted. The degeneracy of the reaction is marked by highlighting the relevant H atoms.

Table 1. BA retro-ene reaction rate constants in modified Arrhenius formula.

Reactant	Alkene Product	Degeneracy	A [s^{-1}]	n	Ea [kcal/mol]
nBA	1-C_4H_8	2	3.48E+03	2.72	46.0
iBA	i-C_4H_8	1	3.18E+06	1.87	48.5
sBA	1-C_4H_8	3	3.58E+07	1.65	45.6
sBA	cis-2-C_4H_8	1	1.96E+09	0.97	46.9
sBA	trans-2-C_4H_8	1	2.52E+09	1.01	46.1
tBA	i-C_4H_8	9	1.09E+10	1.08	42.1

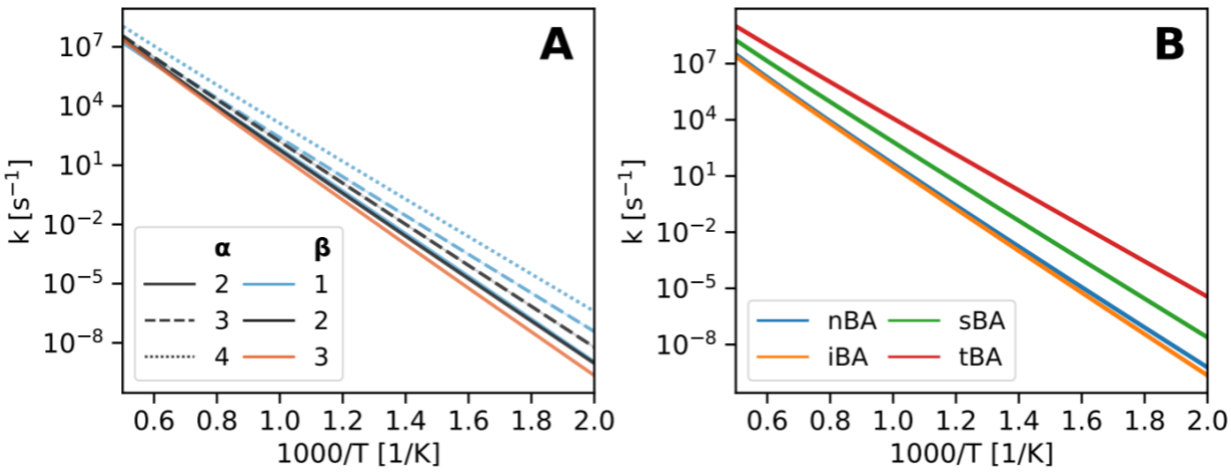

Figure 7. Computed rate constants of retro-ene reactions. **A.** *The rate rules of the acetate retro-ene reactions on a per H atom basis distinguishing the number of non-H substituents on the α- and β-carbons. Retro-ene rate constants of ethyl[9], n-propyl[79], and iso-propyl[80] acetate, along with the 4 butyl acetate isomers, are considered. Reactions with the same α and β atom conditions are grouped, and the group's mean is used to fit the rate rules.* **B.** *Overall retro-ene rate constants of each BA isomer.*

Table 2. Acetate retro-ene rate rules in modified Arrhenius formula on a per H atom basis.

Degree of α-carbon	Degree of β-carbon	A [s^{-1}]	n	Ea [kcal/mol]	Discrepancy factor at 1000 K
2	1	4.53E+13	-0.30	49.9	-
2	2	1.19E+07	1.66	47.1	2.6
2	3	3.18E+06	1.87	48.5	-
3	1	1.21E+08	1.25	43.2	2.1
3	2	1.70E+09	1.03	46.3	1.8
4	1	1.21E+09	1.08	42.1	-

** The discrepancy factor measures the largest difference between the rate constant from a fitted rate rule and individual rate constants used to fit the rate rule, providing a rough estimate of the uncertainty.*

Table 3. Butyl acetate H-atom abstraction rate constants (unit: cm3·mol^{-1}·s^{-1}) calculated in this work.

Reaction	A [$cm^3 \cdot mol^{-1} \cdot s^{-1}$]	n	Ea [kcal/mol]
nBA + OH = nBA-α' + H_2O	1.66E+03	2.95	0.0640
iBA + OH = iBA-α' + H_2O	9.45E+02	3.05	0.0547
sBA + OH = sBA-α' + H_2O	9.38E+02	3.07	0.155
tBA + OH = tBA-α' + H_2O	1.98E+03	2.97	-0.208
nBA + OH = nBA-α + H_2O	8.28E+01	3.18	-3.86
iBA + OH = iBA-α + H_2O	1.51E+01	3.40	-4.13
sBA + OH = sBA-α + H_2O	9.15E+02	2.79	-4.40
nBA + OH = nBA-β + H_2O	6.56E-01	3.81	-4.28
iBA + OH = iBA-β + H_2O	2.23E+01	3.27	-4.63
sBA + OH = sBA-$β_1$ + H_2O	1.01E+01	3.61	-2.76
sBA + OH = sBA-$β_2$ + H_2O	5.88E+00	3.58	-3.70
tBA + OH = tBA-β + H_2O	2.64E+00	3.91	-2.04
nBA + OH = nBA-γ + H_2O	1.48E-05	5.11	-5.70
iBA + OH = iBA-γ + H_2O	4.27E-06	5.36	-5.07
sBA + OH = sBA-γ + H_2O	9.13E-05	4.97	-5.10
nBA + OH = nBA-δ + H_2O	1.06E-07	5.77	-4.47
nBA + HO_2 = nBA-α + H_2O_2	5.13E-06	5.23	9.50
iBA + HO_2 = iBA-α + H_2O_2	9.58E-05	4.92	9.95

H-atom abstractions by OH radical from BA, as primary competitive reactions with retro-ene reactions, were also calculated, and their rate constants in the modified Arrhenius formula are tabulated in Table 3. Following the chemical structure of the investigated isomers reported in Figure 1, nBA and sBA have hydrogens in five different chemical environments, iBA has four different types of hydrogens, and tBA has two. According to the conformer search, all the lowest energy conformer of the transition states (on the CBS-QB3 potential energy surface) shares the configuration where:

1. the H atom in the hydroxyl radical points to the acetyl oxygen and forms a hydrogen bond.
2. at most, one dihedral in the BA fragment is significantly varied from the geometry of the corresponding lowest conformer to fulfill the configuration in item 1.

Rate constants were calculated over 500 – 2000 K (Figure 8 and Figures S13-16). As a reference, rate constants for EA, nPA, and iPA from Mendes et al.[21,23] are plotted alongside. For reactions abstracting α- or α'-hydrogens, rate constants of butyl acetates and ones of lighter acetates have a good agreement (within a factor of two). A slightly larger discrepancy (within a factor of 5) is observed for reactions abstracting β- and γ-hydrogens, where Zhou et al. used a different TS configuration, the H atom in OH pointing to the alkoxyl oxygen, in their rate calculation. Whether the difference in configuration is due to using different levels of theory or a lack of conformer search is unclear and suggested to be investigated in a future study. However, the similarity in the investigated acetates still suggests the applicability of rate rules when investigating even larger esters. Besides, the RMG rate rule estimates are also included in Figure 8 and Figures S13-16. While most estimates from the RMG rate rules are reasonably consistent with the calculated values (within an order of magnitude differences), indicating its good generality, significant discrepancies can be found over a few entries (e.g., abstracting sBA's α-H). It emphasizes the necessity of refining important kinetic parameters during model generation and reveals the irrationals of the manually designed RMG rate rules. Worth to note that RMG is in the process of switching from hand-made rules to rules generated by the substructure isomorphic decision tree algorithm, which aims to solve similar issues.

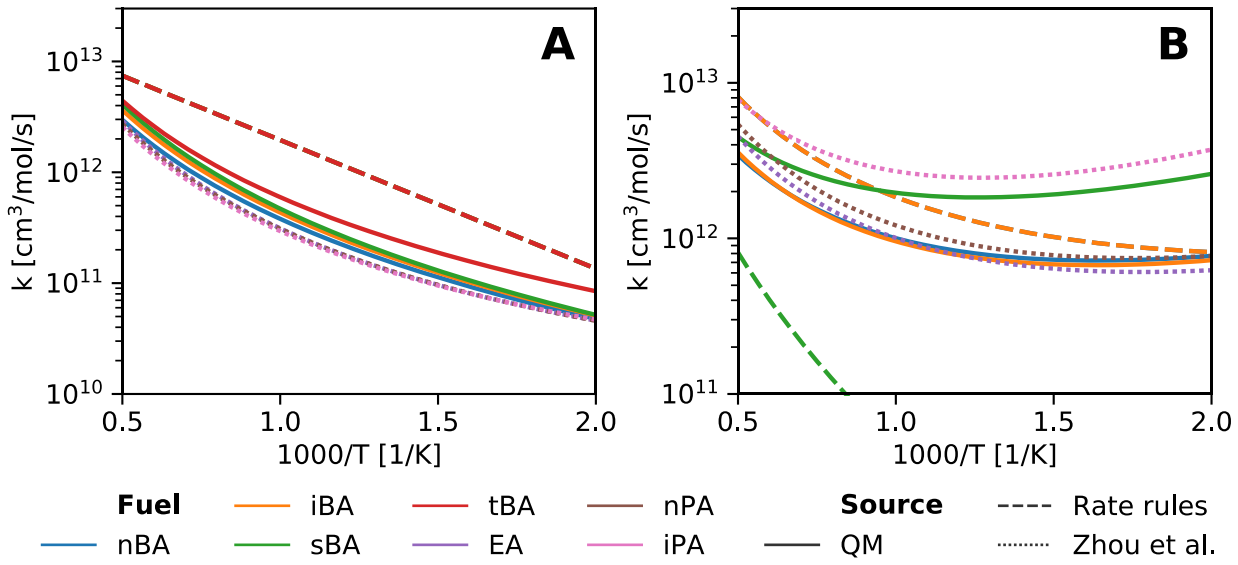

*Figure 8. Rate constants comparisons of H-atom abstraction reactions on a per H atom basis at α' site (**A**) and α site (**B**). Solid lines are calculated in this work, dashed lines are estimated using RMG rate rules, and dotted lines are adapted from Zhou et al.*[23]

Figure 9 shows branching ratios of H-atom abstractions by OH with respect to different carbon atoms and BA isomers. At lower temperatures, the most dominant pathways are the ones abstracting α- and β-hydrogens. At increasing temperatures, the reactivity of each pathway becomes more even, and the contribution sequence becomes more consistent with the order of reaction degeneracy. Regardless of the reactivity complexity at different sites of different BAs, the total H-atom abstraction rate constants are close among BAs and barely variable across the

temperature of interest (Figure 10). Larger differences are observed at lower temperatures, mainly due to tBA missing reactive α-H atoms.

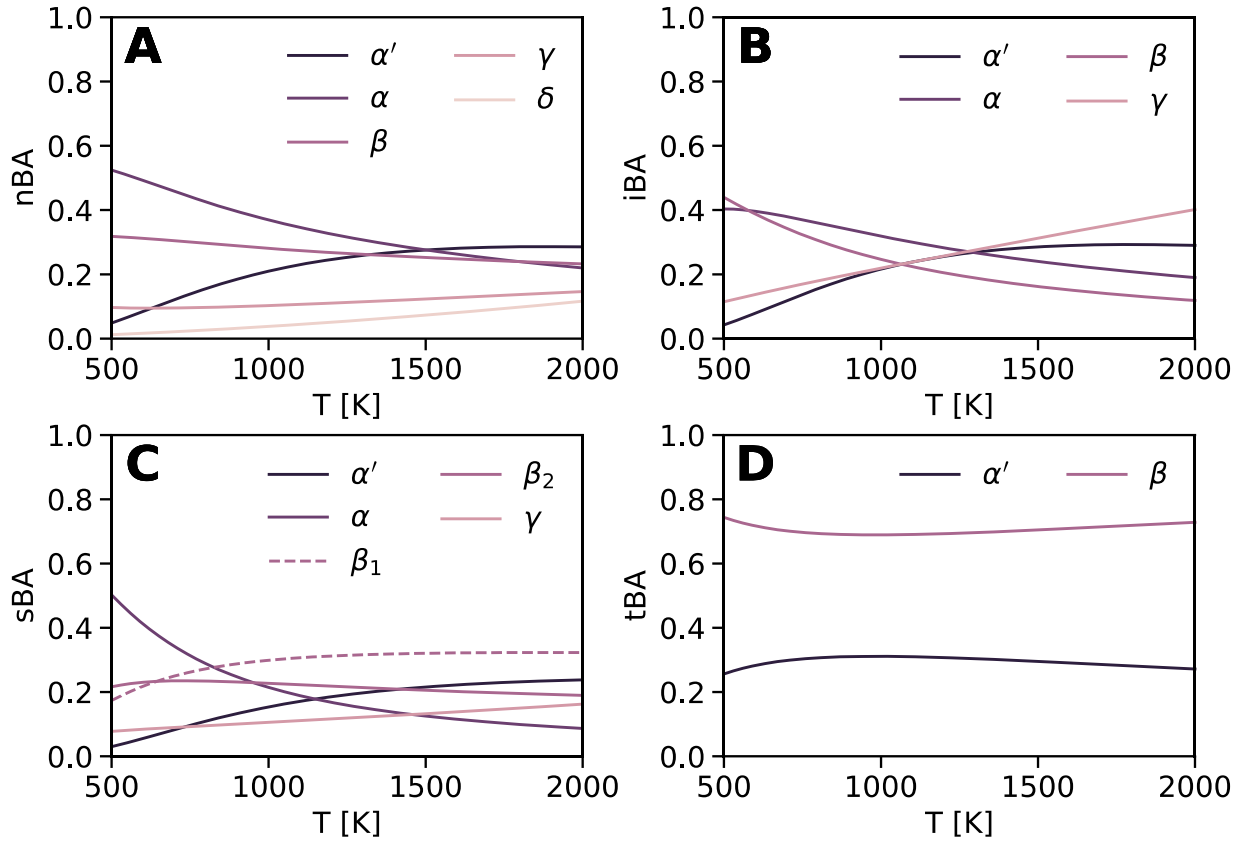

*Figure 9. Branching ratios of the H-atom abstraction by OH in the temperature range from 500–2000 K for BAs studied in this work. (**A**) nBA, (**B**) iBA, (**C**) sBA, and (**D**) tBA.*

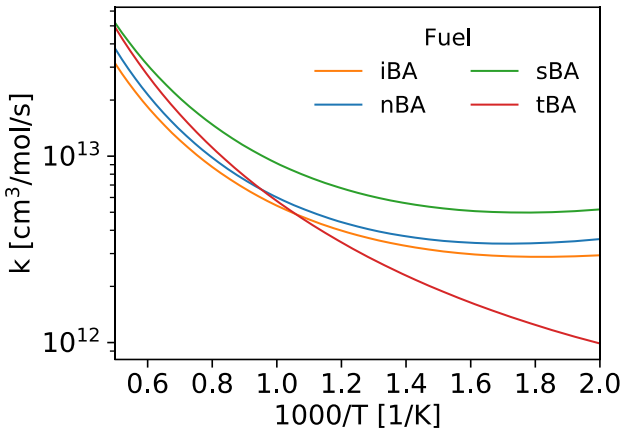

Figure 10. The total rate constants of BA H-atom abstraction reactions.

4.2 Combustion chemistry at elevated temperatures

Ignition delay time (IDT) was evaluated as an alternative measure of the overall reactivity. Figure 11 includes the IDTs at 10 atm across high temperatures (i.e., within 1000–1500 K) and different fuel-to-air ratios (0.5, 1.0, and 2.0), along with the HPST IDTs of relevant butenes[35,81,82] from the retro-ene reactions at the same conditions. Since butene isomers are major intermediates during BA oxidation and decomposition, their IDTs are expected to be relevant to BA ignition. Moreover, HPST IDTs of EA[8,11] under similar conditions but at higher pressures (15 and 20 bar) are also included as references. Indeed, IDTs of EA have been proved to be insensitive to pressure under the investigated temperatures (Figure S17). Comparing EA and BA IDTs provides additional hints about the influence of the retro-ene reactions and acetic acid sub-mechanism on IDTs, which are identified as significant according to Morsch et al.[11] and Figure S18. In addition, IDTs of BAs at intermediate temperatures are compared to IDTs simulated with the same assumption using well-validated models of butenes[35,81,82] and EA[11] (Figure S19). BA IDTs comparison between 5 and 10 atm can be found in Figure S20.

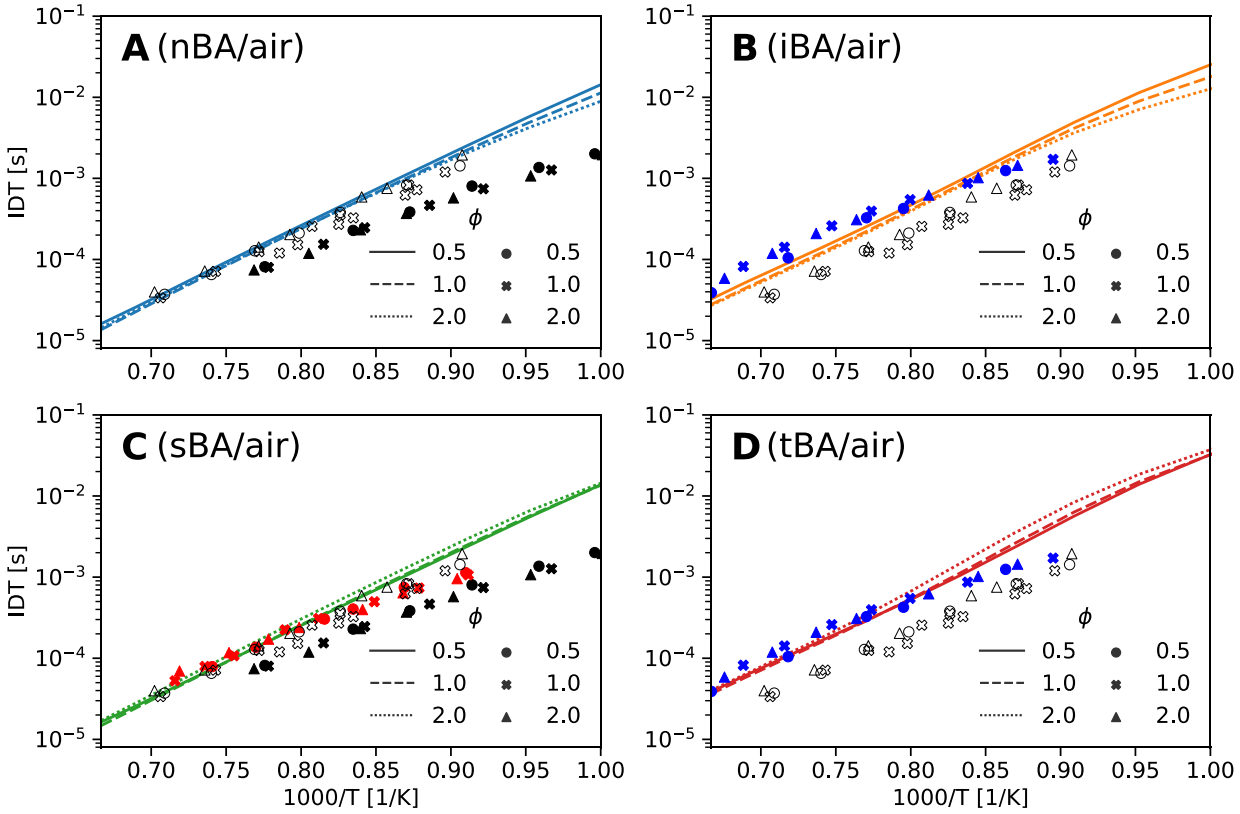

*Figure 11. The estimated ignition delay time of butyl acetate isomers in air at 10 atm as a function of temperature and equivalence ratio. (**A**) nBA, (**B**) iBA, (**C**) sBA, and (**D**) tBA. HPST IDTs of relevant butenes at the same conditions are plotted as solid markers: black - 1-butene[81], red - 2-butene[82], and blue - iso-butene[35]. HPST IDTs of ethyl acetate at 15 (adapted from Ahmed et al.[8]) and 20 bar (adapted from Morsch et al.[11]) are plotted as hollow markers.*

It is worth mentioning that the simulated IDTs for butyl acetate isomers at high temperatures are close to the measured IDTs for butene isomers and ethyl acetate under similar conditions. Specifically, IDTs for nBA and sBA are in line with 1-butene and 2-butene, whereas estimated values for iBA and tBA match the i-butene IDTs. In addition, the BA IDTs show little dependence

on φ and pressure at elevated temperatures, similar to the behavior of butenes and EA. Over 1000 K, retro-ene reactions are fast enough to become the dominant primary reactions. Hence, either the retro-ene reaction or the activation of the butene isomer produced by the retro-ene reaction is the rate-determining step for butyl acetate oxidation at these temperatures. As an example, the flux diagram of sBA oxidation at 1300 K is shown in Figure 12A, where over 98% of the sBA undergoes retro-ene reaction, and most of the diagram is about butene chemistry. The dominance of the retro-ene pathway is consistent with the observations reported by Ahmed et al.[8] about ethyl acetate. At lower temperatures, the contribution of H-atom abstraction increases. The resultant fuel radicals may undergo beta-scission reactions or O_2 addition and the subsequent isomerization/chain branching pathways (as the lower half in Figure 12B). These reactions convert BAs into smaller fragments or unsaturated acetates resembling the butene oxidation intermediates. However, as kinetics of the above-mentioned beta-scission, isomerization, and other reactions were estimated by rate rules in the developed mechanisms, larger uncertainties at lower temperature IDTs are expected. This observation suggests that investigating these reactions is needed for more reliable results at lower temperatures.

Figure 13 shows the temperature sensitivities at ignition delay time (defined by the peak of dT/dt), 900 K, 10 atm, and stoichiometric composition with air. Sensitivities at other fuel-to-air ratios and temperatures can be found in Section 6 of SI. According to Ji et al.[73], temperature sensitivity at the ignition delay state has almost the same direction as the IDT sensitivity. Therefore, it can be used as an alternative to the latter. As shown in Figure 13, nBA, iBA, and sBA share a similar trend in the list of sensitive reactions. Besides the essential C_0 and C_1 chemistry, H-atom abstraction from BAs by HO_2 and OH radicals, retro-ene reactions, beta-scission reactions, and butene chemistry also top the list. The significance of HO_2 chain branching reactions is as expected and similar to observations by Morsch et al.[11] about EA at 850 K. Among them, the most sensitive abstraction reactions take away the hydrogen atom at the α-carbon and are also the most dominant abstraction reactions. On the other hand, retro-ene reactions, as competitors of the abstraction reactions, reduce the reactivity. For tBA, iso-butene oxidation reactions instead of tBA-involved reactions are significant, e.g., O_2, OH, and HO_2 addition and H-atom abstraction. The difference in sensitive reactions is mainly due to the decomposition of tBA much faster than other isomers, resulting in tBA almost fully decomposed to acetic acid and iso-butene before the radical pool becomes large enough to make H-atom abstraction reactions competitive. As evidence, the 20% fuel consumption time for tBA is about three orders of magnitude smaller than its IDT at 900 K, while the time difference of other BAs is within an order of magnitude.

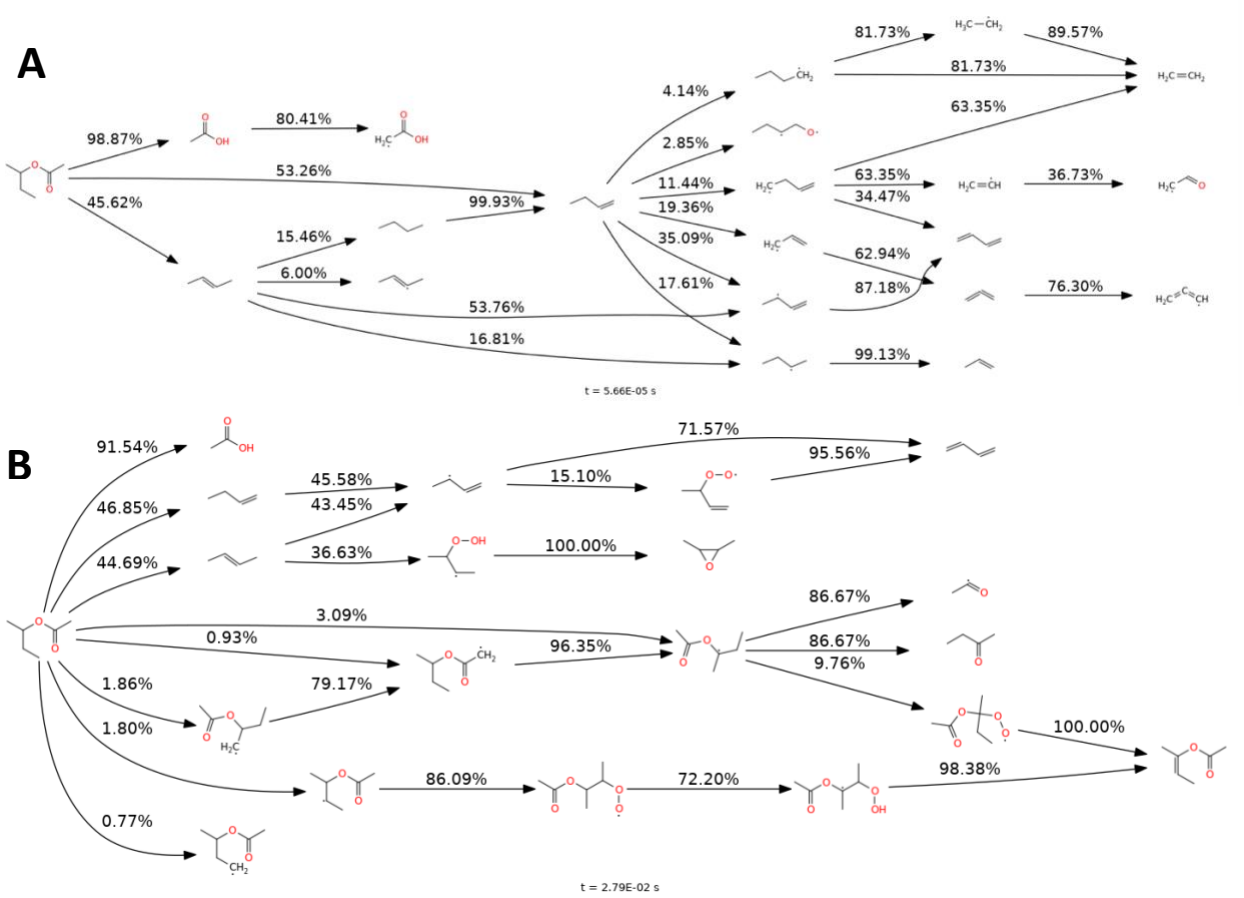

*Figure 12. Flux diagram of sBA oxidation by air at (**A**) 1300 K and (**B**) 900 K, 10 atm, 0.5 IDT, and stoichiometric condition. Percentage values indicate the branching ratio of the accumulated flux out of a species. Fluxes smaller than 0.5% of the fuel consumption are neglected.*

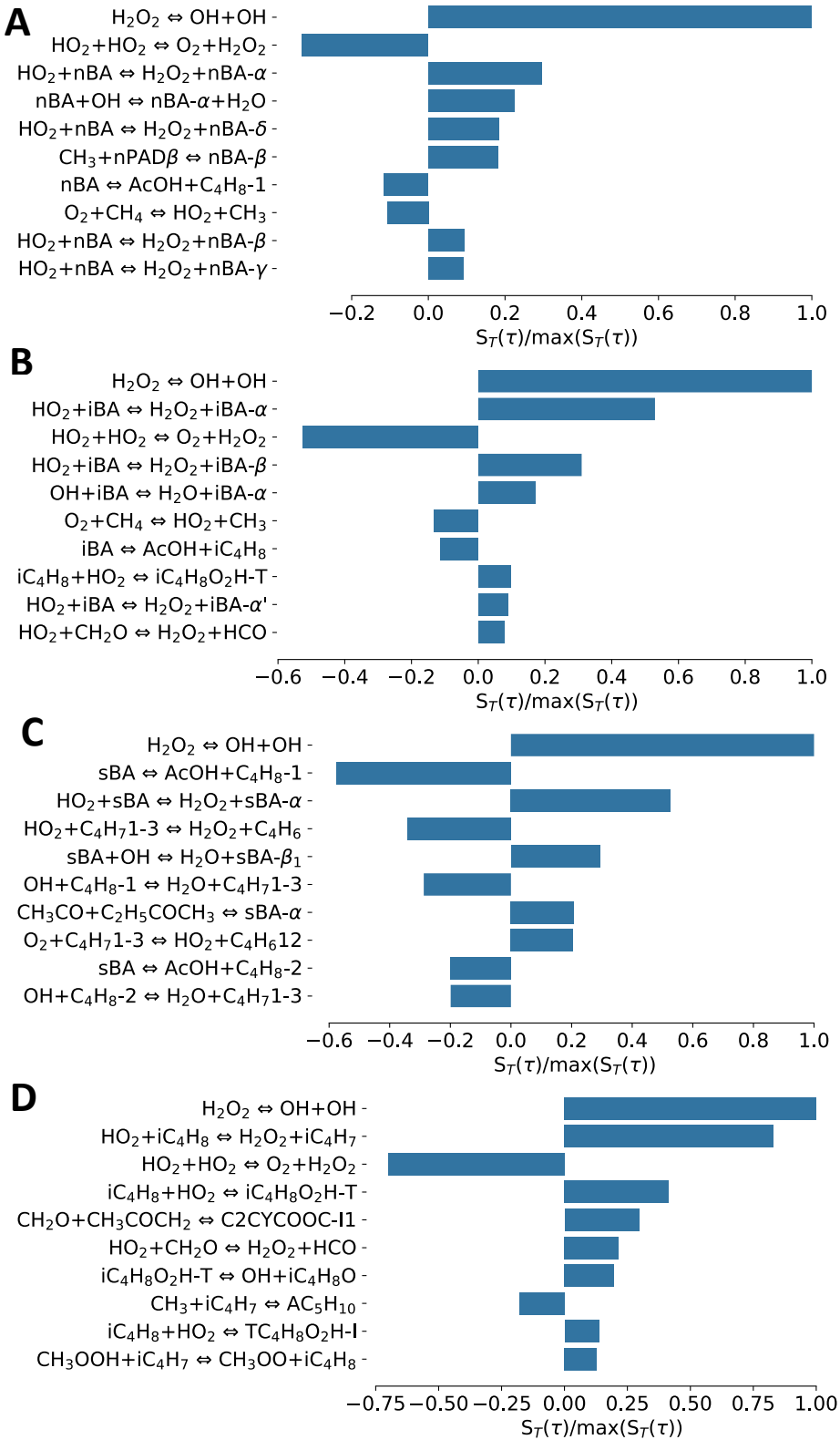

*Figure 13. Normalized temperature sensitivity analysis at ignition delay time, 900 K, 10 atm, and stoichiometric composition with air. (**A**) nBA, (**B**) iBA, (**C**) sBA, and (**D**) tBA.*

4.3 High-temperature pyrolysis

Although the models were not originally developed to predict pyrolysis systems, it is possible to use them for simulating pyrolysis, as the model includes the following essential chemistry:

- the retro-ene reactions that are also the primary reactions in the pyrolysis system
- H-atom abstractions by H and CH_3 for BA isomers and butenes
- relevant beta scissions of BA and butene radicals
- acetic acid decomposition chemistry

Carbon monoxide (CO) mole fraction time histories from shock tube experiments and simulations were compared in Figure 14. For figure clarity, only half of the measurements are included, whereas the remaining data can be found in Figures S32-S39.

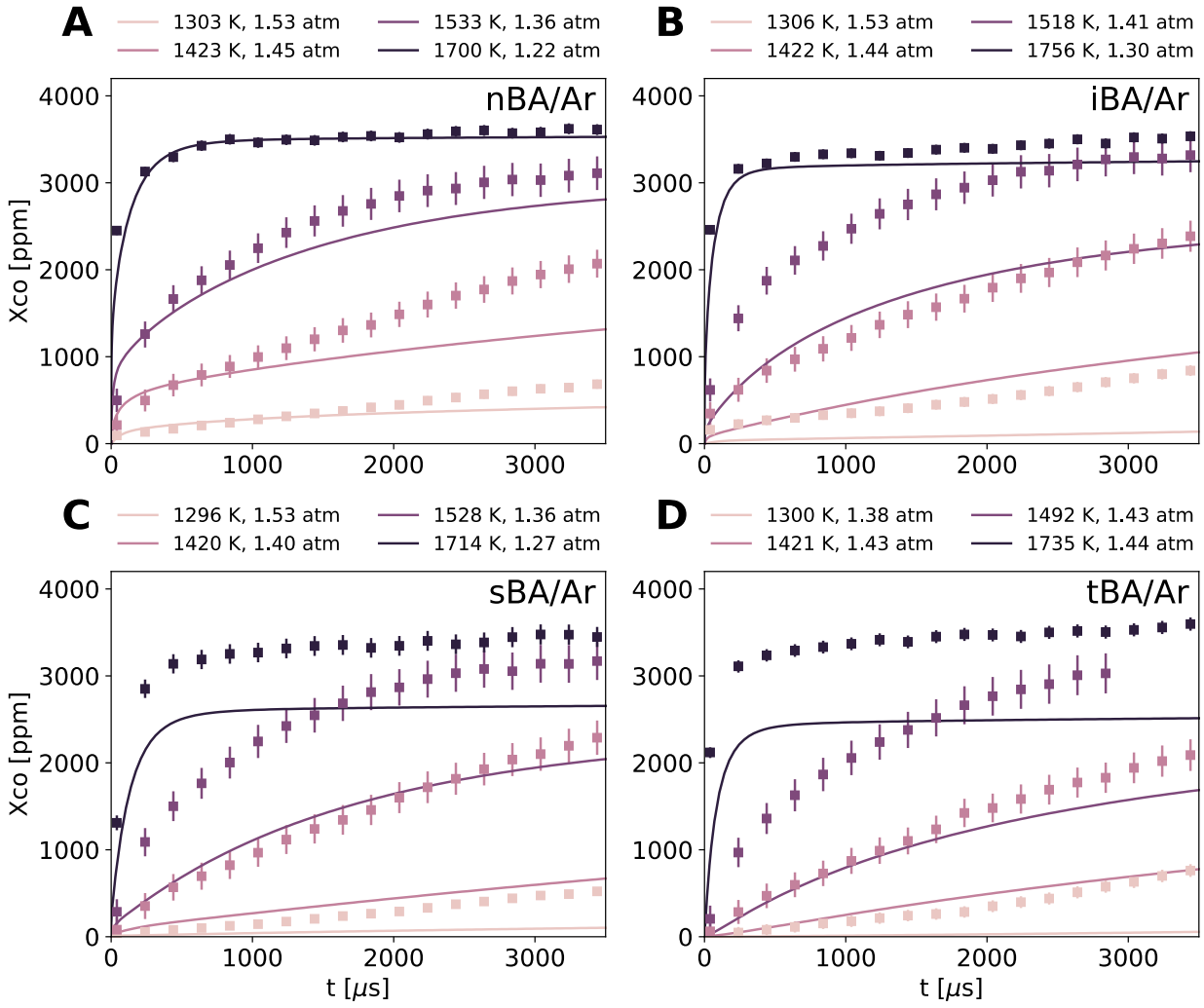

*Figure 14. CO mole fraction time histories in the BA pyrolysis systems. (**A**) nBA, (**B**) iBA, (**C**) sBA, and (**D**) tBA. The lines are predictions from the simulation, and the markers are the measurements from the experiments.*

Generally speaking, the pyrolysis of different BA isomers shows a negligible difference in CO profile according to the experiments. The models can capture the CO generation time history to some extent but underpredict CO production rate.

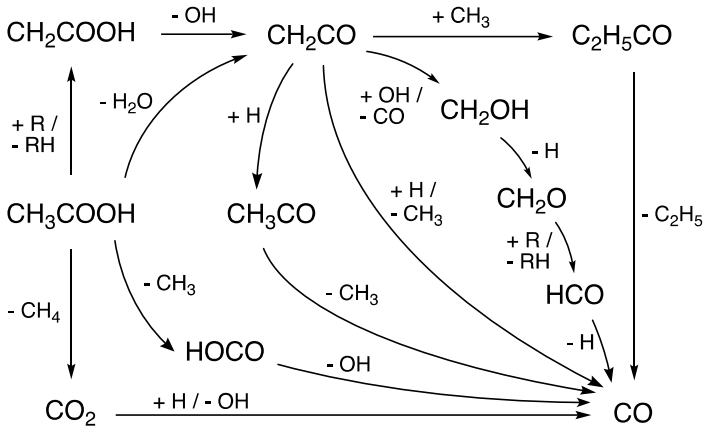

Figure 15. Major pathways in the BA pyrolysis system producing CO between 1200-1700 K. Acetic acid is generated from the retro-ene reaction of BAs. R = H or CH_3.

Figure 15 shows the dominant pathways producing CO from butyl acetates at high temperatures according to the kinetic models. Thermochemistry of all involved species and kinetics of all pathways shown in Figure 15 are from either RMG libraries or published databases and are expected to have reasonable accuracy. All the important pathways start from the acetic acid formed from the butyl acetate and involve radical intermediates, indicating the relevance of the radical pool growth on CO production rate. Indeed, the actual branching of a system depends on the abundance and distribution of each radical species. Sensitivities of CO concentration at 1500 K, 1 atm, and 1 ms from each BA isomer can be found in Section 8 of SI. The results highlight the significance of acetic acid sub-mechanism, C1 - C2 chemistry, a few alkene reactions, BA retro-ene reactions, and BA fission reactions for predicting CO production (Table S2). Among them, BA fission reactions (and their subsequent reactions) are critical to the radical accumulation. However, their exact rate constants at these reaction conditions are unknown; here they are all estimated by RMG rate rules. It is worth mentioning that in addition to the retro-ene reactions and fission reactions, there are other concerted primary reactions (i.e., (1) keto-enol, (2) BA ⇌ ketene + butanol, and (3) BA ⇌ acetaldehyde + butyraldehyde/butanone) that are expected to be involved in the BA decomposition, similar to the EA[9] and iPA[10] pyrolysis. RMG considered most of them insignificant pathways, consistent with the observations of EA and iPA, and included only reaction (2) in the nBA and iBA mechanisms. However, the kinetics of the above reactions were estimated by RMG rate rules, and kinetic parameter refinement is suggested in future studies to confirm their insignificance.

5 Conclusions

This work presents butyl acetate oxidation models created using a predictive modeling approach. Their predictive capability is achieved by gathering accurate parameters for species and reactions in the potential sub-mechanism, calculating primary reactions with a decent quantum chemistry method, implementing a rate-based algorithm to build the kinetic mechanism in the RMG, and

iteratively refining the thermochemistry of critical species. The generated models are for qualitatively and semi-quantitatively predicting oxidation systems, especially at elevated temperatures. Even though no data is available for straightforwardly validating the proposed models, careful comparison and investigation were made to illustrate the rationale of the calculated parameters, reveal the dominant chemistry in the oxidation systems, and demonstrate the adaptability of the model to the pyrolysis predictions. The major weakness of the models is the kinetic parameters of sensitive low-temperature oxidation pathways, e.g., BA peroxide isomerization, still derived from rate rules and with large uncertainties, limiting the accuracy of the model performance at lower temperatures. Other than the generated models, this work makes the following data available:

- QM-based kinetics of H-atom abstraction and retro-ene reactions for BA isomers
- Thermochemical data of over 600 species relevant to the oxidation and decomposition of oxygenated species at the CBS-QB3 level of theory
- CO mole fraction time histories of shock tube BA pyrolysis at 1300-1700 K

These data are valuable for creating ester-specific rate rules, building kinetic mechanisms for oxygenated species, and validating BA pyrolysis models. As a stepstone, this work yields the fundamentals necessary for creating a better BA model in future work and facilitates the evaluation of BA molecules as useful biofuels computationally.

Supporting Information

Supporting Information associated with this article includes the newly generated mechanism in various formats, the quantum chemical calculation detail, data visualization of the model statistics, complementary results for shock tube experiments, and supplementary mechanism analysis in terms of ignition delay time, flux diagram, and sensitivities.

Acknowledgement

This work at MIT and UCF was conducted as part of the Co-Optimization of Fuels & Engines (Co-Optima) project sponsored by the U.S. Department of Energy (DOE) Office of Energy Efficiency and Renewable Energy (EERE) [grant number DE-EE0007982]. The authors would like to thank Dr. Yang Li for helpful discussions about validating IDTs at lower temperatures.

Disclaimer

This report was prepared as an account of work sponsored by an agency of the United States Government. Neither the United States Government nor any agency thereof, nor any of their employees, makes any warranty, express or implied, or assumes any legal liability or responsibility for the accuracy, completeness, or usefulness of any information, apparatus, product, or process disclosed, or represents that its use would not infringe privately owned rights. Reference herein to any specific commercial product, process, or service by trade name, trademark, manufacturer, or otherwise does not necessarily constitute or imply its endorsement, recommendation, or favoring by the United States Government or any agency thereof. The views and opinions of authors expressed herein do not necessarily state or reflect those of the United States Government or any agency thereof.

Reference

(1) Lai, J. Y. W.; Lin, K. C.; Violi, A. Biodiesel Combustion: Advances in Chemical Kinetic Modeling. *Prog. Energy Combust. Sci.* **2011**, *37* (1), 1–14. DOI:10.1016/j.pecs.2010.03.001.

(2) Dagaut, P.; Gail, S.; Sahasrabudhe, M. Rapeseed Oil Methyl Ester Oxidation over Extended Ranges of Pressure, Temperature, and Equivalence Ratio: Experimental and Modeling Kinetic Study. *Proc. Combust. Inst.* **2007**, *31* (2), 2955–2961. DOI:10.1016/j.proci.2006.07.142.

(3) Coniglio, L.; Bennadji, H.; Glaude, P. A.; Herbinet, O.; Billaud, F. Combustion Chemical Kinetics of Biodiesel and Related Compounds (Methyl and Ethyl Esters): Experiments and Modeling-Advances and Future Refinements. *Prog. Energy Combust. Sci.* **2013**, *39* (4), 340–382. DOI:10.1016/j.pecs.2013.03.002.

(4) Felsmann, D.; Zhao, H.; Wang, Q.; Graf, I.; Tan, T.; Yang, X.; Carter, E. A.; Ju, Y.; Kohse-höinghaus, K. Contributions to Improving Small Ester Combustion Chemistry : Theory , Model and Experiments. *Proc. Combust. Inst.* **2017**, *36* (1), 543–551. DOI:10.1016/j.proci.2016.05.012.

(5) Westbrook, C. K.; Pitz, W. J.; Curran, H. J. Chemical Kinetic Modeling Study of the Effects of Oxygenated Hydrocarbons on Soot Emissions from Diesel Engines. *J. Phys. Chem. A* **2006**, *110* (21), 6912–6922. DOI:10.1021/jp056362g.

(6) Dooley, S.; Burke, M. P.; Chaos, M.; Stein, Y.; Dryer, F. L.; Zhukov, V. P.; Finch, O.; Simmie, J. M.; Curran, H. J. Methyl Formate Oxidation: Speciation Data, Laminar Burning Velocities, Ignition Delay Times, and a Validated Chemical Kinetic Model. *Int. J. Chem. Kinet.* **2010**, *42* (9), 527–549. DOI:10.1002/kin.20512.

(7) Le, X. T.; Mai, T. V. T.; Lin, K. C.; Huynh, L. K. Low Temperature Oxidation Kinetics of Biodiesel Molecules: Rate Rules for Concerted HO2 Elimination from Alkyl Ester Peroxy Radicals. *J. Phys. Chem. A* **2018**, *122* (42), 8259–8273. DOI:10.1021/acs.jpca.8b05070.

(8) Ahmed, A.; Pitz, W. J.; Cavallotti, C.; Mehl, M.; Lokachari, N.; Nilsson, E. J. K.; Wang, J. Y.; Konnov, A. A.; Wagnon, S. W.; Chen, B.; et al. Small Ester Combustion Chemistry: Computational Kinetics and Experimental Study of Methyl Acetate and Ethyl Acetate. *Proc. Combust. Inst.* **2019**, *37* (1), 419–428. DOI:10.1016/j.proci.2018.06.178.

(9) Sun, W.; Tao, T.; Zhang, R.; Liao, H.; Huang, C.; Zhang, F.; Zhang, X.; Zhang, Y.; Yang, B. Experimental and Modeling Efforts towards a Better Understanding of the High-Temperature Combustion Kinetics of C3-C5 Ethyl Esters. *Combust. Flame* **2017**, *185*, 173–187. DOI:10.1016/j.combustflame.2017.07.013.

(10) Herzler, J.; Mujaddadi, S. A.; Fikri, M.; Schulz, C.; Peukert, S. Single-Pulse Shock-Tube Study on the Pyrolysis of Small Esters (Ethyl and Propyl Propanoate, Isopropyl Acetate) and Methyl Isopropyl Carbonate. *Proc. Combust. Inst.* **2022**, Article ASAP. DOI:10.1016/j.proci.2022.07.012.

(11) Morsch, P.; Döntgen, M.; Heufer, K. A. Kinetic Investigations on the High- and Low-Temperature Chemistry of Ethyl Acetate. *Combust. Flame* **2022**, *243*, 111995. DOI:10.1016/j.combustflame.2022.111995.

(12) Algayyim, S. J. M.; Wandel, A. P.; Yusaf, T.; Hamawand, I. Production and Application of ABE as a Biofuel. *Renew. Sustain. Energy Rev.* **2018**, *82, Part 1*, 1195–1214. DOI:10.1016/j.rser.2017.09.082.

(13) Ali, S. H.; Al-Rashed, O.; Azeez, F. A.; Merchant, S. Q. Potential Biofuel Additive from Renewable Sources - Kinetic Study of Formation of Butyl Acetate by Heterogeneously

Catalyzed Transesterification of Ethyl Acetate with Butanol. *Bioresour. Technol.* **2011**, *102* (21), 10094–10103. DOI:10.1016/j.biortech.2011.08.033.
(14) Steinigeweg, S.; Gmehling, J. N -Butyl Acetate Synthesis via Reactive Distillation: Thermodynamic Aspects, Reaction Kinetics, Pilot-Plant Experiments, and Simulation Studies. *Ind. Eng. Chem. Res.* **2002**, *41* (22), 5483–5490. DOI:10.1021/ie020179h.
(15) Gangadwala, J.; Kienle, A.; Stein, E.; Mahajani, S. Production of Butyl Acetate by Catalytic Distillation: Process Design Studies. *Ind. Eng. Chem. Res.* **2004**, *43* (1), 136–143. DOI:10.1021/ie021011z.
(16) Rodriguez, G. M.; Tashiro, Y.; Atsumi, S. Expanding Ester Biosynthesis in Escherichia Coli. *Nat. Chem. Biol.* **2014**, *10* (4), 259–265. DOI:10.1038/nchembio.1476.
(17) Feng, J.; Zhang, J.; Ma, Y.; Feng, Y.; Wang, S.; Guo, N.; Wang, H.; Wang, P.; Jiménez-Bonilla, P.; Gu, Y.; et al. Renewable Fatty Acid Ester Production in Clostridium. *Nat. Commun.* **2021**, *12* (1), 4368. DOI:10.1038/s41467-021-24038-3.
(18) Wang, Y.; Chen, Z.; Haefner, M.; Guo, S.; DiReda, N.; Ma, Y.; Wang, Y.; Thomas Avedisian, C. Combustion of N-Butyl Acetate Synthesized by a New and Sustainable Biological Process and Comparisons with an Ultrapure Commercial n-Butyl Acetate Produced by Conventional Fischer Esterification. *Fuel* **2021**, *304*, 121324. DOI:10.1016/j.fuel.2021.121324.
(19) Xing, J. H.; Takahashi, K.; Hurley, M. D.; Wallington, T. J. Kinetics of the Reactions of Chlorine Atoms with a Series of Acetates. *Chem. Phys. Lett.* **2009**, *474* (4–6), 268–272. DOI:10.1016/j.cplett.2009.04.083.
(20) Glassman, I.; Yetter, R. A. *Combustion*, 4th ed.; Academic Press, Ed.; Elsevier: San Diego, California, 2008.
(21) Mendes, J.; Zhou, C. W.; Curran, H. J. Theoretical and Kinetic Study of the Hydrogen Atom Abstraction Reactions of Esters with HO2 Radicals. *J. Phys. Chem. A* **2013**, *117* (51), 14006–14018. DOI:10.1021/jp409133x.
(22) Wang, Q. De; Wang, X. J.; Liu, Z. W.; Kang, G. J. Theoretical and Kinetic Study of the Hydrogen Atom Abstraction Reactions of Ethyl Esters with Hydrogen Radicals. *Chem. Phys. Lett.* **2014**, *616–617* (25), 109–114. DOI:10.1016/j.cplett.2014.10.032.
(23) Mendes, J.; Zhou, C. W.; Curran, H. J. Theoretical Study of the Rate Constants for the Hydrogen Atom Abstraction Reactions of Esters with ·OH Radicals. *J. Phys. Chem. A* **2014**, *118* (27), 4889–4899. DOI:10.1021/jp5029596.
(24) Herbinet, O.; Pitz, W. J.; Westbrook, C. K. Detailed Chemical Kinetic Oxidation Mechanism for a Biodiesel Surrogate. *Combust. Flame* **2008**, *154* (3), 507–528. DOI:10.1016/j.combustflame.2008.03.003.
(25) Wang, Q. De; Ni, Z. H. Theoretical and Kinetic Study of the Hydrogen Atom Abstraction Reactions of Unsaturated C6 Methyl Esters with Hydroxyl Radical. *Chem. Phys. Lett.* **2016**, *650*, 119–125. DOI:10.1016/j.cplett.2016.02.071.
(26) Zádor, J.; Taatjes, C. A.; Fernandes, R. X. Kinetics of Elementary Reactions in Low-Temperature Autoignition Chemistry. *Prog. Energy Combust. Sci.* **2011**, *37* (4), 371–421. DOI:10.1016/j.pecs.2010.06.006.
(27) Zádor, J.; Klippenstein, S. J.; Miller, J. A. Pressure-Dependent OH Yields in Alkene + HO2 Reactions: A Theoretical Study. *J. Phys. Chem. A* **2011**, *115* (36), 10218–10225. DOI:10.1021/jp2059276.
(28) Miller, J. A.; Klippenstein, S. J. Dissociation of Propyl Radicals and Other Reactions on a C3H7 Potential. *J. Phys. Chem. A* **2013**, *117* (13), 2718–2727. DOI:10.1021/jp312712p.

(29) Cavallotti, C.; Pelucchi, M.; Frassoldati, A. Analysis of Acetic Acid Gas Phase Reactivity: Rate Constant Estimation and Kinetic Simulations. *Proc. Combust. Inst.* **2019**, *37* (1), 539–546. DOI:10.1016/j.proci.2018.06.137.
(30) Zhou, C. W.; Klippenstein, S. J.; Simmie, J. M.; Curran, H. J. Theoretical Kinetics for the Decomposition of Iso-Butanol and Related (CH3)2ĊH + ĊH2OH Reactions. *Proc. Combust. Inst.* **2013**, *34* (1), 501–509. DOI:10.1016/j.proci.2012.06.034.
(31) Mendes, J.; Zhou, C. W.; Curran, H. J. Theoretical Chemical Kinetic Study of the H-Atom Abstraction Reactions from Aldehydes and Acids by Ḣ Atoms and ȮH, HȮ2, and ĊH3 Radicals. *J. Phys. Chem. A* **2014**, *118* (51), 12089–12104. DOI:10.1021/jp5072814.
(32) Antonov, I. O.; Kwok, J.; Zádor, J.; Sheps, L. A Combined Experimental and Theoretical Study of the Reaction OH + 2-Butene in the 400-800 K Temperature Range. *J. Phys. Chem. A* **2015**, *119* (28), 7742–7752. DOI:10.1021/acs.jpca.5b01012.
(33) Tan, T.; Yang, X.; Ju, Y.; Carter, E. A. Ab Initio Unimolecular Reaction Kinetics of CH2C(=O)OCH3 and CH3C(=O)OCH2 Radicals. *J. Phys. Chem. A* **2015**, *119* (42), 10553–10562. DOI:10.1021/acs.jpca.5b08331.
(34) Zhou, C. W.; Simmie, J. M.; Somers, K. P.; Goldsmith, C. F.; Curran, H. J. Chemical Kinetics of Hydrogen Atom Abstraction from Allylic Sites by 3O2; Implications for Combustion Modeling and Simulation. *J. Phys. Chem. A* **2017**, *121* (9), 1890–1899. DOI:10.1021/acs.jpca.6b12144.
(35) Zhou, C. W.; Li, Y.; O'Connor, E.; Somers, K. P.; Thion, S.; Keesee, C.; Mathieu, O.; Petersen, E. L.; DeVerter, T. A.; Oehlschlaeger, M. A.; et al. A Comprehensive Experimental and Modeling Study of Isobutene Oxidation. *Combust. Flame* **2016**, *167*, 353–379. DOI:10.1016/j.combustflame.2016.01.021.
(36) Tan, T.; Yang, X.; Ju, Y.; Carter, E. A. Ab Initio Reaction Kinetics of CH3OC(=O) and CH2OC(=O)H Radicals. *J. Phys. Chem. B* **2016**, *120* (8), 1590–1600. DOI:10.1021/acs.jpcb.5b07959.
(37) Tian, Z.; Li, J.; Yan, Y. Theoretical Ab-Initio Kinetics of the Reactions between Isobutene plus Hydroxyl. *Chem. Phys. Lett.* **2019**, *720*, 83–92. DOI:10.1016/j.cplett.2019.01.057.
(38) Pounds, A. J. *Introduction to Quantum Mechanics: A Time-Dependent Perspective (David J. Tannor)*, 1st ed.; University Science Books: Sausalito, USA, 2007. DOI:10.1021/ed085p919.
(39) Montgomery, J. A.; Frisch, M. J.; Ochterski, J. W.; Petersson, G. A. A Complete Basis Set Model Chemistry. VI. Use of Density Functional Geometries and Frequencies. *J. Chem. Phys.* **1999**, *110* (6), 2822–2827. DOI:10.1063/1.477924.
(40) Montgomery, J. A.; Frisch, M. J.; Ochterski, J. W.; Petersson, G. A. A Complete Basis Set Model Chemistry. VII. Use of the Minimum Population Localization Method. *J. Chem. Phys.* **2000**, *112* (15), 6532–6542. DOI:10.1063/1.481224.
(41) Goldsmith, C. F.; Magoon, G. R.; Green, W. H. Database of Small Molecule Thermochemistry for Combustion. *J. Phys. Chem. A* **2012**, *116* (36), 9033–9057. DOI:10.1021/jp303819e.
(42) Green, W. H. Moving from Postdictive to Predictive Kinetics in Reaction Engineering. *AIChE J.* **2020**, *66* (11), e17059. DOI:10.1002/aic.17059.
(43) Zhang, P.; Yee, N. W.; Filip, S. V.; Hetrick, C. E.; Yang, B.; Green, W. H. Modeling Study of the Anti-Knock Tendency of Substituted Phenols as Additives: An Application of the Reaction Mechanism Generator (RMG). *Phys. Chem. Chem. Phys.* **2018**, *20* (16), 10637–10649. DOI:10.1039/C7CP07058F.

(44) Liu, M.; Grinberg Dana, A.; Johnson, M. S.; Goldman, M. J.; Jocher, A.; Payne, A. M.; Grambow, C. A.; Han, K.; Yee, N. W.; Mazeau, E. J.; et al. Reaction Mechanism Generator v3.0: Advances in Automatic Mechanism Generation. *J. Chem. Inf. Model.* **2021**, *61* (6), 2686–2696. DOI:10.1021/acs.jcim.0c01480.
(45) Gao, C. W.; Allen, J. W.; Green, W. H.; West, R. H. Reaction Mechanism Generator: Automatic Construction of Chemical Kinetic Mechanisms. *Comput. Phys. Commun.* **2016**, *203*, 212–225. DOI:10.1016/j.cpc.2016.02.013.
(46) Johnson, M. S.; Dong, X.; Grinberg Dana, A.; Chung, Y.; Farina, D.; Gillis, R. J.; Liu, M.; Yee, N. W.; Blondal, K.; Mazeau, E.; et al. RMG Database for Chemical Property Prediction. *J. Chem. Inf. Model.* **2022**, *62* (20), 4906–4915. DOI:10.1021/acs.jcim.2c00965.
(47) Pio, G.; Dong, X.; Salzano, E.; Green, W. H. Automatically Generated Model for Light Alkene Combustion. *Combust. Flame* **2022**, *241*, 112080. DOI:10.1016/j.combustflame.2022.112080.
(48) Goodwin, D. G.; Speth, R. L.; Moffat, H. K.; Weber, B. W. Cantera: An Object-Oriented Software Toolkit for Chemical Kinetics, Thermodynamics, and Transport Processes. 2018. http://www.cantera.org. DOI:10.5281/zenodo.1174508 (accessed 2020-03-10).
(49) Johnson, M. S.; Pang, H.-W.; Payne, A. M.; Dong, X.; Green, W. H. Reaction Mechanism Simulator (RMS). Cambridge 2022. https://github.com/ReactionMechanismGenerator/ReactionMechanismSimulator.jl (accessed 2021-10-15).
(50) Sharma, S.; Raman, S.; Green, W. H. Intramolecular Hydrogen Migration in Alkylperoxy and Hydroperoxyalkylperoxy Radicals: Accurate Treatment of Hindered Rotors. *J. Phys. Chem. A* **2010**, *114* (18), 5689–5701. DOI:10.1021/jp9098792.
(51) Frisch, M. J.; Trucks, G. W.; Schlegel, H. B.; Scuseria, G. E.; Robb, M. A.; Cheeseman, J. R.; Montgomery Jr., J. A.; Vreven, T.; Kudin, K. N.; Burant, J. C.; et al. Gaussian 09 Revision D.01. Wallingford, CT 2013.
(52) Frisch, M. J.; Trucks, G. W.; Schlegel, H. B.; Scuseria, G. E.; Robb, M. A.; Cheeseman, J. R.; Scalmani, G.; Barone, V.; Petersson, G. A.; Nakatsuji, H.; et al. Gaussian 16 Revision B.01. Wallingford, CT 2016.
(53) Grinberg Dana, A.; Ranasinghe, D.; Wu, H.; Grambow, C.; Dong, X.; Johnson, M.; Goldman, M.; Liu, M.; Green, W. H. ARC - Automated Rate Calculator. Cambridge, MA, US. https://github.com/ReactionMechanismGenerator/ARC. DOI:10.5281/zenodo.3356849 (accessed 2019-10-01).
(54) Dana, A. G.; Johnson, M. S.; Allen, J. W.; Sharma, S.; Raman, S.; Liu, M.; Gao, C. W.; Grambow, C. A.; Goldman, M. J.; Ranasinghe, D. S.; et al. Automated Reaction Kinetics and Network Exploration (Arkane): A Statistical Mechanics, Thermodynamics, Transition State Theory, and Master Equation Software. *ChemRxiv* **2022**. DOI:10.26434/chemrxiv-2022-4klsm.
(55) Riniker, S.; Landrum, G. A. Better Informed Distance Geometry: Using What We Know To Improve Conformation Generation. *J. Chem. Inf. Model.* **2015**, *55* (12), 2562–2574. DOI:10.1021/acs.jcim.5b00654.
(56) Tosco, P.; Stiefl, N.; Landrum, G. Bringing the MMFF Force Field to the RDKit: Implementation and Validation. *J. Cheminform.* **2014**, *6* (1), 37. DOI:10.1186/S13321-014-0037-3.
(57) Halgren, T. A. MMFF VI. MMFF94s Option for Energy Minimization Studies. *J.*

Comput. Chem. **1999**, *20* (7), 720–729. DOI:10.1002/(SICI)1096-987X(199905)20:7<720::AID-JCC7>3.0.CO;2-X.
(58) Grinberg Dana, A.; Wu, H.; Ranasinghe, D. S.; Pickard, F. C.; Wood, G. P. F.; Zelesky, T.; Sluggett, G. W.; Mustakis, J.; Green, W. H. Kinetic Modeling of API Oxidation: (1) The AIBN/H2O/CH3OH Radical "Soup." *Mol. Pharm.* **2021**, *18* (8), 3037–3049. DOI:10.1021/acs.molpharmaceut.1c00261.
(59) Zhou, C.-W.; Simmie, J. M.; Curran, H. J. Rate Constants for Hydrogen-Abstraction by ȮH from n-Butanol. *Combust. Flame* **2011**, *158* (4), 726–731. DOI:10.1016/j.combustflame.2010.11.002.
(60) Zhou, C.-W.; Simmie, J. M.; Curran, H. J. Rate Constants for Hydrogen Abstraction by HȮ2 from N-Butanol. *Int. J. Chem. Kinet.* **2012**, *44* (3), 155–164. DOI:10.1002/kin.20708.
(61) Tan, T.; Yang, X.; Krauter, C. M.; Ju, Y.; Carter, E. A. Ab Initio Kinetics of Hydrogen Abstraction from Methyl Acetate by Hydrogen, Methyl, Oxygen, Hydroxyl, and Hydroperoxy Radicals. *J. Phys. Chem. A* **2015**, *119* (24), 6377–6390. DOI:10.1021/acs.jpca.5b03506.
(62) Power, J.; Somers, K. P.; Nagaraja, S. S.; Curran, H. J. Hierarchical Study of the Reactions of Hydrogen Atoms with Alkenes: A Theoretical Study of the Reactions of Hydrogen Atoms with C 2 –C 4 Alkenes. *J. Phys. Chem. A* **2021**, *125* (23), 5124–5145. DOI:10.1021/acs.jpca.1c03168.
(63) Xiao, F.; Sun, X.; Li, Z.; Li, X. Theoretical Study of Radical–Molecule Reactions with Negative Activation Energies in Combustion: Hydroxyl Radical Addition to Alkenes. *ACS Omega* **2020**, *5* (22), 12777–12788. DOI:10.1021/acsomega.0c00400.
(64) Villano, S. M.; Carstensen, H.-H.; Dean, A. M. Rate Rules, Branching Ratios, and Pressure Dependence of the HO2 + Olefin Addition Channels. *J. Phys. Chem. A* **2013**, *117* (30), 6458–6473. DOI:10.1021/jp405262r.
(65) Hashemi, H.; Christensen, J. M.; Gersen, S.; Levinsky, H.; Klippenstein, S. J.; Glarborg, P. High-Pressure Oxidation of Methane. *Combust. Flame* **2016**, *172*, 349–364. DOI:10.1016/j.combustflame.2016.07.016.
(66) Li, X.; Jasper, A. W.; Zádor, J.; Miller, J. A.; Klippenstein, S. J. Theoretical Kinetics of O + C2H4. *Proc. Combust. Inst.* **2017**, *36* (1), 219–227. DOI:10.1016/j.proci.2016.06.053.
(67) Burke, M. P.; Chaos, M.; Ju, Y.; Dryer, F. L.; Klippenstein, S. J. Comprehensive H2/O2 Kinetic Model for High-Pressure Combustion. *Int. J. Chem. Kinet.* **2012**, *44* (7), 444–474. DOI:10.1002/kin.20603.
(68) Yaws, C. L. *Yaws' Critical Property Data for Chemical Engineers and Chemists*; Knovel, 2012.
(69) Smith, G. P.; Tao, Y.; Wang, H. *Foundational fuel chemistry model version 1.0 (FFCM-1)*. ChemRxiv. http://nanoenergy.stanford.edu/ffcm1 (accessed 2021-09-03).
(70) Benson, S. W. Thermochemical Kinetics: Methods for the Estimation of Thermochemical Data and Rate Parameters; John Wiley & Sons, Inc.: Hoboken, USA, 1976. DOI:10.1002/bbpc.19690730226.
(71) Kee, R. J.; Rupley, F. M.; Miller, J. A.; Coltrin, M. E.; Grcar, J. F.; Meeks, E.; Moffat, H. K.; Lutz, A. E.; Dixon-Lewis, G.; Smooke, M. D.; et al. CHEMKIN-Pro. Reaction Design: San Diego 2020.
(72) Johnson, M. S.; McGill, C. J.; Green, W. H. Transitory Sensitivity in Automatic Chemical Kinetic Mechanism Analysis. **2022**. DOI:10.26434/chemrxiv-2022-zsfjc.

(73) Ji, W.; Ren, Z.; Law, C. K. Evolution of Sensitivity Directions during Autoignition. *Proc. Combust. Inst.* **2019**, *37* (1), 807–815. DOI:10.1016/j.proci.2018.07.005.
(74) Koroglu, B.; Vasu, S. S. Measurements of Propanal Ignition Delay Times and Species Time Histories Using Shock Tube and Laser Absorption. *Int. J. Chem. Kinet.* **2016**, *48* (11), 679–690. DOI:10.1002/kin.21024.
(75) Pryor, O.; Barak, S.; Koroglu, B.; Ninnemann, E.; Vasu, S. S. Measurements and Interpretation of Shock Tube Ignition Delay Times in Highly CO2 Diluted Mixtures Using Multiple Diagnostics. *Combust. Flame* **2017**, *180*, 63–76. DOI:10.1016/j.combustflame.2017.02.020.
(76) Ninnemann, E.; Koroglu, B.; Pryor, O.; Barak, S.; Nash, L.; Loparo, Z.; Sosa, J.; Ahmed, K.; Vasu, S. New Insights into the Shock Tube Ignition of H2/O2 at Low to Moderate Temperatures Using High-Speed End-Wall Imaging. *Combust. Flame* **2018**, *187*, 11–21. DOI:10.1016/j.combustflame.2017.08.021.
(77) Campbell, M. F. Studies of Biodiesel Surrogates Using Novel Shock Tube Techniques, Ph.D. Dissertation, Palo Alto, U.S.A., 2014.
(78) Rothman, L. S.; Gordon, I. E.; Barber, R. J.; Dothe, H.; Gamache, R. R.; Goldman, A.; Perevalov, V. I.; Tashkun, S. A.; Tennyson, J. HITEMP, the High-Temperature Molecular Spectroscopic Database. *J. Quant. Spectrosc. Radiat. Transf.* **2010**, *111* (15), 2139–2150. DOI:10.1016/j.jqsrt.2010.05.001.
(79) Dayma, G.; Thion, S.; Lailliau, M.; Serinyel, Z.; Dagaut, P.; Sirjean, B.; Fournet, R. Kinetics of Propyl Acetate Oxidation: Experiments in a Jet-Stirred Reactor, Ab Initio Calculations, and Rate Constant Determination. *Proc. Combust. Inst.* **2019**, *37* (1), 429–436. DOI:10.1016/j.proci.2018.05.178.
(80) Herzler, J.; Mujaddadi, S. A.; Fikri, M.; Schulz, C.; Peukert, S. Single-Pulse Shock-Tube Study on the Pyrolysis of Small Esters (Ethyl and Propyl Propanoate, Isopropyl Acetate) and Methyl Isopropyl Carbonate. *Proc. Combust. Inst.* **2022**. DOI:10.1016/j.proci.2022.07.012.
(81) Li, Y.; Zhou, C.-W.; Curran, H. J. An Extensive Experimental and Modeling Study of 1-Butene Oxidation. *Combust. Flame* **2017**, *181*, 198–213. DOI:10.1016/j.combustflame.2017.03.023.
(82) Li, Y.; Zhou, C.-W.; Somers, K. P.; Zhang, K.; Curran, H. J. The Oxidation of 2-Butene: A High Pressure Ignition Delay, Kinetic Modeling Study and Reactivity Comparison with Isobutene and 1-Butene. *Proc. Combust. Inst.* **2017**, *36* (1), 403–411. DOI:10.1016/j.proci.2016.05.052.

Butyl Acetate Pyrolysis and Combustion Chemistry: Mechanism Generation and Shock Tube Experiments

Xiaorui Dong[a], Gianmaria Pio[b], Farhan Arafin[c], Andrew Laich[c], Jessica Baker[c], Erik Ninnemann[c], Subith S. Vasu[c], and William H. Green[a*]

[a] *Department of Chemical Engineering, Massachusetts Institute of Technology, Cambridge, MA, 02139, USA*
[b] *Department of Civil, Chemical, Environmental, and Materials Engineering (DICAM), Alma Mater Studiorum, University of Bologna, Bologna, 40126, Italy*
[c] *Center for Advanced Turbomachinery and Energy Research (CATER), Mechanical and Aerospace Engineering, University of Central Florida, Orlando, FL, 32816, USA*

* Corresponding author. *Email address*: whgreen@mit.edu (W. H. Green).

1 Quantum Chemical Calculation Details

1.1 Calculation Environment

The quantum chemistry calculations are conducted using

- Gaussian 09 revision D.01[1] running on the MIT C3DDB cluster (each node has four 16-core AMD 6376 CPUs and 256 GB RAM)
- Gaussian 16 revision B.01[2] running on the MIT Supercloud cluster (each node has two 24-core Intel Xeon Platinum 8620 CPUs and 192 GB RAM)

Each calculation job typically uses eight threads and 15 GB RAM.

1.2 Quantum Chemistry Calculation Schemes

- **Non-TS Geometry Optimization**
  #P b3lyp/cbsb7 opt=(calcfc, noeigentest, tight) guess=mix scf=(tight, direct) integral=(grid=ultrafine, Acc2E=12) iop(2/9=2000)

- **TS Geometry Optimization**
  #P b3lyp/cbsb7 opt=(ts, calcfc, noeigentest, tight, maxstep=5, maxcycles=200) guess=mix scf=(tight, direct) integral=(grid=ultrafine, Acc2E=12) iop(2/9=2000)

- **Frequency Calculation**
  #P b3lyp/cbsb7 freq scf=(tight, direct) integral=(grid=ultrafine, Acc2E=12) iop(2/9=2000) iop(7/33=1)

- **Single Point Energy Calculation**
  #P cbs-qb3 sp scf=(tight, direct) integral=(grid=ultrafine, Acc2E=12) iop(2/9=2000)

- **Non-TS Rotor Scan**
  #P b3lyp/cbsb7 opt=(calcfc, noeig, modredundant) guess=mix scf=(tight, direct) integral=(grid=ultrafine, Acc2E=12) iop(2/9=2000)

- **TS Rotor Scan**
  #P b3lyp/cbsb7 opt=(ts, calcfc, noeig, modredundant) guess=mix scf=(tight, direct) integral=(grid=ultrafine, Acc2E=12) iop(2/9=2000)

Notes

1. guess=mix is effective only for molecules with multiplicity=1.
2. iop(7/33=1) was used to write the Hessian matrix into the log file.
3. Scans were done in 45 steps with a step size of 8 degrees.
4. The actual schemes may be slightly different due to ARC's troubleshooting suggestions.[3] E.g., including scf=xqc for converging SCF in some cases, freezing several internal coordinates in the rotor scans to yield relevant results, etc.

1.3 Energy Corrections

Atomization energy corrections and Petersson-type bond additivity corrections were applied when calculating the thermochemistry of non-TS molecules. Relevant theoretical background can be found in the ARKANE introductory paper[4], and the correction values used are stored at

https://github.com/ReactionMechanismGenerator/RMG-database/blob/main/input/quantum_corrections/data.py

1.4 Accessibility

All relevant quantum chemical calculation output files can be found at https://doi.org/10.5281/zenodo.7244945

Calculated rate constants are reported in the manuscript Table 1 and 2. The same data in the RMG reaction library format can also be found at

- H abstraction reactions:

  https://github.com/ReactionMechanismGenerator/RMG-database/blob/butyl_acetate_xdong_gpio/input/kinetics/libraries/BA_habs/reactions.py

- Retro-ene reactions:

  https://github.com/ReactionMechanismGenerator/RMG-database/blob/butyl_acetate_xdong_gpio/input/kinetics/libraries/BA_retroene/reactions.py

- Calculated thermochemical data can be found at

  https://github.com/ReactionMechanismGenerator/RMG-database/blob/butyl_acetate_xdong_pio/input/thermo/libraries/butyl_acetate_xdong_gpio.py

1.5 Statistics of the Thermochemistry Results

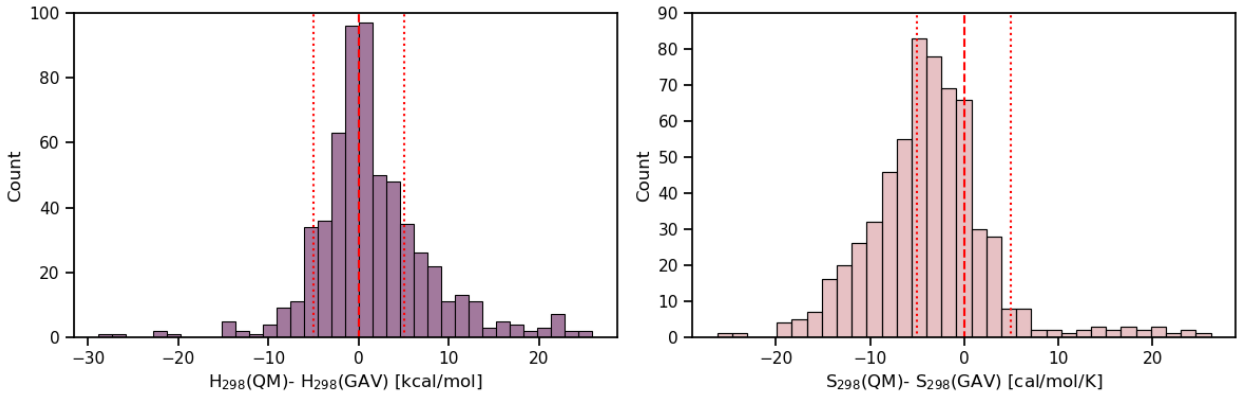

Figure S1. The distribution of deviations between the estimated and quantum mechanically calculated enthalpy and entropy at 298 K. The dashed line represents the case when the estimated value equals the calculated value. The dotted reference lines indicate a +/- 5 kcal/mol (H_{298}) or 5 cal/mol/K(S_{298}) difference between the estimated and calculated values.

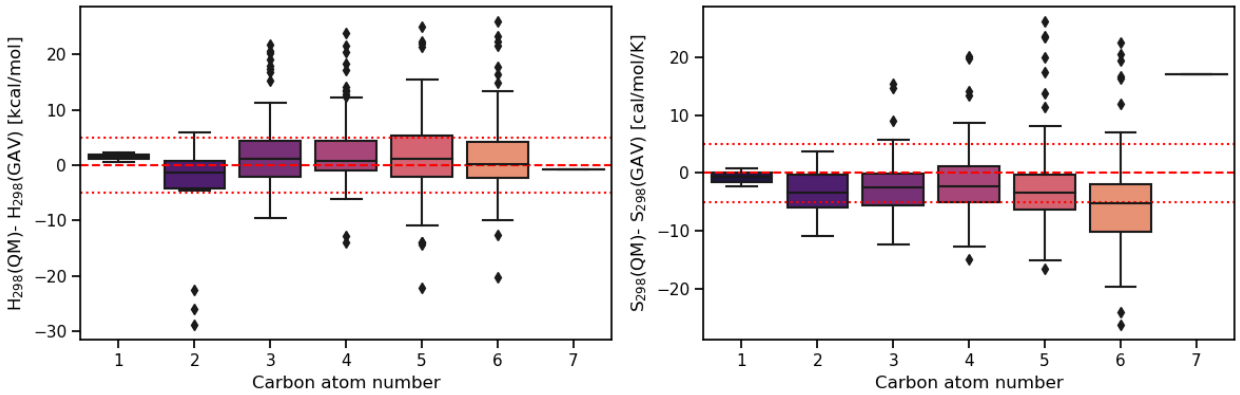

Figure S2. The distribution of deviations between the estimated and quantum mechanically calculated enthalpy and entropy at 298 K when categorized by the number of carbon atoms. The dashed line represents the case when the estimated value equals the calculated value. The dotted reference lines indicate a +/- 5 kcal/mol (H_{298}) or 5 cal/mol/K(S_{298}) difference between the estimated and calculated values.

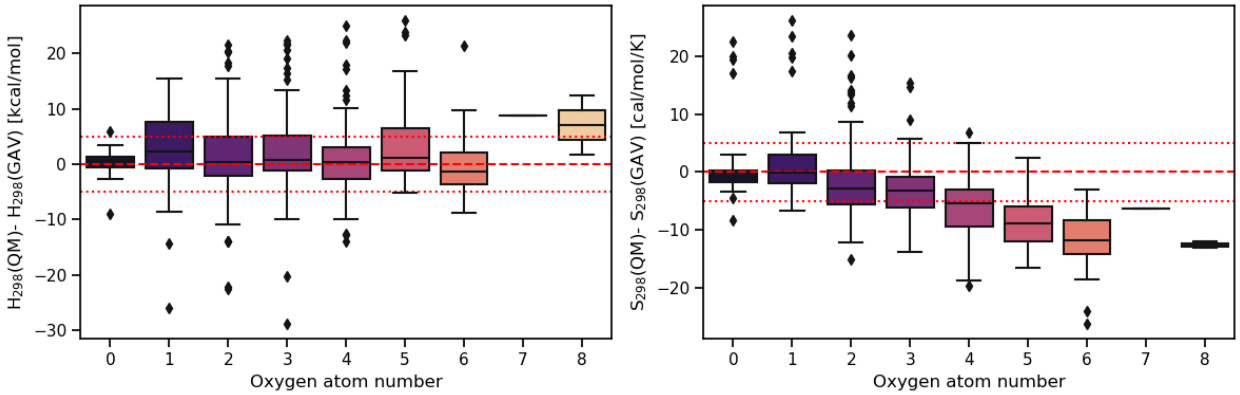

Figure S3. The distribution of deviations between the estimated and quantum mechanically calculated enthalpy and entropy at 298 K when categorized by the number of oxygen atoms. The dashed line represents the case when the estimated value equals the calculated value. The dotted reference lines indicate a +/- 5 kcal/mol (H_{298}) or 5 cal/mol/K(S_{298}) difference between the estimated and calculated values.

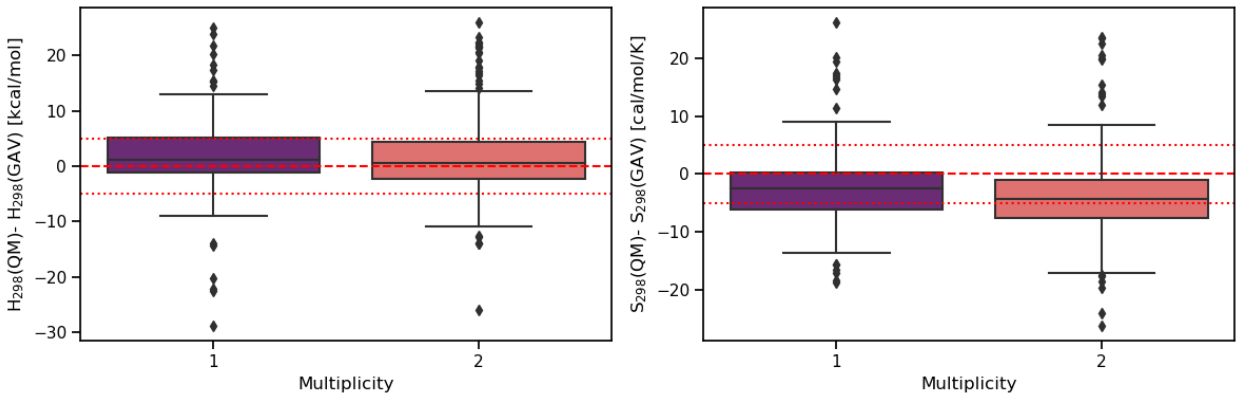

Figure S4. The distribution of deviations between the estimated and quantum mechanically calculated enthalpy and entropy at 298 K when categorized by the molecule multiplicity. The dashed line represents the case when the estimated value equals the calculated value. The dotted reference lines indicate a +/- 5 kcal/mol (H_{298}) or 5 cal/mol/K(S_{298}) difference between the estimated and calculated values.

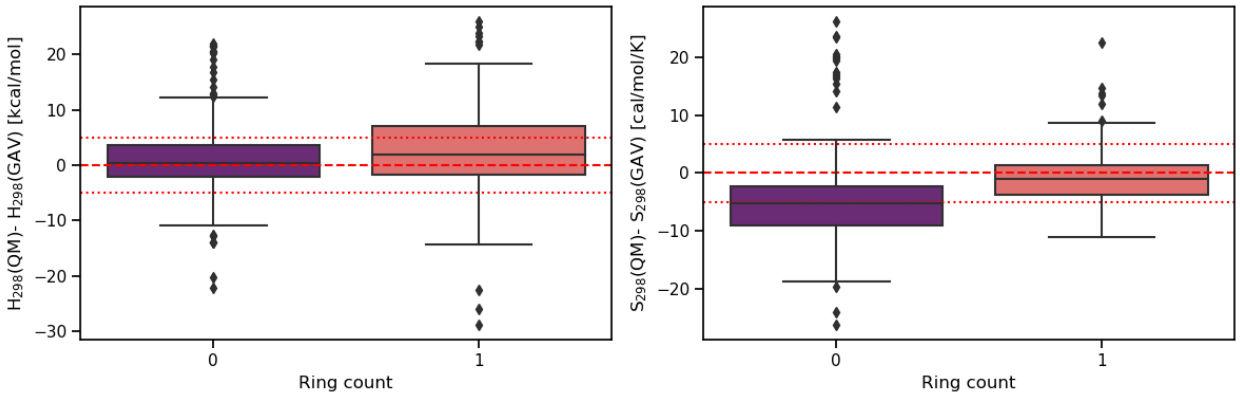

Figure S5. The distribution of deviations between the estimated and quantum mechanically calculated enthalpy and entropy at 298 K when categorized by the number of rings. The dashed line represents the case when the estimated value equals the calculated value. The dotted reference lines indicate a +/- 5 kcal/mol (H_{298}) or 5 cal/mol/K(S_{298}) difference between the estimated and calculated values.

From the above figures, for most species, the estimated enthalpy of formation at 298 K is within a 5 kcal/mol difference, and a systemic bias is not observed. However, the group additivity approach overestimated the entropy of formation, where a 5 cal/mol/K bias can be observed in Figure S1. The differences are mainly due to species with higher multiplicity, more internal rotational modes, and higher tendencies to form intramolecular hydrogen bonds (Figure S2 - S5). It is also worth mentioning that these calculations were done under the 1D separable hindered rotor approximation, and the limitations due to the approximation also partially attribute to the difference.

2 Kinetic Models of BA isomers

2.1 Input Arguments in the Model Generation

The automated generation of the detailed kinetic mechanism was performed using RMG-Py[5–7] (RMG-Py version 3.0.0 at commit hash ID 4aedaf, RMG-database version 3.0.0 at commit hash ID d8ec1a). Besides the calculated thermochemical and kinetic data, the following libraries stored in the RMG database are also used:

- 'Klippenstein_Glarborg2016'[8] and 'C2H4+O_Klipp2017'[9] were used as the seed mechanism. All involved species and reactions in these libraries were introduced into the final models.
- 'primaryThermoLibrary', 'DFT_QCI_thermo'[10], 'thermo_DFT_CCSDTF12_BAC', 'CBS_QB3_1dHR', 'CHO'[11], and 'FFCM1(-)'[12] were used as the reference thermochemistry libraries. If the thermochemistry can be found in one of these libraries, the corresponding parameters will be used in the final model. If multiple targets are hit, the priority follows the above sequence, from high to low.
- 'BurkeH2O2inN2'[13] was used as the reaction library
- Two new libraries were created according to Section 2.2 in the main text, namely 'BA_oxidation' and 'alkene_chemistry'. They can be found at
    - https://github.com/ReactionMechanismGenerator/RMG-database/blob/butyl_acetate_xdong_gpio/input/kinetics/libraries/BA_oxidation/reactions.py
    - https://github.com/ReactionMechanismGenerator/RMG-database/blob/butyl_acetate_xdong_gpio/input/kinetics/libraries/alkene_chemistry/reactions.py, respectively.
    - The parameters from these two libraries are adapted into the model during the post-processing.

The main arguments adopted for the model generation jobs are reported below, and the notation reference can be found in the User's guide[14].

> toleranceMoveToCore=0.01, toleranceKeepInEdge=0.0, toleranceInterruptSimulation=0.02, maximumEdgeSpecies=100000, maxNumObjsPerIter=5, terminateAtMaxObjects=True, filterReactions=True, atol=1e-16, rtol=1e-8, maximumCarbonAtoms=15, maximumOxygenAtoms=8, maximumRadicalElectrons=2, maximumSingletCarbenes=1, maximumCarbeneRadicals=0, allowSingletO2=True, terminationTime=(50, 's')

2.2 Accessibility

Models can be found in the compressed file distributed as the other SI file. For each isomer, the mechanism file in the CHEMKIN[15] format (.inp, tested on Chemkin Pro 2020 R2), Cantera[16] format (.cti, tested on Cantera v2.4.0), and RMS[17] format (.rms, tested on version commit hash ID 2f76997) are prepared for the reader's convenience. Besides, a species dictionary file and a gas transport data file corresponding to each mechanism is distributed and formatted in an RMG-readable style.

2.3 Model Simulations

The simulation results can be found in Sections 4.2 - 4.4 of the manuscript and Sections 4 - 6 in the current SI.

2.4 Model Statistics

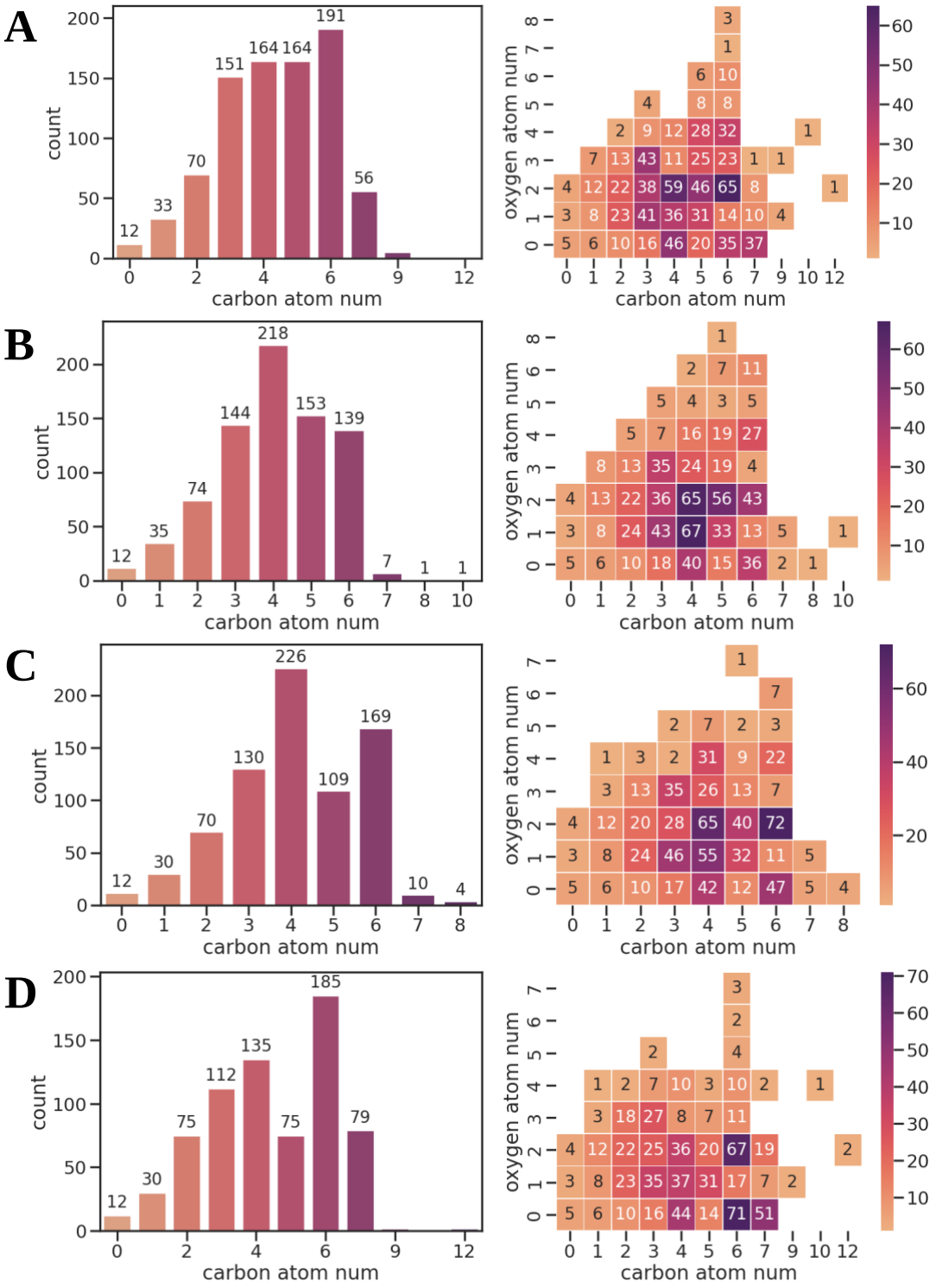

Figure S6. Species distribution with respect to the number of carbon atoms and the number of oxygen atoms. (A) iBA, (B) nBA, (C) sBA, and (D) tBA.

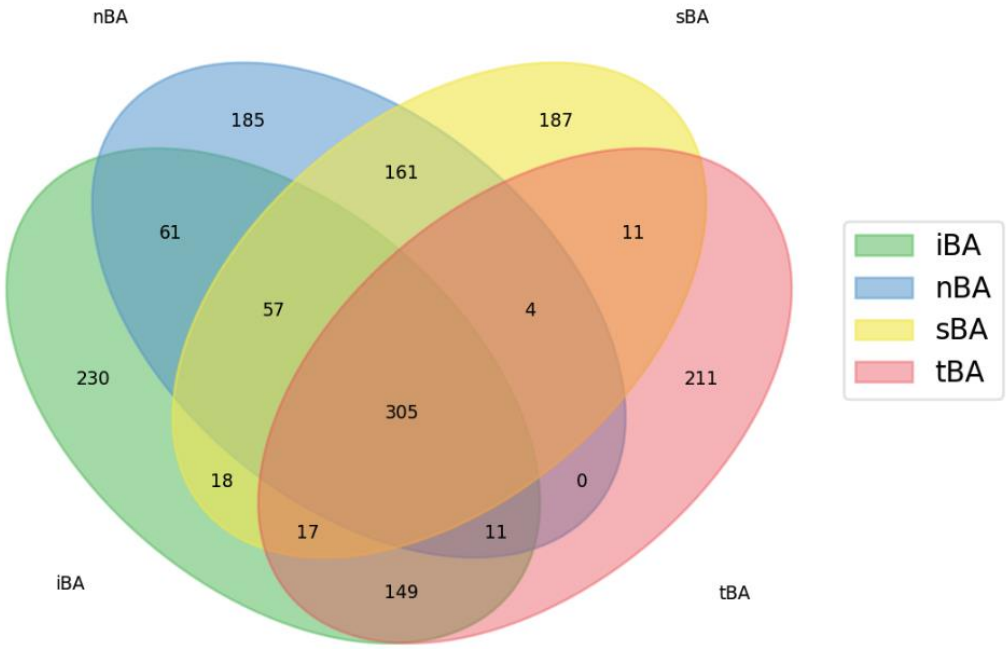

Figure S7. The Venn diagram indicating the intersection of the species among the BA isomer models.

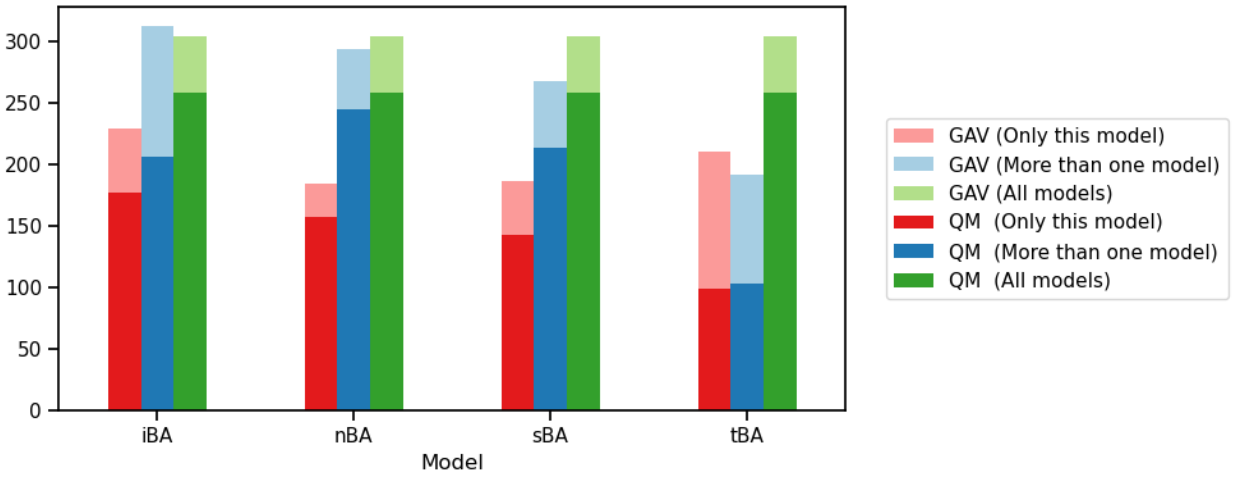

Figure S8. The distribution of species based on the source of data (values from the group additivity estimator, GAV, or values derived quantum-mechanically, QM) and the model coverage (only in one of the models, in more than one model, in all models).

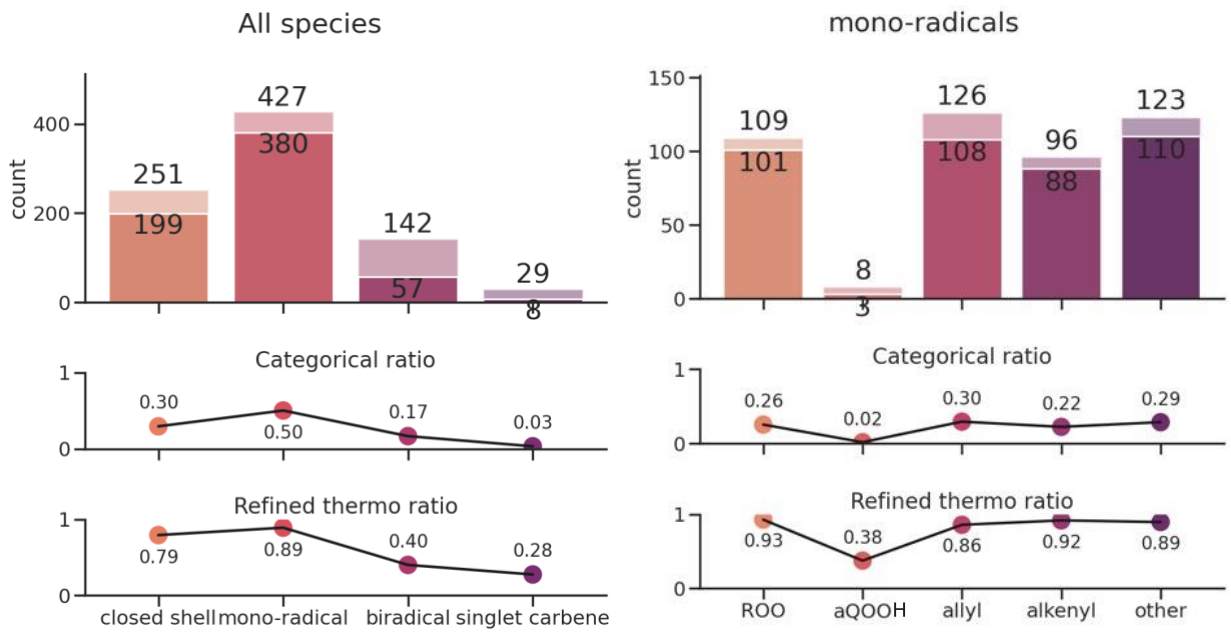

*Figure S9. The statistics of all species (left) and mono-radical species (right) in the **iBA** model. In the left figure, species are categorized into closed-shell species, mono-radicals, bi-radical species, and singlet carbenes. In the right figure Species are divided into five categories ROO (radical site at the terminal oxygen atom), aQOOH (radical site at the alpha position to the -OOH group), allyl (radical site at the alpha position to an unsaturated bond), alkenyl (radical site at an unsaturated bond), and other (species not belonging to any of those categories). The upper bar plot indicates the population number of species and species with refined thermochemistry parameters in each category. The middle subfigure indicates the population proportion of each category. Note, there are overlaps between the different definitions of radicals, therefore the sum may exceed unity. The bottom subfigure shows the proportion of species with refined thermochemistry in each category.*

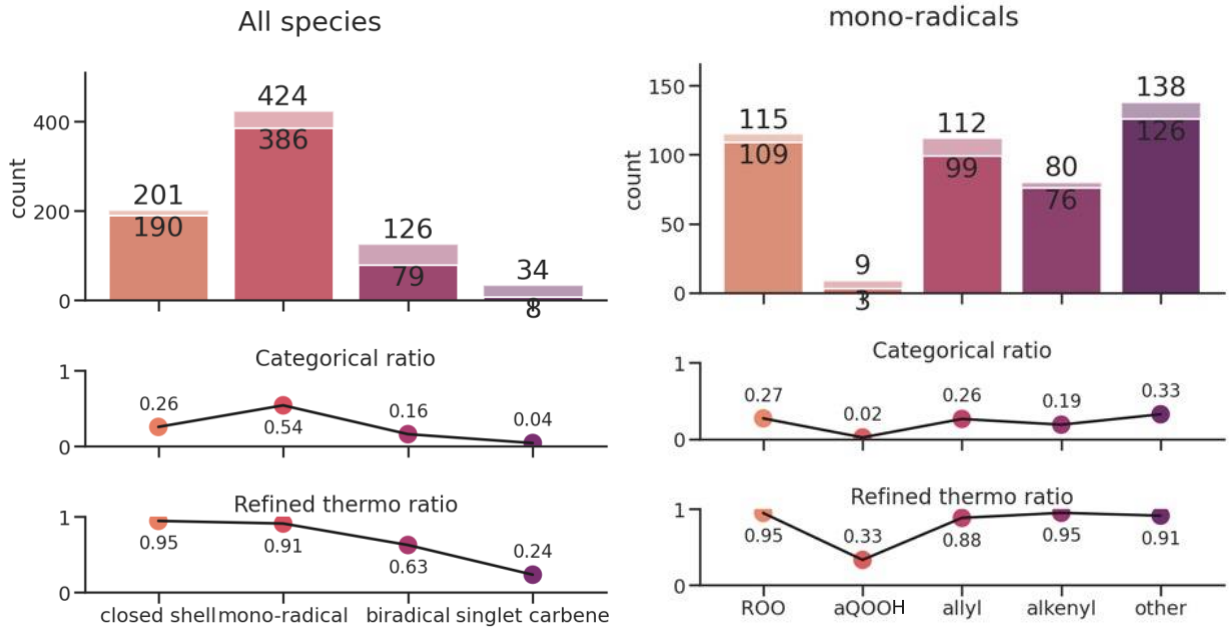

*Figure S10. The statistics of all species (left) and mono-radical species (right) in the **nBA** model. The figure interpretation can be found in Figure S9's caption.*

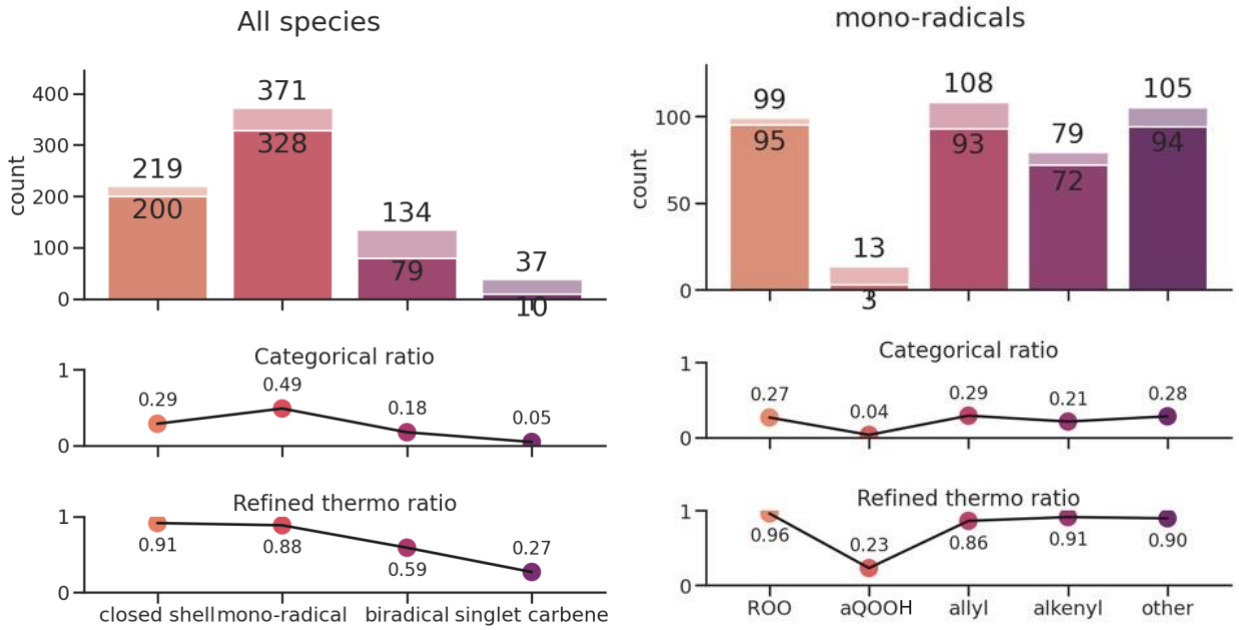

*Figure S11. The statistics of all species (left) and mono-radical species (right) in the **sBA** model. The figure interpretation can be found in Figure S9's caption.*

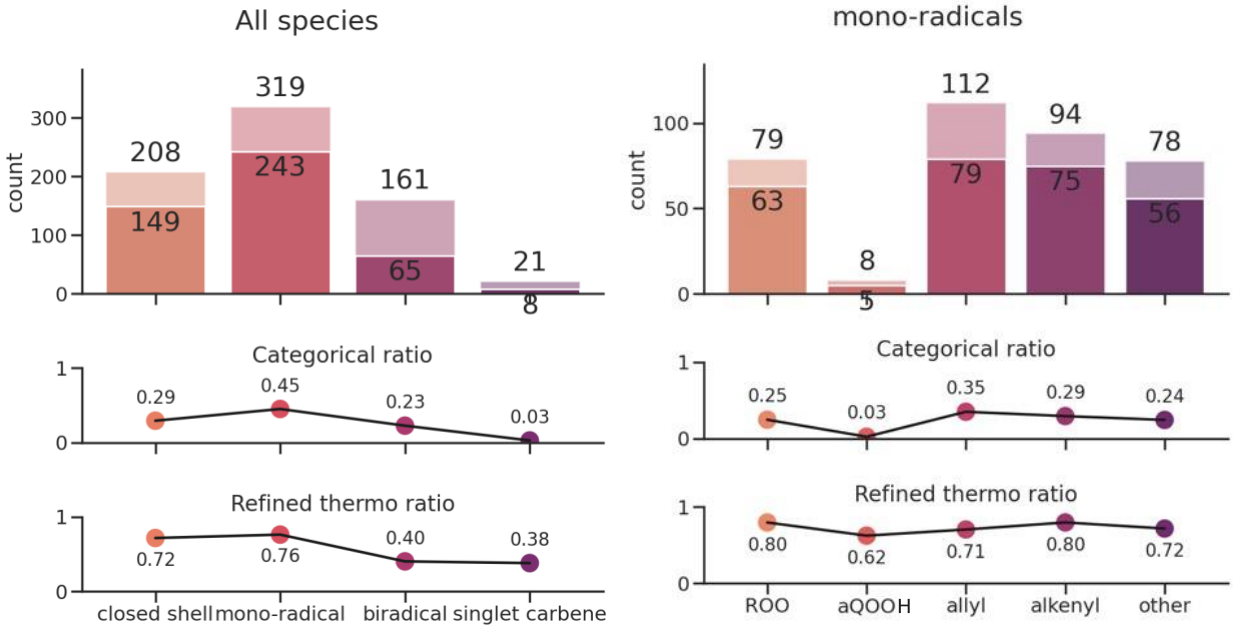

*Figure S12. The statistics of all species (left) and mono-radical species (right) in the **tBA** model. The figure interpretation can be found in Figure S9's caption.*

2.5 Discussion about Mechanism Changes across Iterations

In principle, a generated mechanism can suffer from truncation and parameter errors. The implemented iterative workflow with a parameter update step in each iteration directly helps reduce parameter errors and potentially mitigate the truncation error of the model generated in the following iteration.

The reaction pathways not included in a reaction mechanism generated by RMG can be categorized as follow:

1) Missing reactions due to (accurate) low rates under the investigated conditions
2) Missing reactions due to inaccurate estimations of thermodynamic and kinetic parameters
3) Missing reactions due to limitations in RMG reaction families

Clearly, (1) is essential to limit the size of the generated mechanisms and is ruled by the adopted termination criteria and tolerances used during the generation process. For non-essential low-flux reactions, omitting them results in no risk. However, there are reactions with low fluxes that have great significance to the overall reactivity (e.g., chain branching reactions). RMG used to have difficulty picking them up. But with advanced algorithms (e.g., branching algorithms), RMG is more capable of correctly selecting them as important reactions, though occasional missing is still inevitable.

The workflow with parameter updates in each iteration is designed to tackle (2). The update of parameters enables RMG to have a better judgment on the pathways' importance. E.g., correcting an underestimated radical generation reaction may lead RMG further to explore the chemical space relevant to this radical.

RMG needs the user's help to solve (3). RMG is unaware of any missing reaction templates and won't generate a reaction that is not defined in its library or defined by its reaction templates. However, users are allowed to add new reaction data or types to RMG. This scenario happened when we were developing models for this work. Previously, the retro-ene reaction type was not defined in RMG; therefore, RMG couldn't generate a single retro-ene reaction despite its importance. We, the authors, got to be aware of the importance of retro-ene during reading literature. Later, we collected the kinetics of over ten retro-ene reactions and added this reaction type to RMG in-house.

3 H abstraction results

3.1 Transition State Geometries

iBA + HO_2 = iBA-α + H_2O_2

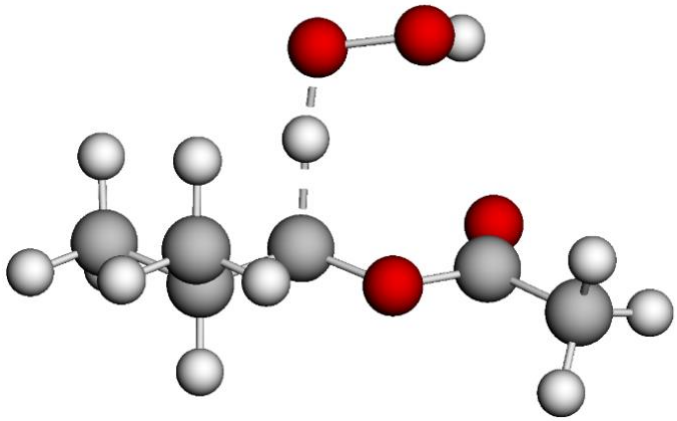

O	0.924988	2.187349	0.692270
O	-0.354270	2.141947	0.098484
H	1.505750	2.311464	-0.074812
C	2.823322	-1.296164	0.557774
C	1.807031	-0.605399	-0.307662
O	2.039104	0.122401	-1.237140
O	0.539861	-0.894942	0.116536
C	-0.532827	-0.304026	-0.565804
C	-1.865518	-0.839722	-0.101551
C	-2.065024	-0.662301	1.411161
C	-2.996193	-0.185421	-0.908224
H	3.803905	-1.227710	0.091599
H	2.847269	-0.799711	1.531731
H	2.546872	-2.338207	0.723784
H	-0.488384	1.032588	-0.224077
H	-0.357977	-0.251596	-1.641640
H	-1.864807	-1.919064	-0.322682
H	-3.020373	-1.091894	1.722882
H	-2.060226	0.398861	1.673562
H	-1.269088	-1.153001	1.973822
H	-3.961538	-0.611473	-0.625381
H	-3.038287	0.891397	-0.720750
H	-2.865322	-0.337495	-1.983417

nBA + HO_2 = nBA-α + H_2O_2

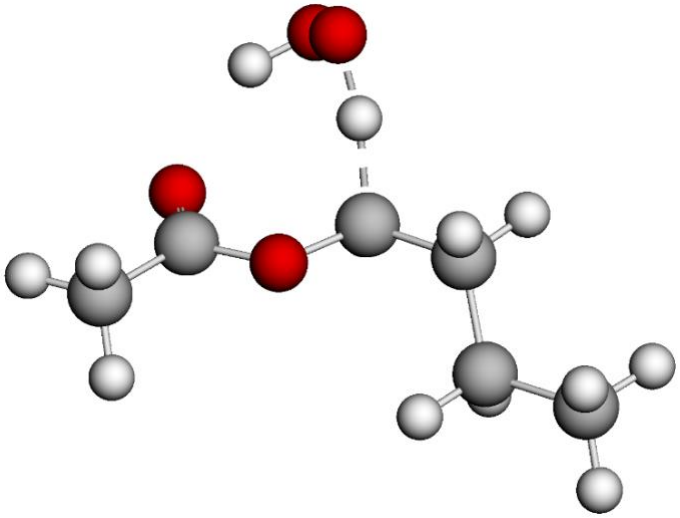

C	-4.145682	0.048346	0.006852
C	-2.704151	0.291038	-0.446528
C	-1.692988	-0.610184	0.293435
C	-0.271976	-0.399674	-0.132158
O	0.201485	0.867996	0.263204
C	1.460485	1.232228	-0.098149
O	2.215017	0.513390	-0.706007
C	1.764024	2.631449	0.360958
O	1.412273	-2.021932	0.812579
O	2.080388	-2.345982	-0.385777
H	-4.263020	0.247643	1.076254
H	-4.449616	-0.987245	-0.173102
H	-4.841955	0.697198	-0.530824
H	-2.431682	1.337647	-0.280152
H	-2.619578	0.113034	-1.524477
H	-1.773103	-0.439315	1.372651
H	-1.941068	-1.662383	0.118230
H	0.556826	-1.343619	0.473618
H	-0.006201	-0.636244	-1.165054
H	1.648307	2.696402	1.445077
H	1.057111	3.333742	-0.086543
H	2.780733	2.892853	0.076904
H	2.551677	-1.516707	-0.581032

iBA + OH = iBA-α + H_2O

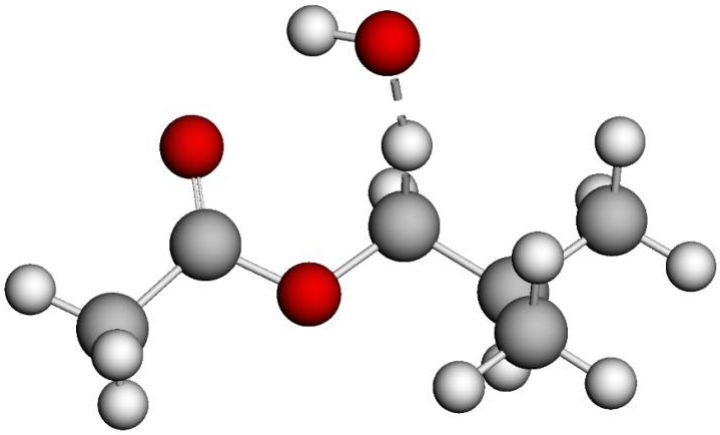

C	-2.984713	-1.097748	0.166276
C	-1.905466	-0.113692	-0.197391
O	-2.078596	1.046501	-0.479632
O	-0.683403	-0.697781	-0.159067
C	0.440612	0.106890	-0.509646
C	1.728553	-0.672677	-0.315951
C	2.912853	0.178296	-0.794882
C	1.903230	-1.128804	1.138613
O	0.242843	2.220732	0.919963
H	-2.875030	-1.385511	1.214941
H	-3.959083	-0.639356	0.012649
H	-2.890173	-2.004018	-0.434542
H	0.470128	1.048161	0.207379
H	0.310722	0.516917	-1.514482
H	1.658017	-1.564936	-0.954517
H	2.987680	1.101503	-0.213360
H	3.850128	-0.371249	-0.680036
H	2.812191	0.451542	-1.849244
H	1.064740	-1.748808	1.460969
H	1.963316	-0.264885	1.806972
H	2.821025	-1.711775	1.250200
H	-0.630819	2.383218	0.520840

nBA + OH = nBA-α + H_2O

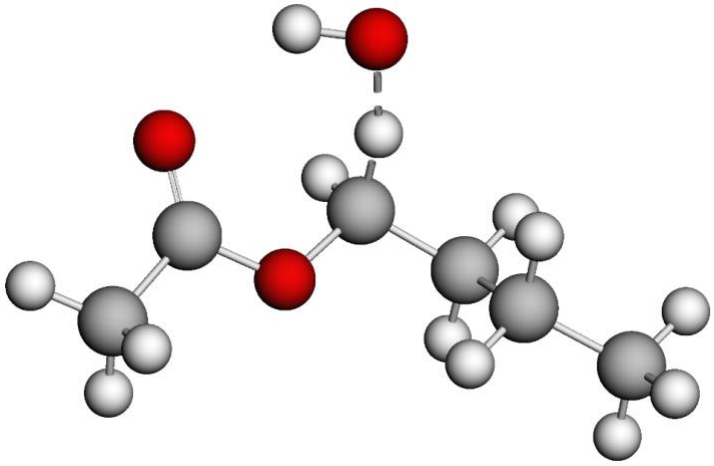

C	-3.695943	-0.652820	-0.371565
C	-2.212406	-0.292333	-0.478288
C	-1.582876	0.029225	0.883378
C	-0.128191	0.431940	0.811399
O	0.643179	-0.640107	0.268573
C	1.959253	-0.414562	0.041935
O	2.496335	0.646943	0.243811
C	2.632900	-1.648769	-0.495189
O	0.361782	2.425742	-0.711254
H	-4.275435	0.170946	0.056744
H	-3.847736	-1.530621	0.264572
H	-4.118647	-0.878667	-1.353849
H	-2.083344	0.570954	-1.139464
H	-1.662525	-1.118797	-0.938019
H	-2.124765	0.853643	1.360209
H	-1.675090	-0.836672	1.553008
H	-0.033817	1.369294	0.093296
H	0.300605	0.759619	1.761448
H	2.233671	-1.878496	-1.486288
H	2.424956	-2.504981	0.149030
H	3.704600	-1.475612	-0.562893
H	1.310735	2.322667	-0.516848

sBA + OH = sBA-α + H_2O

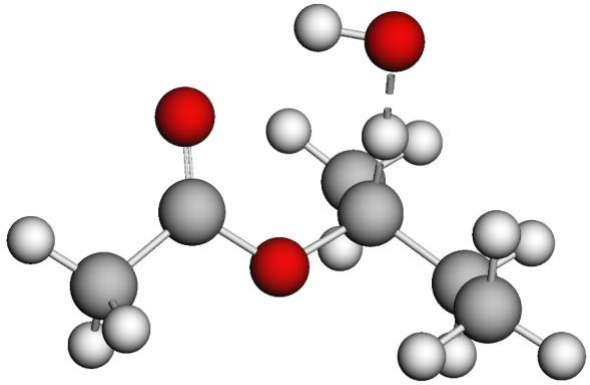

C	-2.080620	-1.426582	-0.919332
C	-1.969000	-0.676637	0.410732
C	-0.733924	0.203228	0.515343
O	0.420452	-0.652417	0.368174
C	1.599914	-0.143084	-0.049349
O	1.771993	1.010694	-0.362809
C	2.660970	-1.212485	-0.078148
O	-0.728423	1.798926	-1.513867
H	-2.048494	-0.726136	-1.757129
H	-1.258812	-2.135621	-1.038128
H	-2.839559	-0.028229	0.550131
H	-1.962722	-1.383729	1.250489
H	-0.780314	0.931377	-0.407206
H	3.616123	-0.767425	-0.347871
H	2.389462	-1.978295	-0.808651
H	2.730480	-1.699523	0.896418
H	0.232250	1.938844	-1.427307
H	-3.018267	-1.984943	-0.971268
C	-0.632670	1.052215	1.768243
H	-1.509835	1.697389	1.848708
H	-0.585307	0.413819	2.656793
H	0.254793	1.684916	1.738101

iBA + OH = iBA-β + H_2O

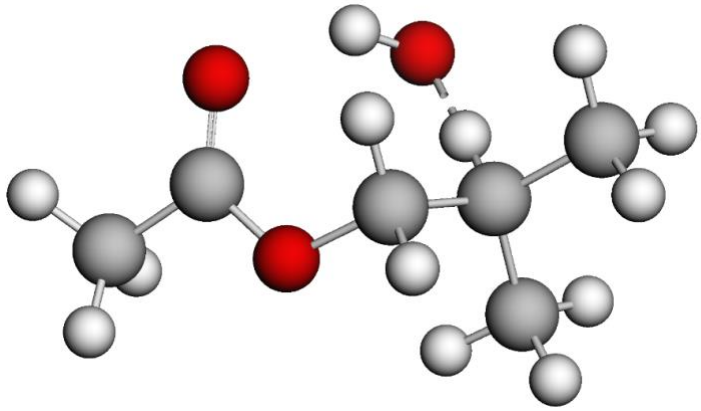

C	3.011543	-0.500230	0.515450
C	1.788616	-0.045009	-0.235568
O	0.836202	-0.997971	-0.244260
C	-0.412575	-0.698065	-0.917066
O	1.662263	1.042580	-0.750844
C	-1.477555	-0.165750	0.034802
O	-0.514030	2.128166	0.858379
H	3.878180	0.057300	0.164439
H	2.865680	-0.281076	1.577261
H	3.166897	-1.573087	0.407327
C	-1.716416	-1.066623	1.241912
C	-2.754213	0.176921	-0.728485
H	-1.085990	0.844511	0.459645
H	0.211495	2.114590	0.205419
H	-0.217409	0.011179	-1.721997
H	-0.729079	-1.654071	-1.343552
H	-2.419009	-0.602030	1.937333
H	-0.787423	-1.267996	1.777138
H	-2.140554	-2.028126	0.926072
H	-3.491161	0.626251	-0.059672
H	-3.203369	-0.723565	-1.165146
H	-2.560147	0.886463	-1.536734

nBA + OH = nBA-β + H_2O

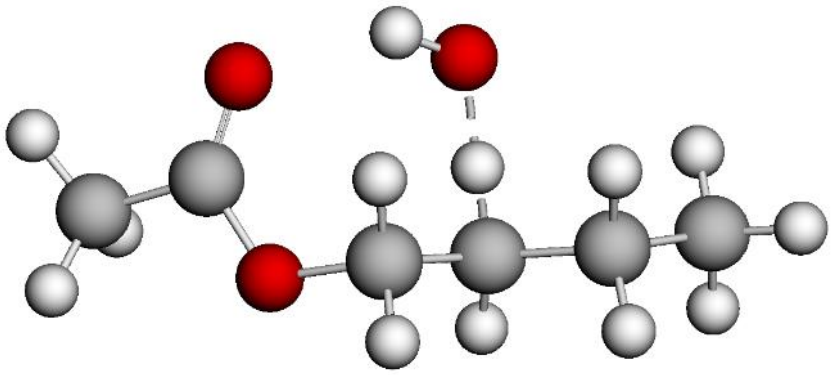

C	3.334471	-0.062400	0.692841
C	2.063869	-0.017245	-0.113657
O	1.249921	-1.043277	0.203790
C	-0.022728	-1.131524	-0.484430
O	1.792593	0.833457	-0.929985
C	-1.133144	-0.454951	0.290852
O	-0.643971	2.046028	0.138029
H	4.086438	0.564734	0.218151
H	3.127743	0.328019	1.693361
H	3.692578	-1.086324	0.800579
H	-1.113362	-0.750538	1.345018
C	-2.511676	-0.610048	-0.335439
H	-0.914988	0.720800	0.330607
H	0.122871	1.913027	-0.450087
H	0.082129	-0.706157	-1.483794
H	-0.212290	-2.204808	-0.569426
C	-3.597150	0.171446	0.410166
H	-2.773358	-1.677451	-0.362636
H	-2.472276	-0.276007	-1.378269
H	-3.681607	-0.162143	1.448784
H	-4.572477	0.037673	-0.064192
H	-3.361593	1.237835	0.415237

sBA + OH = sBA-β1+ H2O

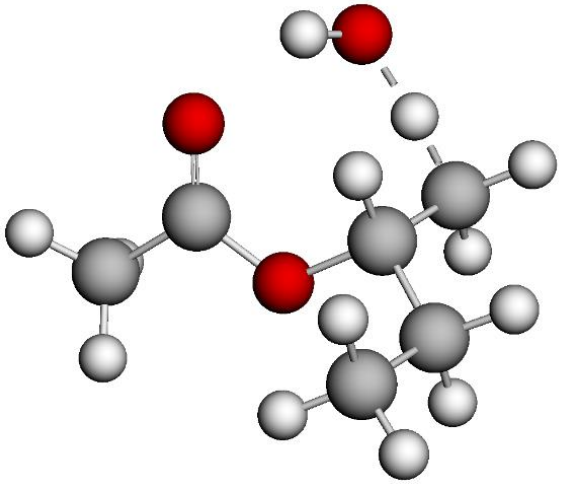

C	-1.573763	-2.210033	-0.647584
C	-0.992237	-1.044395	0.108249
O	0.089008	-0.544695	-0.519956
C	0.758929	0.615755	0.063198
C	2.256999	0.429720	-0.195296
C	2.848210	-0.805628	0.488467
O	-1.448715	-0.595247	1.135053
C	0.208764	1.875656	-0.563320
H	-2.156103	-2.827671	0.033836
H	-0.795979	-2.795093	-1.137498
H	-2.242104	-1.818609	-1.420133
H	0.558198	0.606127	1.136991
H	-0.972773	2.033556	-0.264783
H	0.693119	2.777300	-0.185848
H	0.205205	1.844389	-1.654220
H	2.420832	0.379651	-1.276835
H	2.766380	1.331571	0.159619
H	2.373116	-1.719476	0.126306
H	3.919677	-0.882378	0.288305
H	2.713421	-0.760528	1.573251
O	-2.189959	2.059765	0.173664
H	-2.127078	1.306125	0.788635

sBA + OH = sBA-β2+ H2O

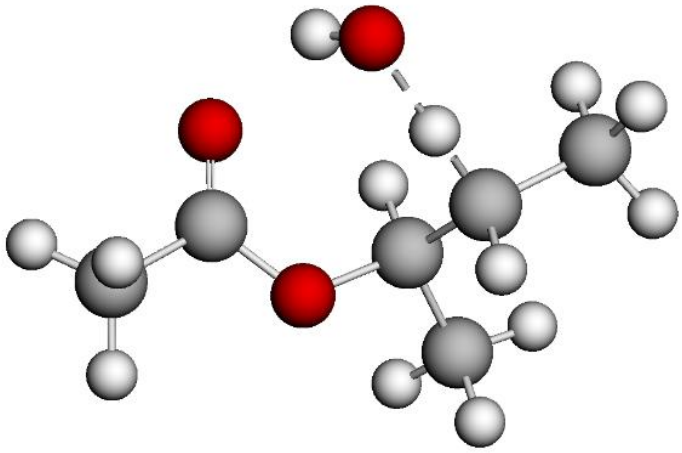

C	2.947550	-0.288534	-0.581810
C	1.665998	-0.128938	0.192137
O	0.667063	-0.840020	-0.363449
C	-0.663672	-0.748409	0.232910
C	-1.464440	0.304224	-0.519189
C	-2.852185	0.589016	0.030485
O	1.538093	0.571310	1.171425
C	-1.256040	-2.150569	0.150016
O	-0.165429	2.496751	-0.224350
H	3.013902	-1.271334	-1.046895
H	3.794246	-0.109815	0.078932
H	2.959717	0.467510	-1.372481
H	-0.538066	-0.446241	1.274590
H	-0.608501	-2.862121	0.666428
H	-2.240459	-2.179626	0.621295
H	-1.357649	-2.467262	-0.891028
H	-0.867712	1.332348	-0.461641
H	-1.470102	0.087642	-1.592370
H	-2.815847	0.818236	1.099092
H	-3.293475	1.448170	-0.478263
H	-3.527038	-0.262008	-0.111566
H	0.369897	2.159426	0.517605

tBA + OH = tBA-β + H_2O

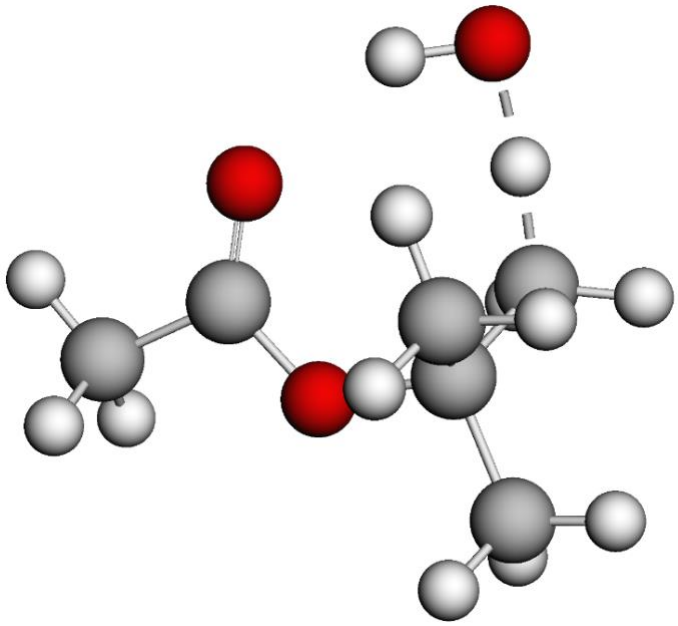

C	-2.910876	-0.458451	-0.163668
C	-1.514687	0.089092	0.014898
O	-0.606509	-0.883314	-0.158238
C	0.850961	-0.685149	0.016706
C	1.392796	-2.092402	-0.269113
O	-1.271845	1.243849	0.281322
C	1.396026	0.288878	-1.017847
C	1.161895	-0.263914	1.454560
O	1.159490	2.637910	-0.161828
H	-3.628286	0.357970	-0.117699
H	-2.991220	-0.982429	-1.117803
H	-3.123364	-1.182995	0.626157
H	0.712028	-0.966636	2.159971
H	2.244525	-0.272605	1.604499
H	0.805493	0.742895	1.656962
H	1.150814	-2.398913	-1.288812
H	2.477343	-2.110500	-0.144900
H	0.947963	-2.811246	0.422480
H	0.883026	0.230741	-1.978117
H	2.474776	0.178222	-1.143597
H	1.317296	1.461164	-0.657015
H	0.223824	2.498445	0.074614

iBA + OH = iBA-γ + H_2O

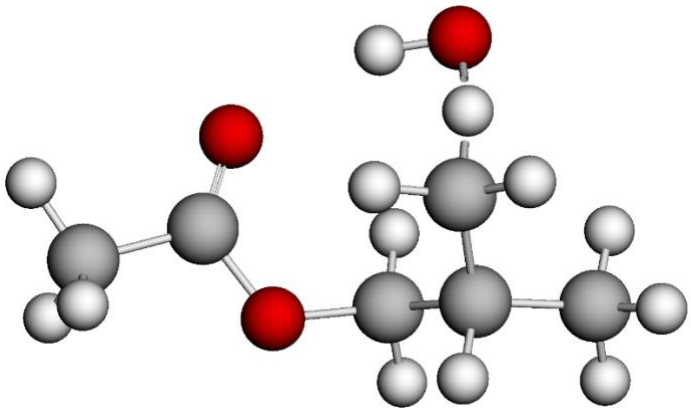

O	1.180465	2.297177	-0.282583
H	0.225191	2.158599	-0.429427
C	-3.165875	-0.405938	0.409092
C	-1.816625	0.005966	-0.121955
O	-1.532957	1.126650	-0.478298
O	-0.976086	-1.045252	-0.157495
C	0.345980	-0.870501	-0.733173
C	1.435943	-0.846898	0.340981
C	1.291479	0.332268	1.289461
C	2.812065	-0.849659	-0.341644
H	-3.052626	-0.978426	1.331145
H	-3.774888	0.478877	0.580502
H	-3.658171	-1.054073	-0.320446
H	0.479073	-1.730612	-1.390768
H	0.367493	0.048461	-1.317812
H	1.332317	-1.768835	0.931835
H	1.338450	1.358487	0.628390
H	2.126597	0.435582	1.985126
H	0.341130	0.371215	1.822340
H	2.955098	0.072895	-0.910160
H	2.921199	-1.698560	-1.022429
H	3.609963	-0.913647	0.402136

nBA + OH = nBA-γ + H_2O

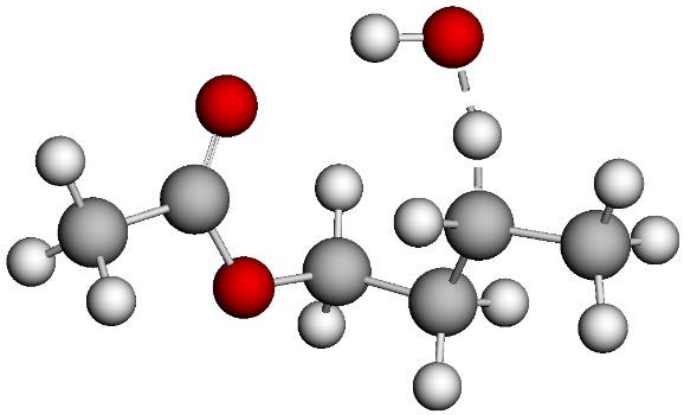

O	1.320512	2.126006	-0.551547
H	0.365868	2.112200	-0.345302
C	-3.048585	-0.265536	0.944772
C	-1.832694	0.136588	0.149152
O	-1.448384	1.275975	0.015421
O	-1.244089	-0.941227	-0.399975
C	-0.104444	-0.750905	-1.284896
C	1.203884	-1.121818	-0.598221
C	1.629510	-0.179585	0.520516
H	-2.804641	-1.085512	1.622234
H	-3.419270	0.592498	1.501134
H	-3.824133	-0.623696	0.263003
H	-0.299030	-1.414190	-2.128234
H	-0.079010	0.283037	-1.625329
H	1.615917	0.919807	0.066052
C	3.028174	-0.417384	1.064624
H	0.888028	-0.144349	1.323604
H	1.979085	-1.136108	-1.373590
H	1.129024	-2.146530	-0.210617
H	3.778352	-0.357761	0.271142
H	3.104303	-1.412548	1.520239
H	3.286129	0.318953	1.828796

sBA + OH = sBA-γ + H_2O

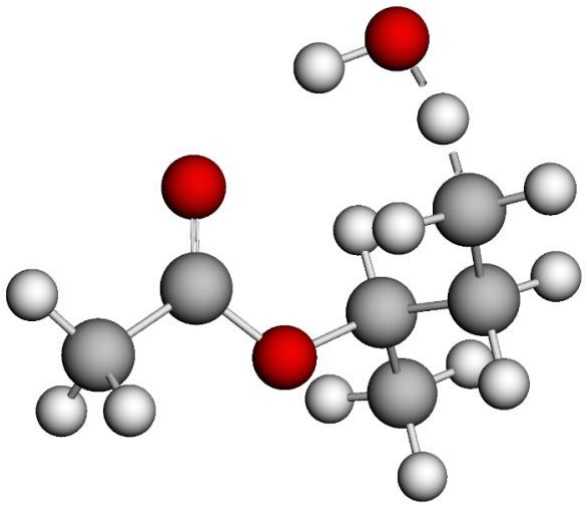

O	-1.707070	-2.073531	-0.908108
H	-0.737622	-2.014311	-1.008079
C	2.895583	-0.283230	0.546244
C	1.517106	-0.332320	-0.063897
O	1.117304	-1.226629	-0.774705
O	0.803510	0.754056	0.280341
C	-0.527788	0.960781	-0.298827
C	-1.585168	0.678788	0.769253
C	-1.636999	-0.762384	1.238727
H	2.832832	-0.043174	1.608830
H	3.392714	-1.239475	0.398634
H	3.475289	0.508696	0.065084
H	-0.650744	0.251842	-1.116903
H	-1.789276	-1.477380	0.259804
H	-0.720993	-1.113304	1.714866
H	-2.556230	0.960603	0.349550
H	-1.406010	1.343223	1.625686
H	-2.504164	-0.990145	1.860549
C	-0.554901	2.392604	-0.810188
H	-1.522718	2.608402	-1.269487
H	-0.391515	3.101571	0.005597
H	0.221488	2.546843	-1.562227

nBA + OH = nBA-δ + H_2O

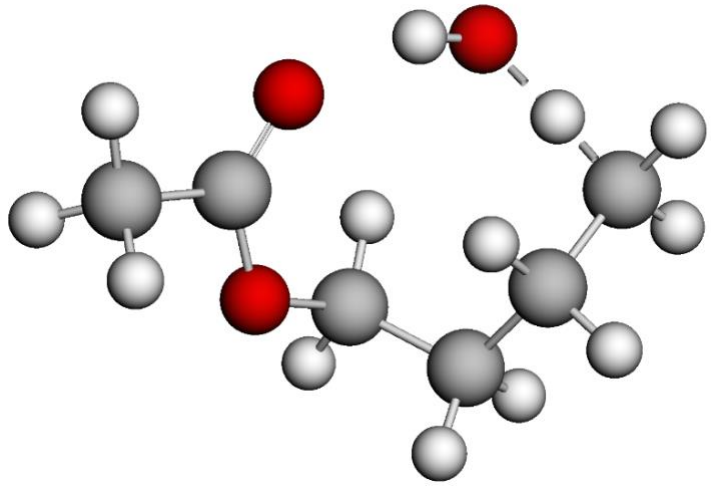

O	-1.581819	2.060696	0.741099
H	-0.686598	2.021258	0.351487
C	3.113585	0.113241	-0.610375
C	1.706664	0.284634	-0.094913
O	1.058892	1.301318	-0.210595
O	1.281174	-0.834294	0.510555
C	-0.033231	-0.858897	1.143388
C	-1.032719	-1.616958	0.275162
C	-1.529712	-0.873220	-0.976237
C	-2.554164	0.216713	-0.715623
H	3.393243	0.983043	-1.200564
H	3.798358	0.005325	0.234398
H	3.188358	-0.795729	-1.209826
H	0.134355	-1.390731	2.080494
H	-0.359402	0.157408	1.355556
H	-0.570937	-2.564991	-0.018929
H	-1.890905	-1.872949	0.908331
H	-1.994036	-1.610149	-1.645997
H	-0.681647	-0.463777	-1.533525
H	-2.128817	1.103515	-0.001502
H	-2.863010	0.744047	-1.619463
H	-3.427475	-0.131101	-0.157331

3.2 Rate coefficient comparisons

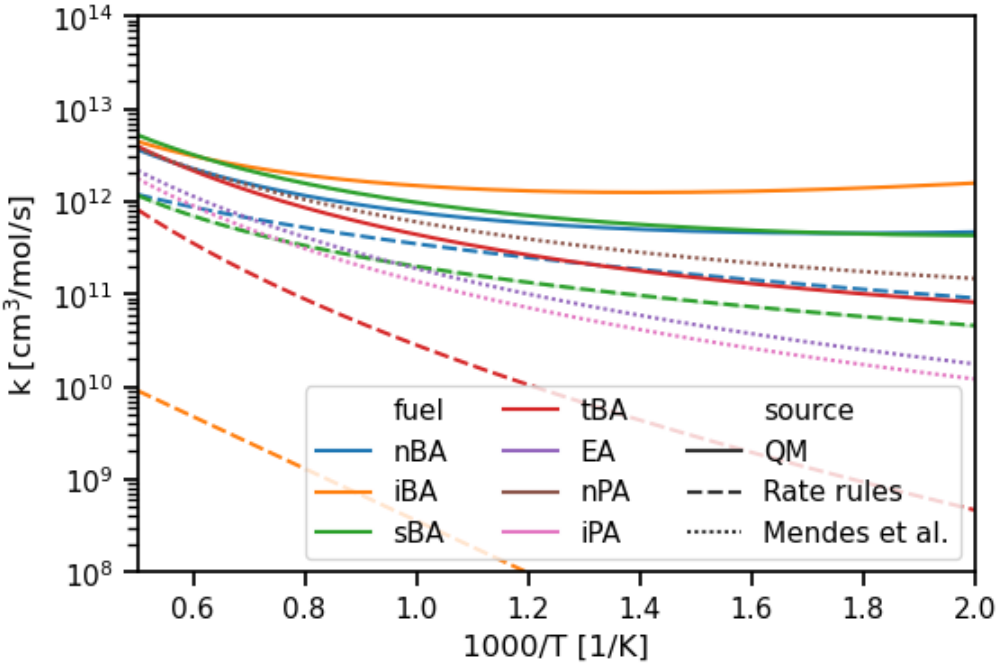

Figure S13. A comparison of kinetic coefficients for the hydrogen abstraction by OH from β carbon atom with respect to the temperature. Butyl acetate isomers (nBA, iBA, sBA, and tBA), ethyl acetate (EA), n-propyl acetate (nPA), and iso-propyl acetate (iPA) are considered. Solid lines refer to coefficients derived by quantum chemistry calculations, dashed lines by the RMG rate rules, and dotted lines from the Mendes et al.[18]

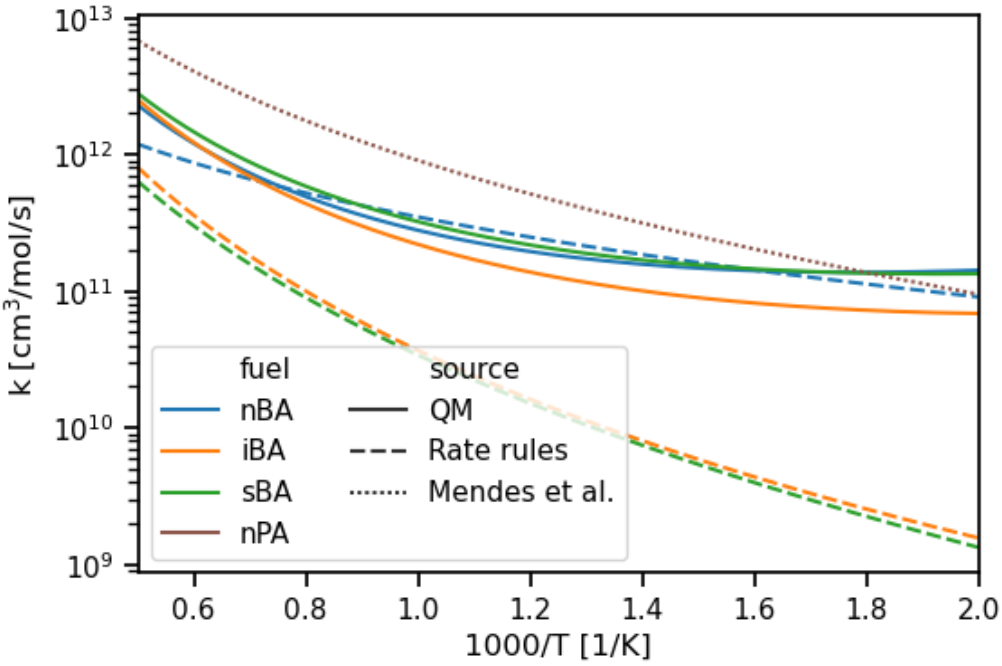

Figure S14. A comparison of kinetic coefficients for the hydrogen abstraction by OH from γ carbon atom with respect to the temperature. Butyl acetate isomers (nBA, iBA, and sBA) and n-propyl acetate (nPA) are considered. Solid lines refer to coefficients derived by quantum chemistry calculations, dashed lines by the RMG rate rules, and dotted lines from the Zhou et al.[18]

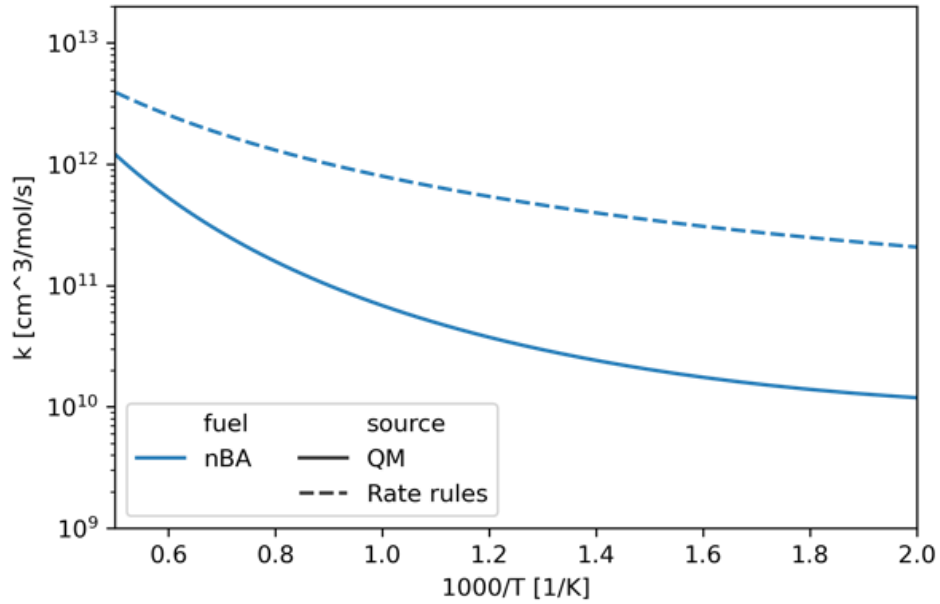

Figure S15. A comparison of kinetic coefficients for the hydrogen abstraction by OH from δ carbon atom with respect to the temperature. Butyl acetate isomers (nBA, iBA, and sBA) and n-propyl acetate (nPA) are considered. Solid lines refer to coefficients derived by quantum chemistry calculations and dashed lines by the RMG rate rules.

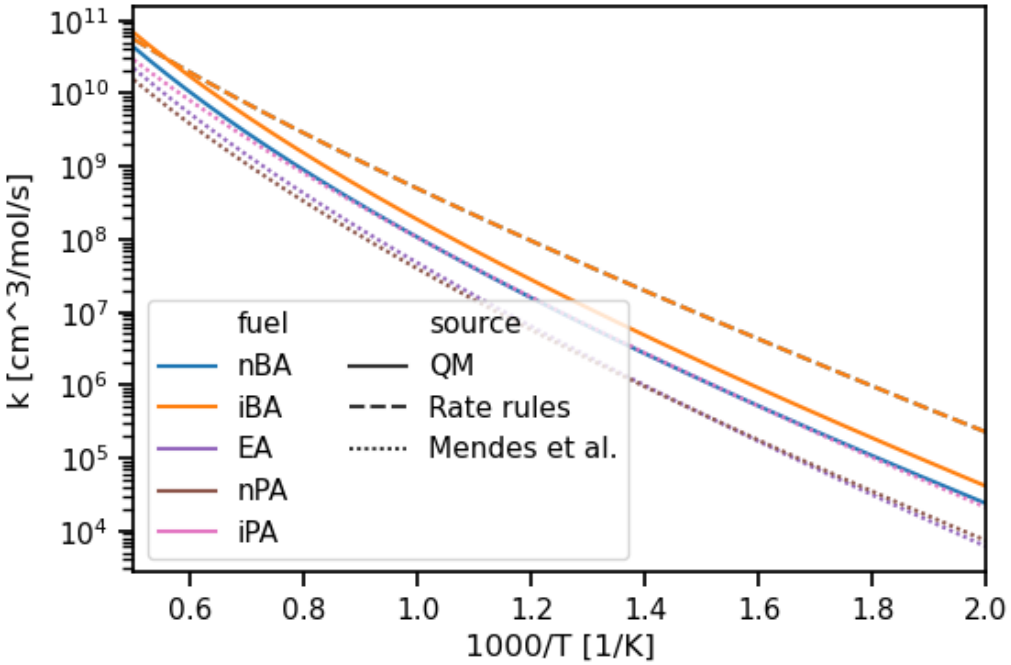

Figure S16. A comparison of kinetic coefficients for the hydrogen abstraction by HO_2 from α carbon atom with respect to the temperature. Butyl acetate isomers (nBA and iBA), ethyl acetate (EA), n-propyl acetate (nPA), and iso-propyl acetate (iPA) are considered. Solid lines refer to coefficients derived by quantum chemistry calculations and dashed lines by the RMG rate rules, and dotted lines from the Zhou et al.[18]

4 Ignition Delay Time (IDT)

4.1 EA IDT

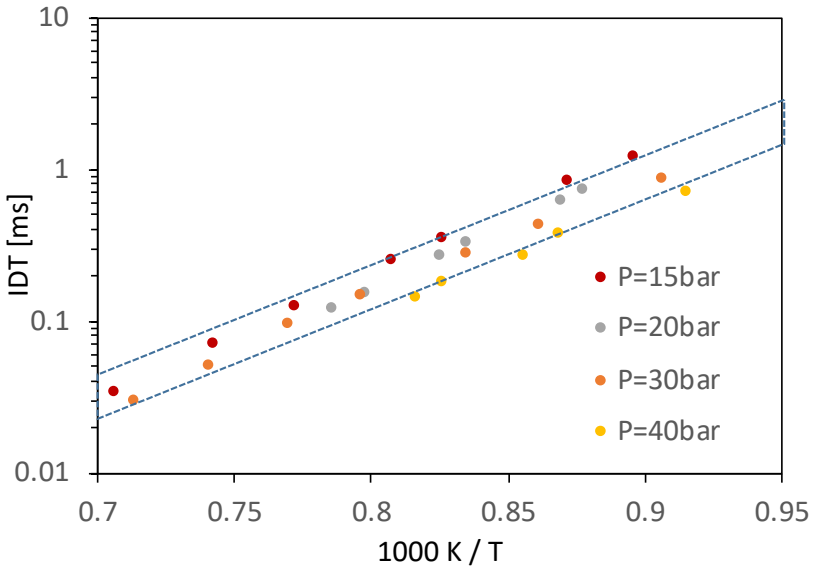

Figure S17. Ethyl acetate IDTs measured in high-pressure shock tubes by Ahmed et al.[19] (15 bar and 30 bar) and Morsch et al.[20] (20 and 40 bar). Data within the shaded area has a difference smaller than a factor of 2 at the same temperature.

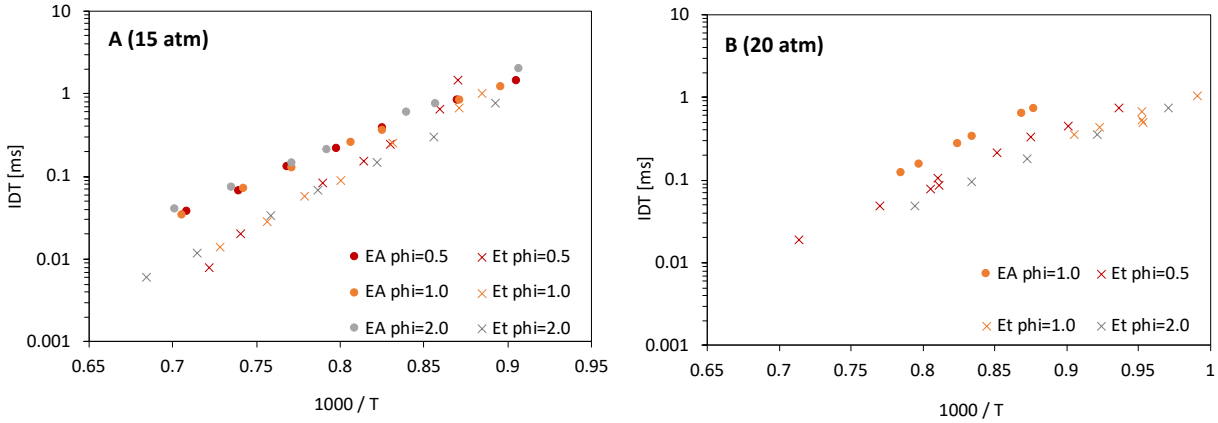

Figure S18. Comparison of experiment IDTs between ethyl acetate and ethylene indicates an IDT difference larger than a factor of 2. (A) measurements at about 15 atm. EA - Ahmed et al.[19] and ethylene - Penyazkov et al.[21]. (B) measurements at about 20 atm. EA - Morsch et al.[20] and ethylene: Wan et al.[22] and Kopp et al.[23]

4.2 BA Ignition delay time

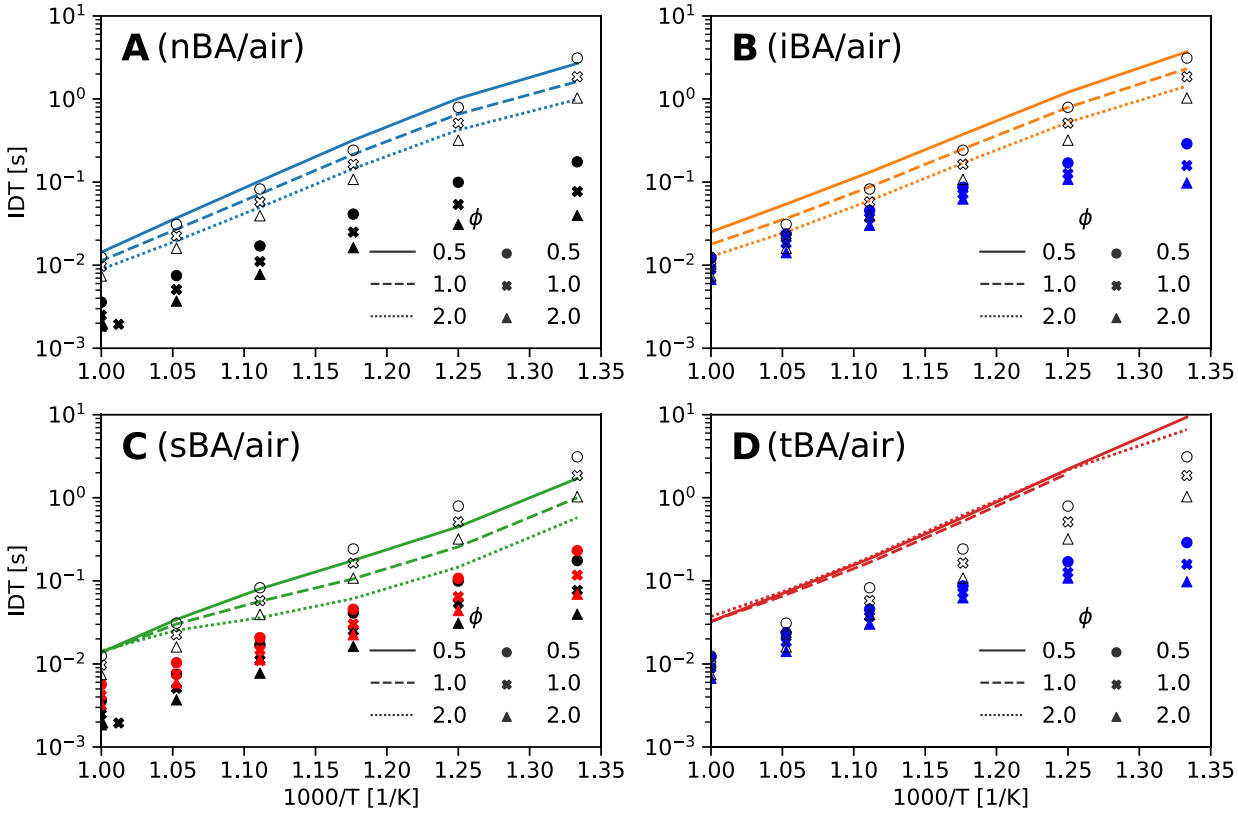

*Figure S19. The estimated ignition delay time of butyl acetate isomers in air at 10 atm and intermediate temperatures as a function of temperature and equivalence ratio. (**A**) nBA, (**B**) iBA, (**C**) sBA, and (**D**) tBA. Simulated IDTs of relevant butenes at the same conditions are plotted as solid markers: black - 1-butene[24], red - 2-butene[25], and blue - iso-butene[26]. Simulated IDTs of ethyl acetate using the model by Morsch et al.[20] are plotted as hollow markers.*

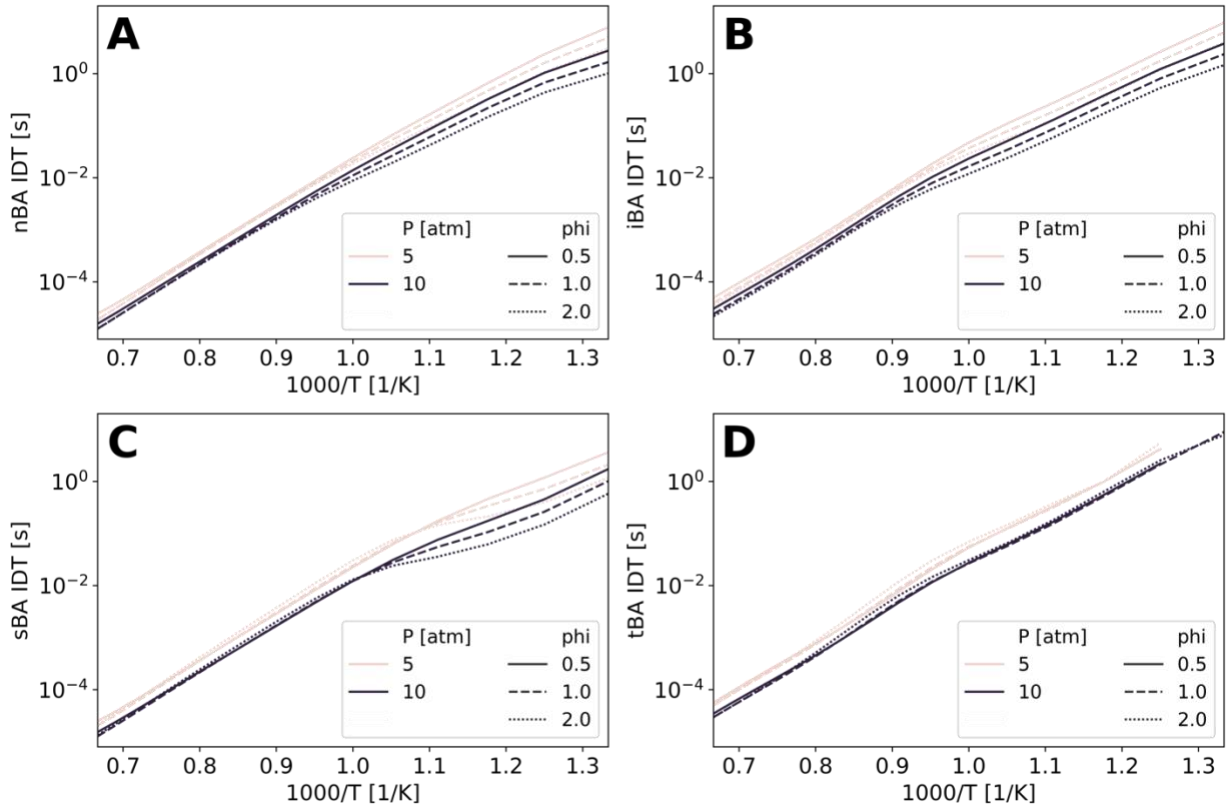

*Figure S20. Estimated ignition delay time of butyl acetate isomers in air at 5 and 10 atm as a function of initial temperature and equivalence ratio. (**A**) nBA, (**B**) iBA, (**C**) sBA, and (**D**) tBA.*

5 Flux Diagrams of BA oxidation

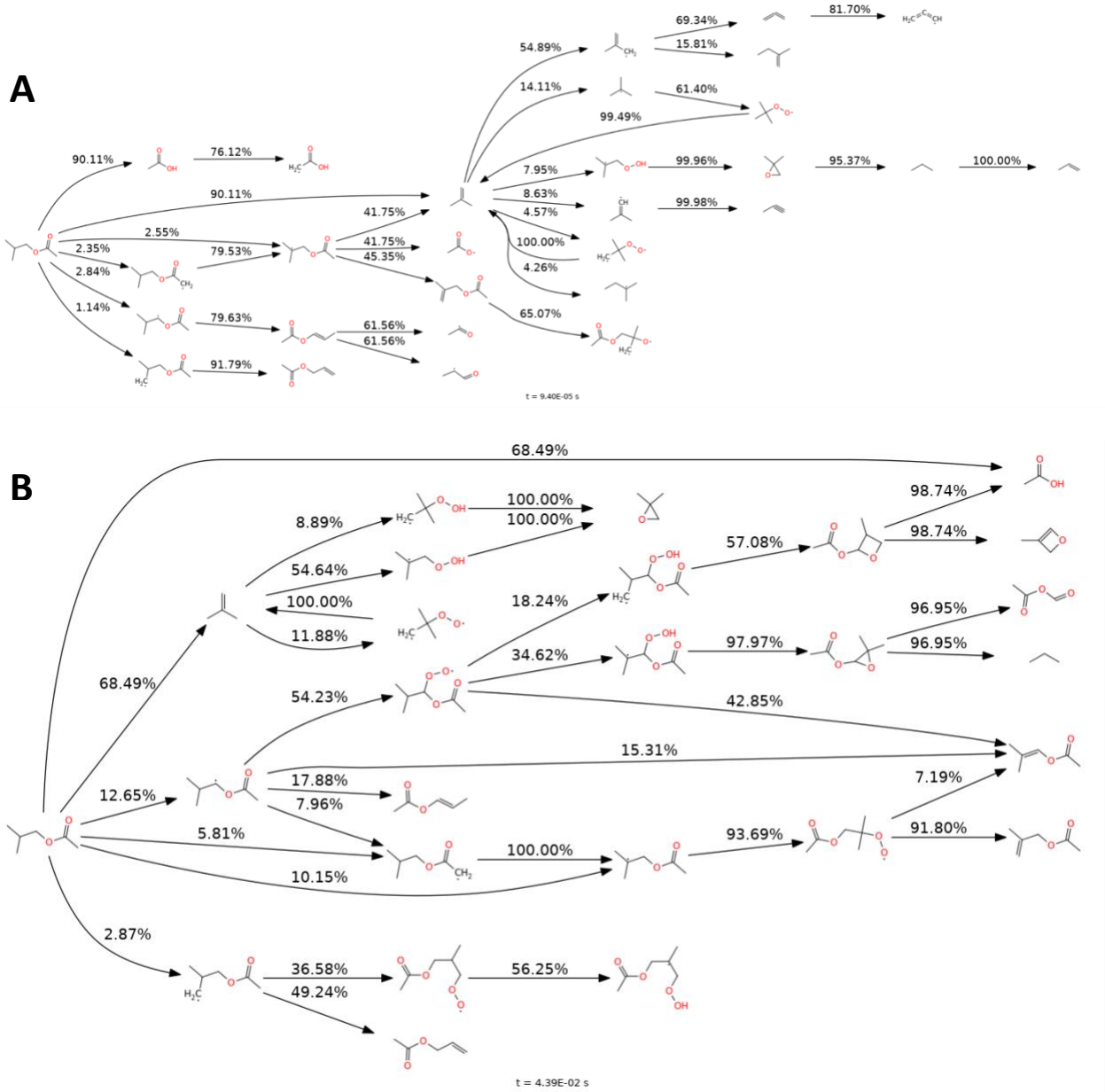

*Figure S21. Flux diagram of **iBA** oxidation by air at (**A**) 1300 K and (**B**) 900 K, 10 atm, 0.5 IDT, and stoichiometric condition. Percentage values indicate the branching ratio of the accumulated flux out of a species. Fluxes smaller than 0.5% of the fuel consumption are neglected.*

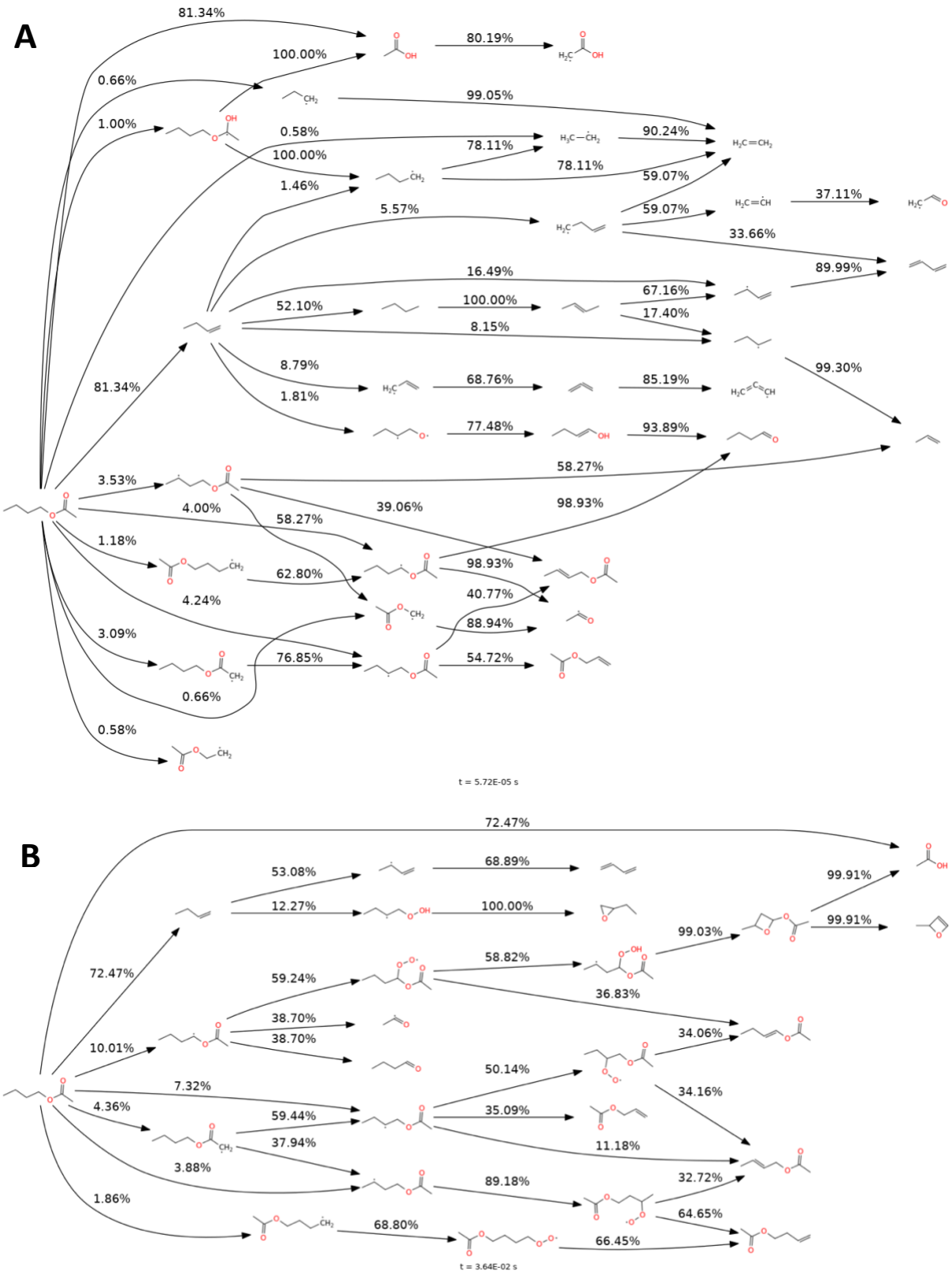

*Figure S22. Flux diagram of **nBA** oxidation by air at (**A**) 1300 K and (**B**) 900 K, 10 atm, 0.5 IDT, and stoichiometric condition. Percentage values indicate the branching ratio of the accumulated flux out of a species. Fluxes smaller than 0.5% of the fuel consumption are neglected.*

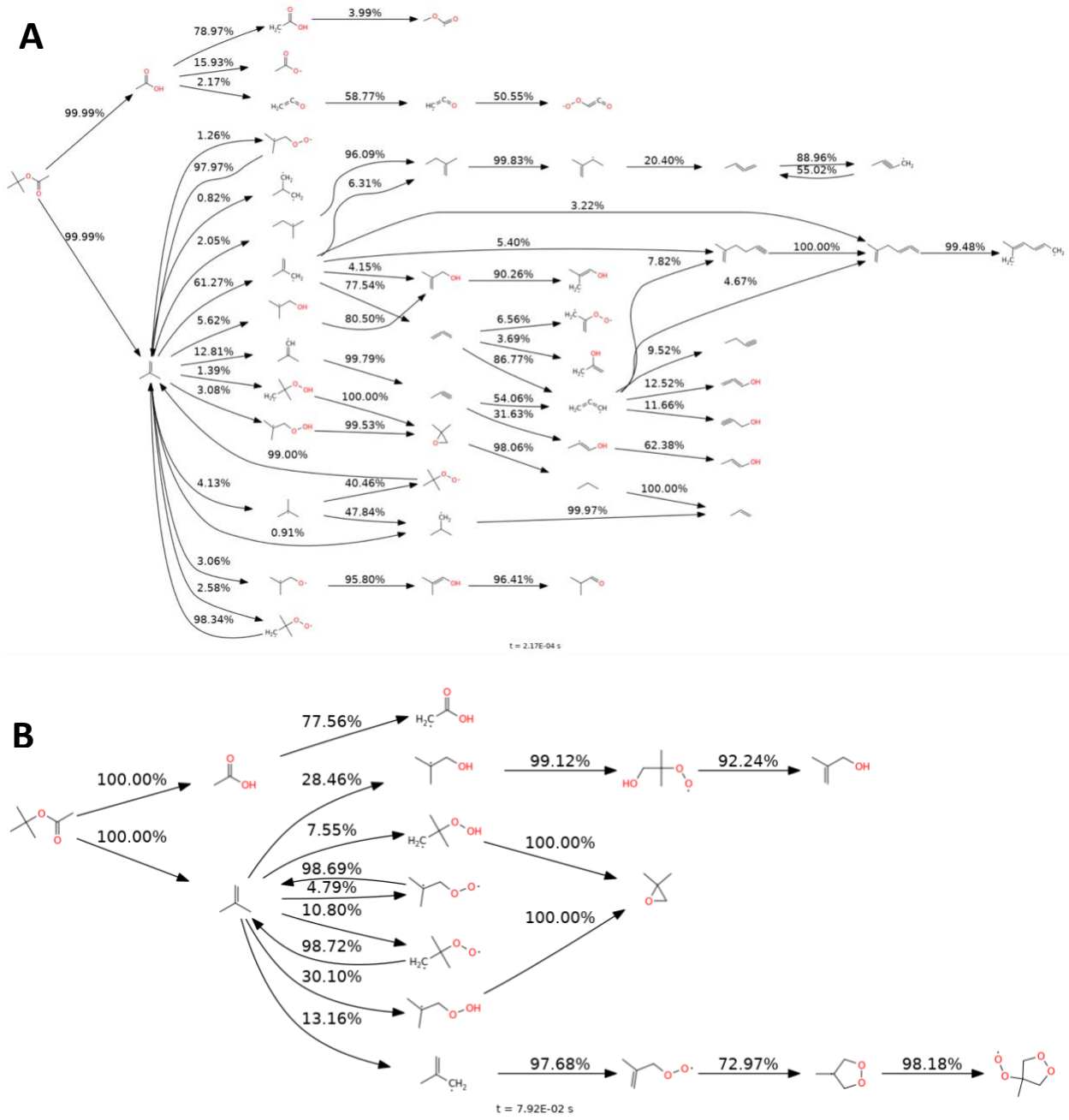

*Figure S23. Flux diagram of **tBA** oxidation by air at (**A**) 1300 K and (**B**) 900 K, 10 bar, 0.5 atm, and stoichiometric condition. Percentage values indicate the branching ratio of the accumulated flux out of a species. Fluxes smaller than 0.5% of the fuel consumption are neglected.*

6 Sensitivity analysis

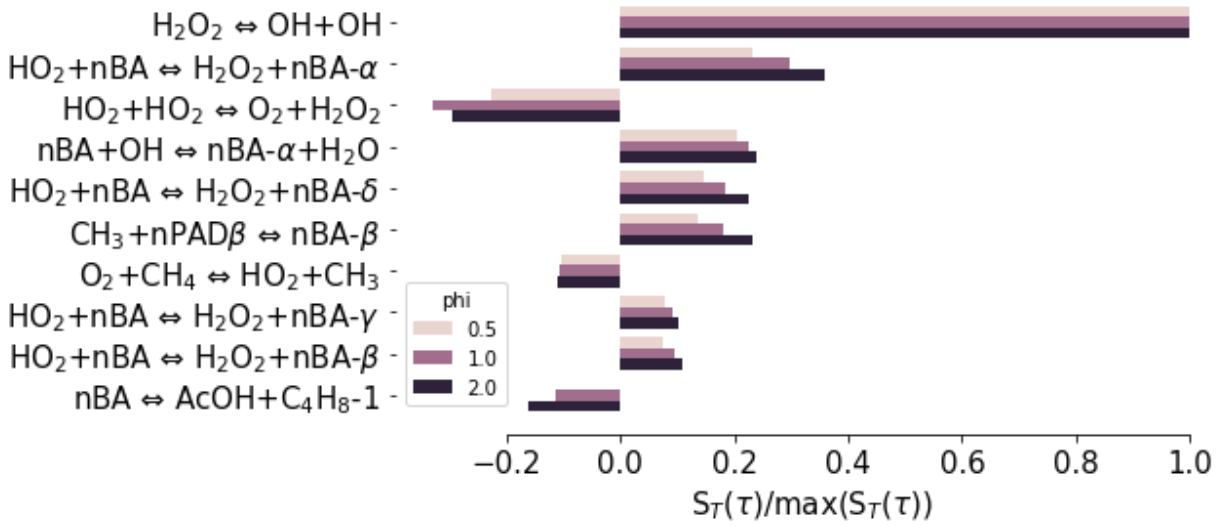

*Figure S24. Temperature sensitivity analysis of **nBA**/air system at ignition delay time, 900 K, 10 atm, and different fuel-to-air ratios.*

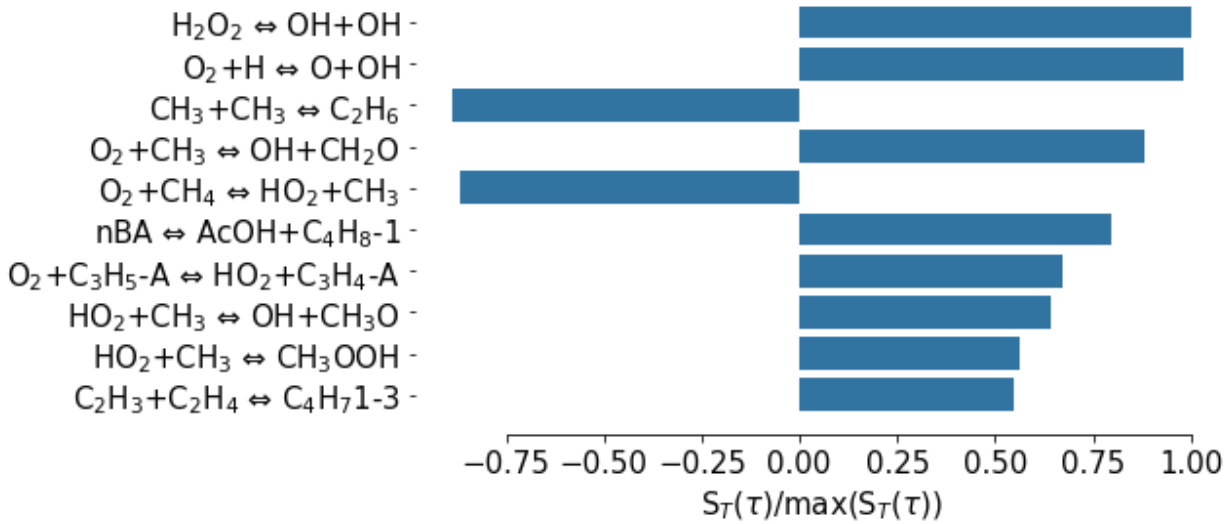

*Figure S25. Temperature sensitivity analysis of **nBA**/air system at ignition delay time, 1300 K, 10 atm, and φ = 1.0.*

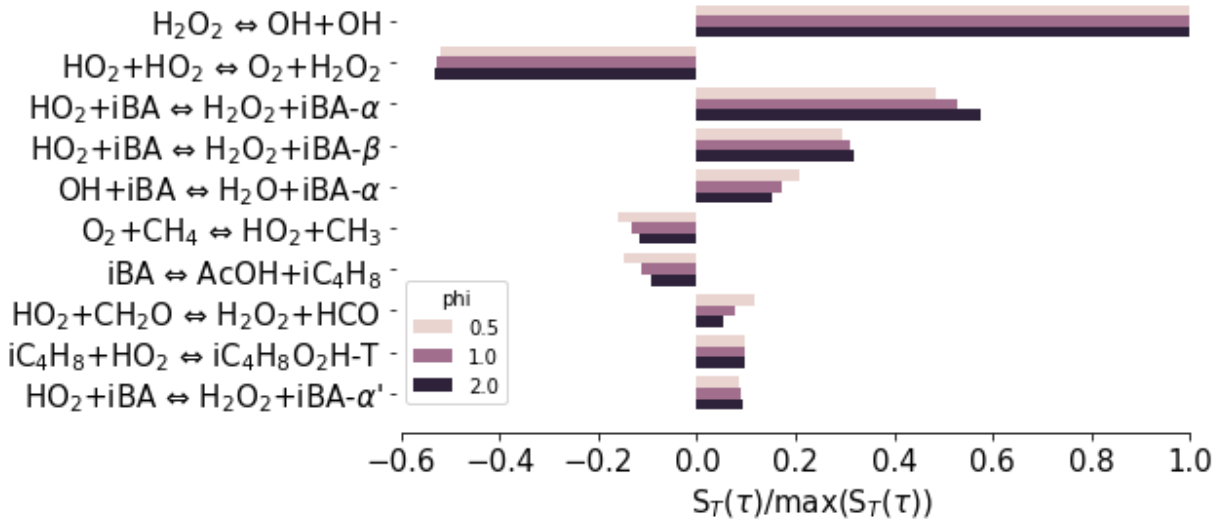

*Figure S26. Temperature sensitivity analysis of **iBA**/air system at ignition delay time, 900 K, 10 atm, and different fuel-to-air ratios.*

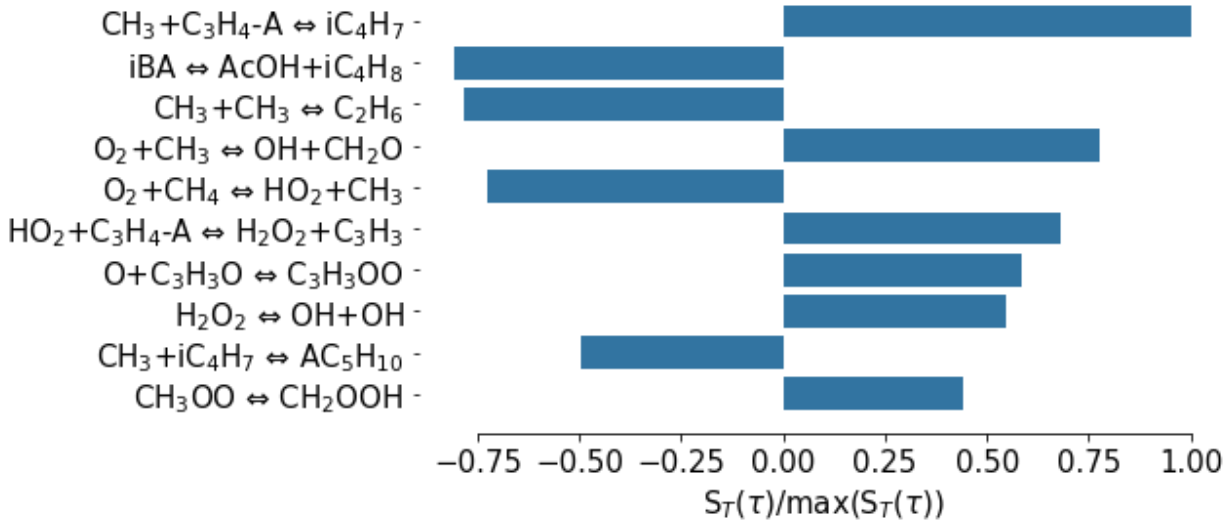

*Figure S27. Temperature sensitivity analysis of **iBA**/air system at ignition delay time, 1300 K, 10 atm, and φ = 1.0.*

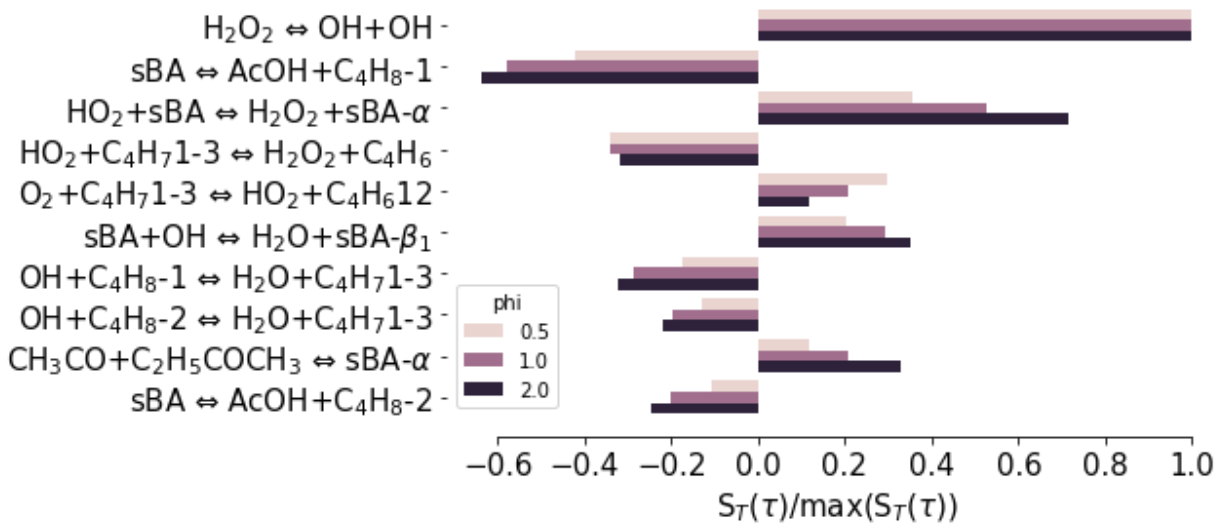

*Figure S28. Temperature sensitivity analysis of **sBA**/air system at ignition delay time, 900 K, 10 atm, and different fuel-to-air ratios.*

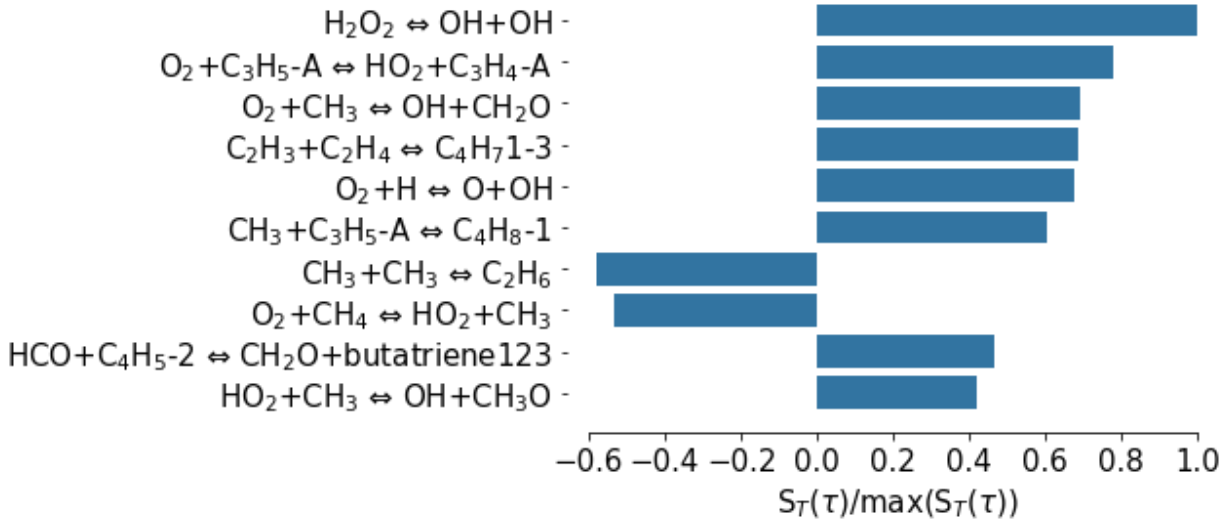

*Figure S29. Temperature sensitivity analysis of **sBA**/air system at ignition delay time, 1300 K, 10 atm, and φ = 1.0.*

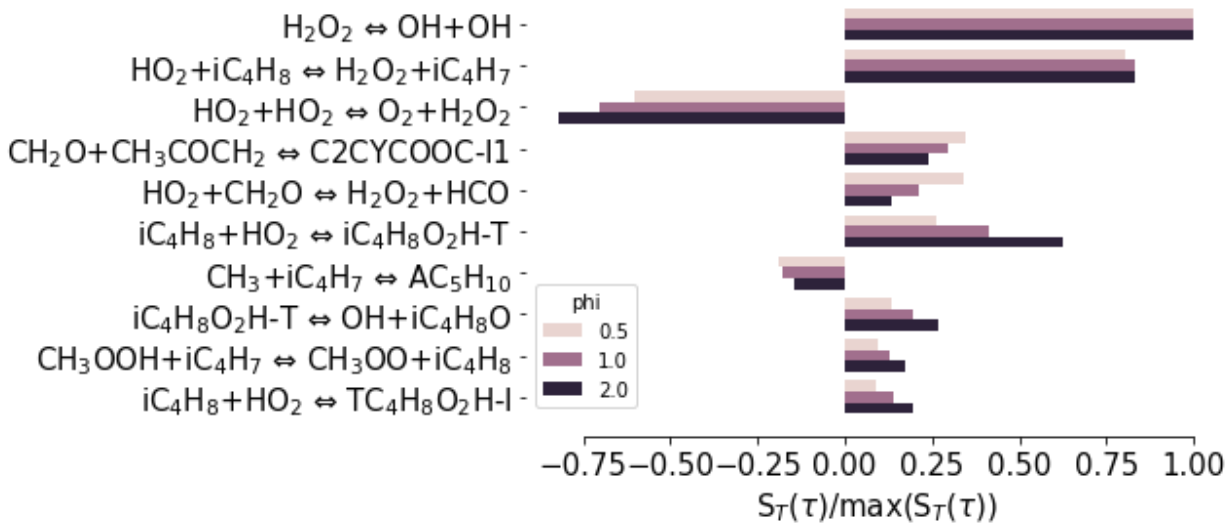

*Figure S30. Temperature sensitivity analysis of **tBA**/air system at ignition delay time, 900 K, 10 atm, and different fuel-to-air ratios.*

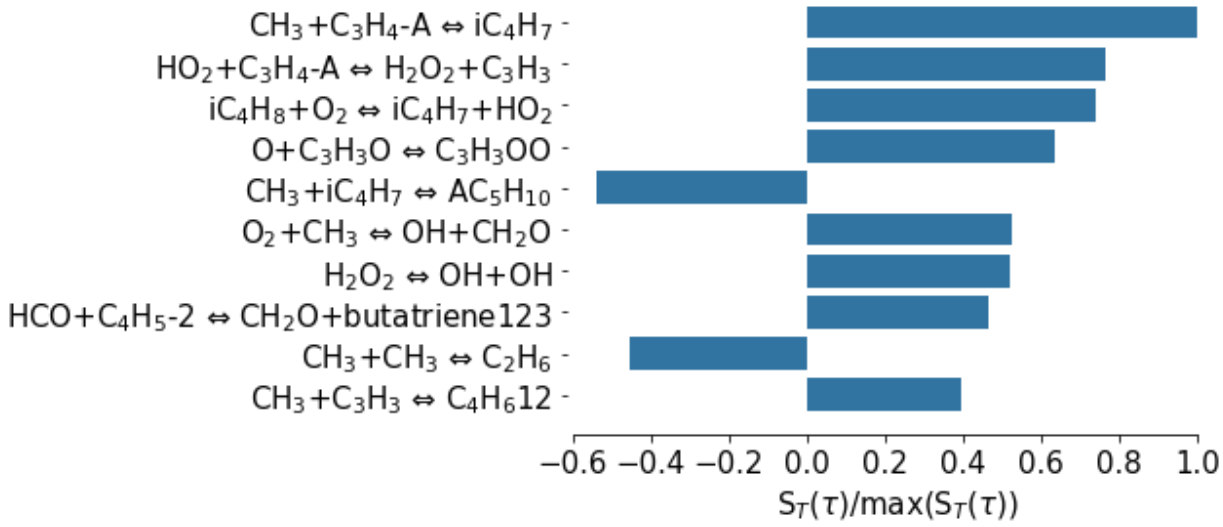

*Figure S31. Temperature sensitivity analysis of **tBA**/air system at ignition delay time, 1300 K, 10 atm, and φ = 1.0.*

7 Shock Tube Experimental Data

7.1 Experimental Conditions

Table S1. Reflected Shock conditions during pyrolysis of butyl acetate isomers

0.5% iBA / 99.5% Ar		0.5% nBA / 99.5% Ar		0.5% sBA / 99.5% Ar		0.5% tBA / 99.5% Ar	
T_5 (K)	P_5 (atm)	T_5 (K)	P_5 (atm)	T_5 (K)	P_5 (atm)	T_5 (K)	P_5 (atm)
1306	1.53	1303	1.53	1296	1.53	1300	1.38
1352	1.47	1366	1.50	1385	1.52	1362	1.37
1413	1.42	1423	1.45	1420	1.40	1421	1.43
1422	1.44	1441	1.48	1458	1.42	1431	1.40
1490	1.44	1485	1.42	1528	1.36	1492	1.43
1518	1.41	1533	1.36	1626	1.29	1592	1.45
1619	1.35	1611	1.25	1714	1.27	1735	1.44
1756	1.30	1700	1.22				

7.2 iBA Results

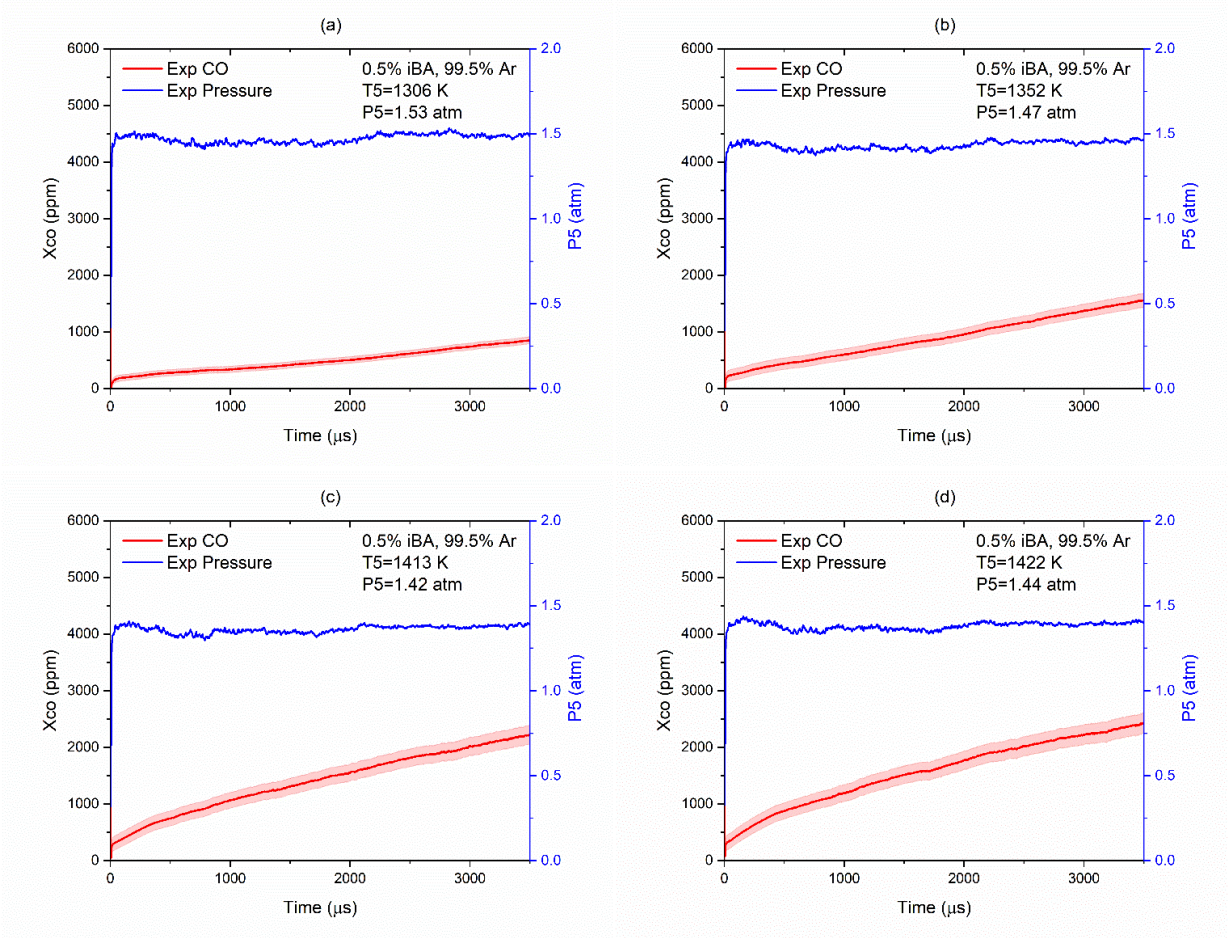

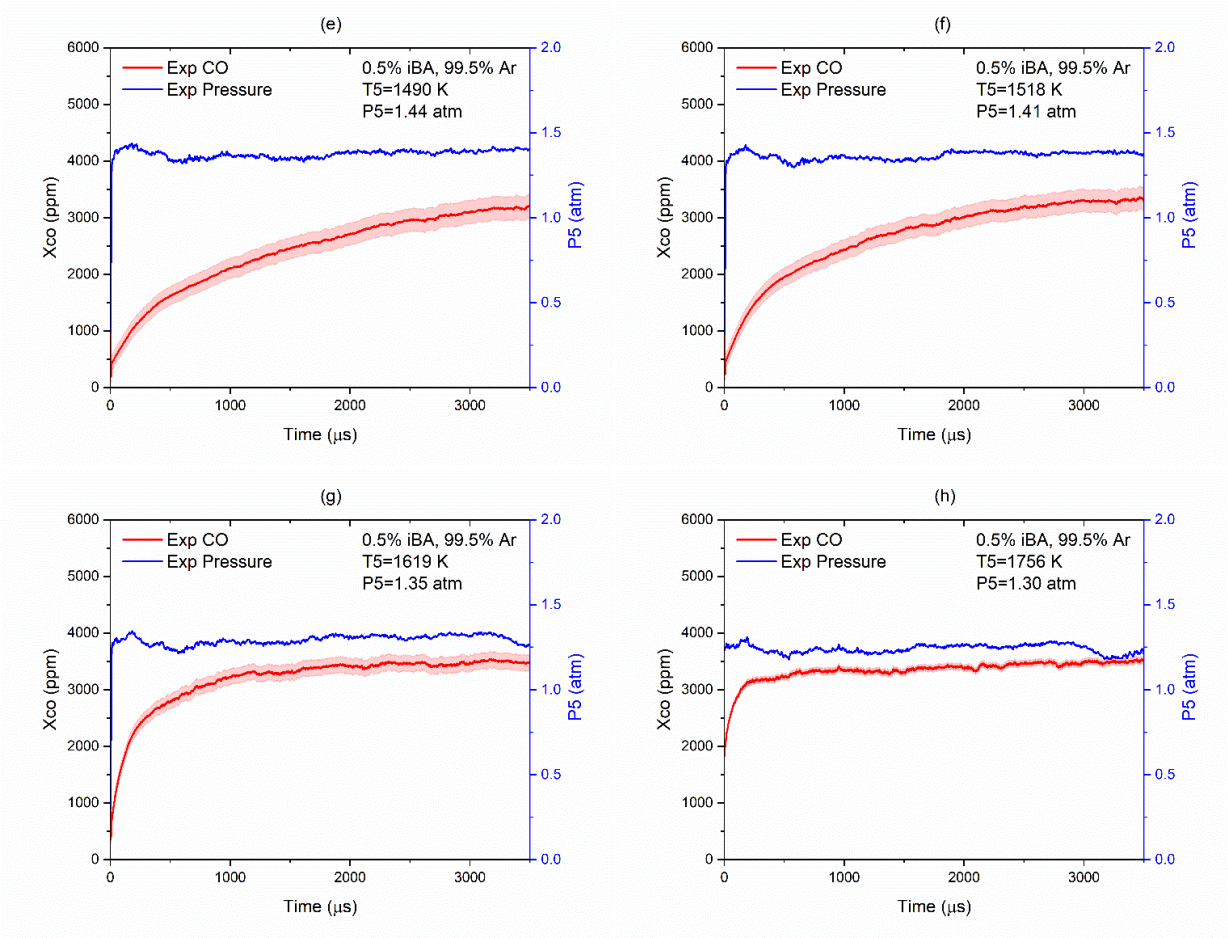

Figure S32. Pressure (blue) and carbon monoxide time-histories (red) during pyrolysis of 0.5% iBA in Ar bath at different reflected shock conditions (a-g).

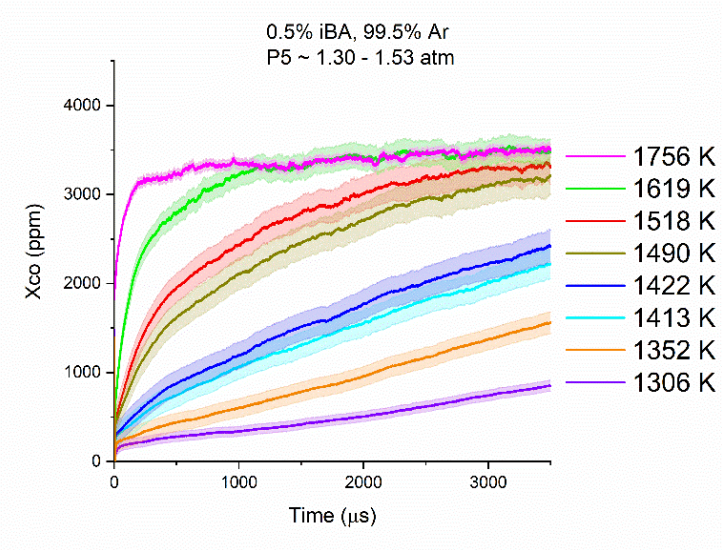

Figure S33. Comparison of CO time-histories during iBA pyrolysis at different temperatures.

7.3 nBA Results

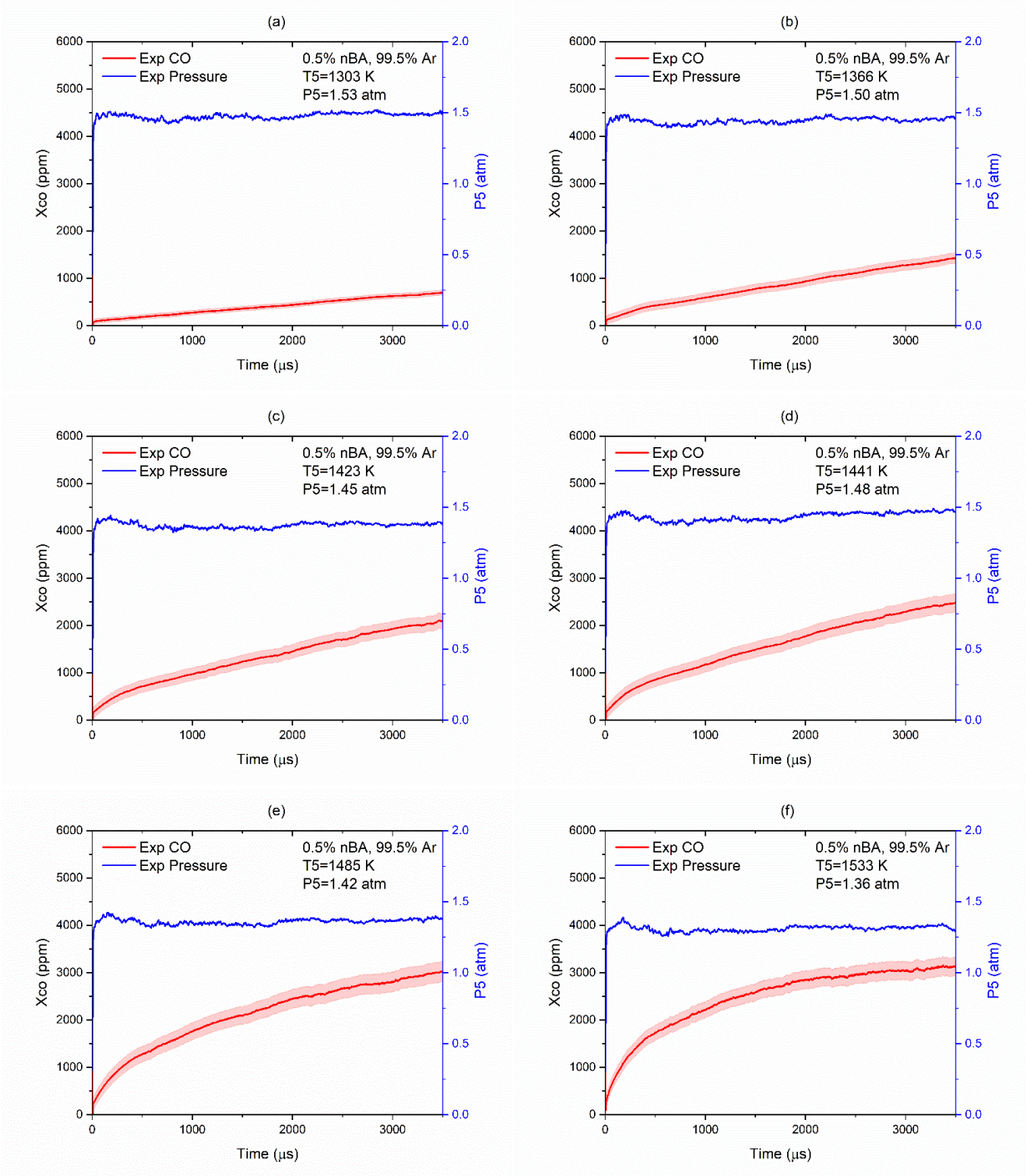

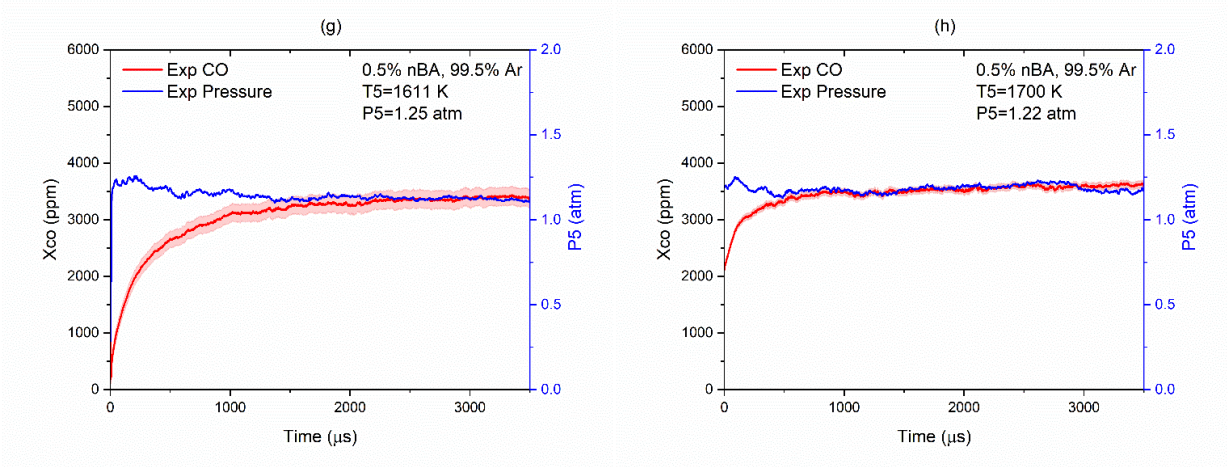

Figure S34. Pressure (blue) and carbon monoxide time-histories (red) during pyrolysis of 0.5% nBA in Ar bath at different reflected shock conditions (a-h).

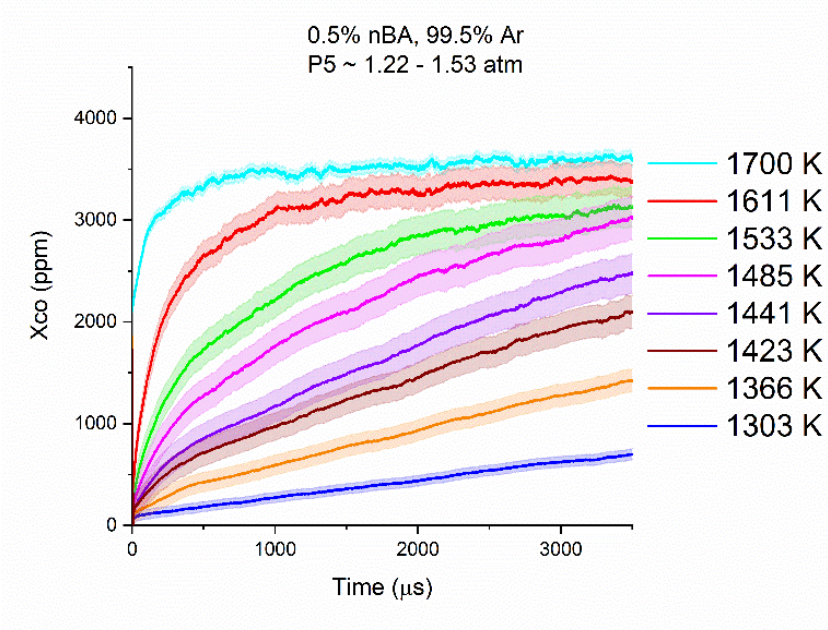

Figure S35. Comparison of CO time-histories during nBA pyrolysis at different temperatures.

7.4 sBA Results

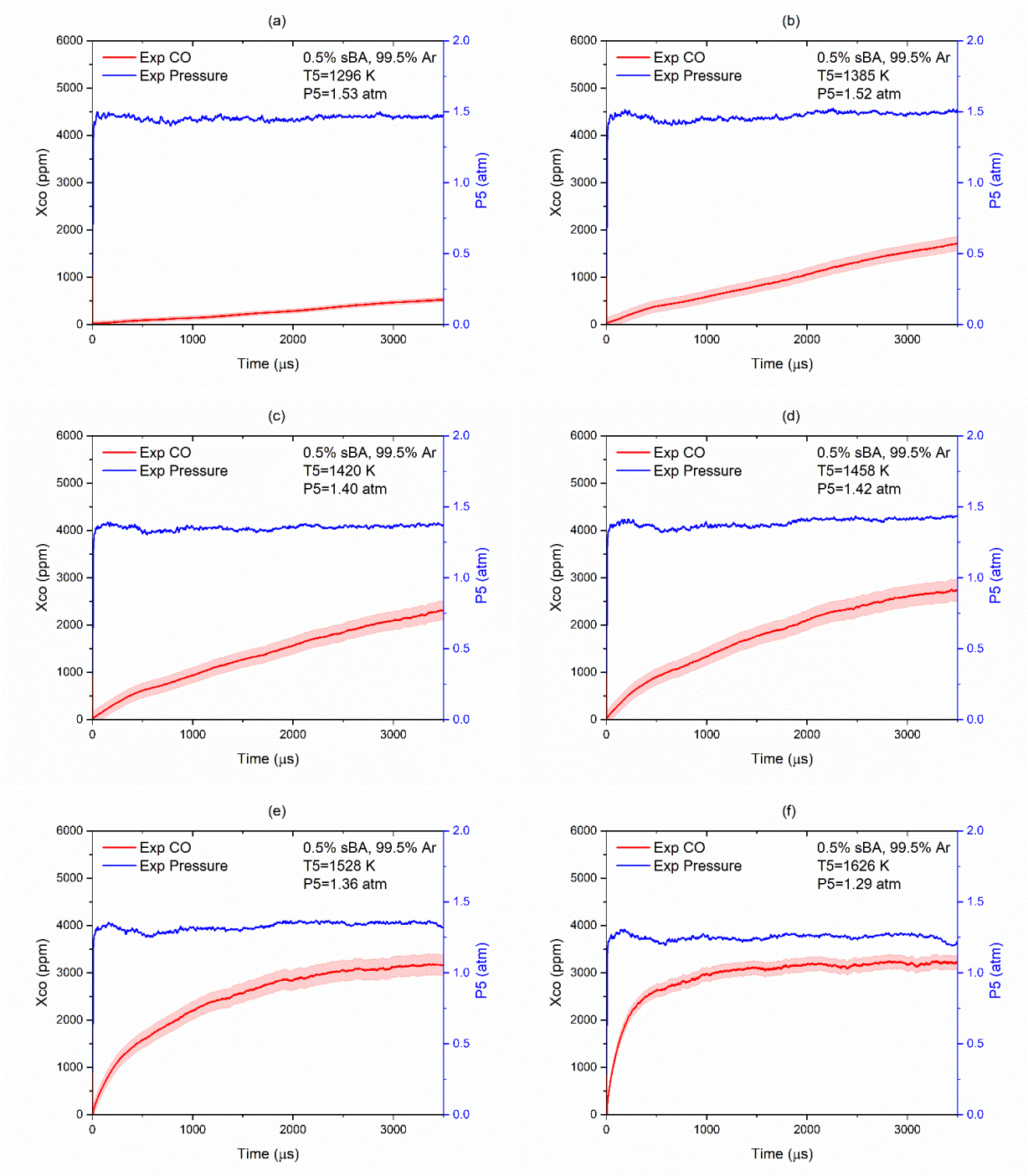

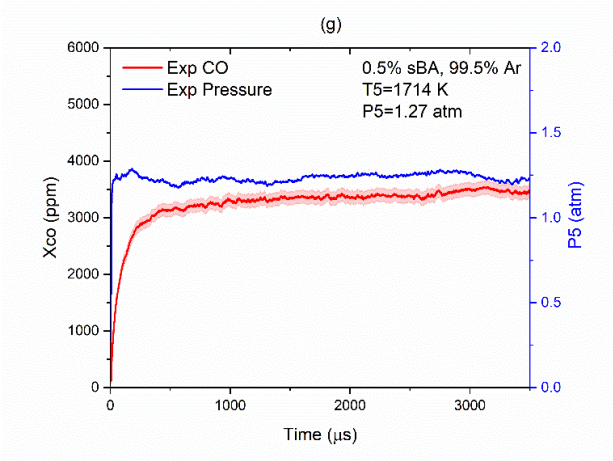

Figure S36. Pressure (blue) and carbon monoxide time-histories (red) during pyrolysis of 0.5% sBA in Ar bath at different reflected shock conditions (a-g).

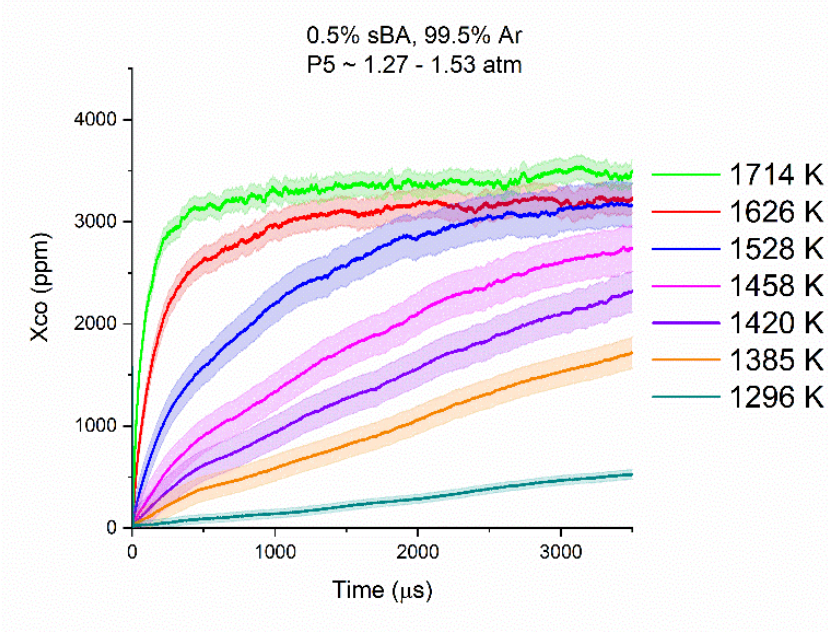

Figure S37. Comparison of CO time-histories during sBA pyrolysis at different temperatures.

7.5 tBA Results

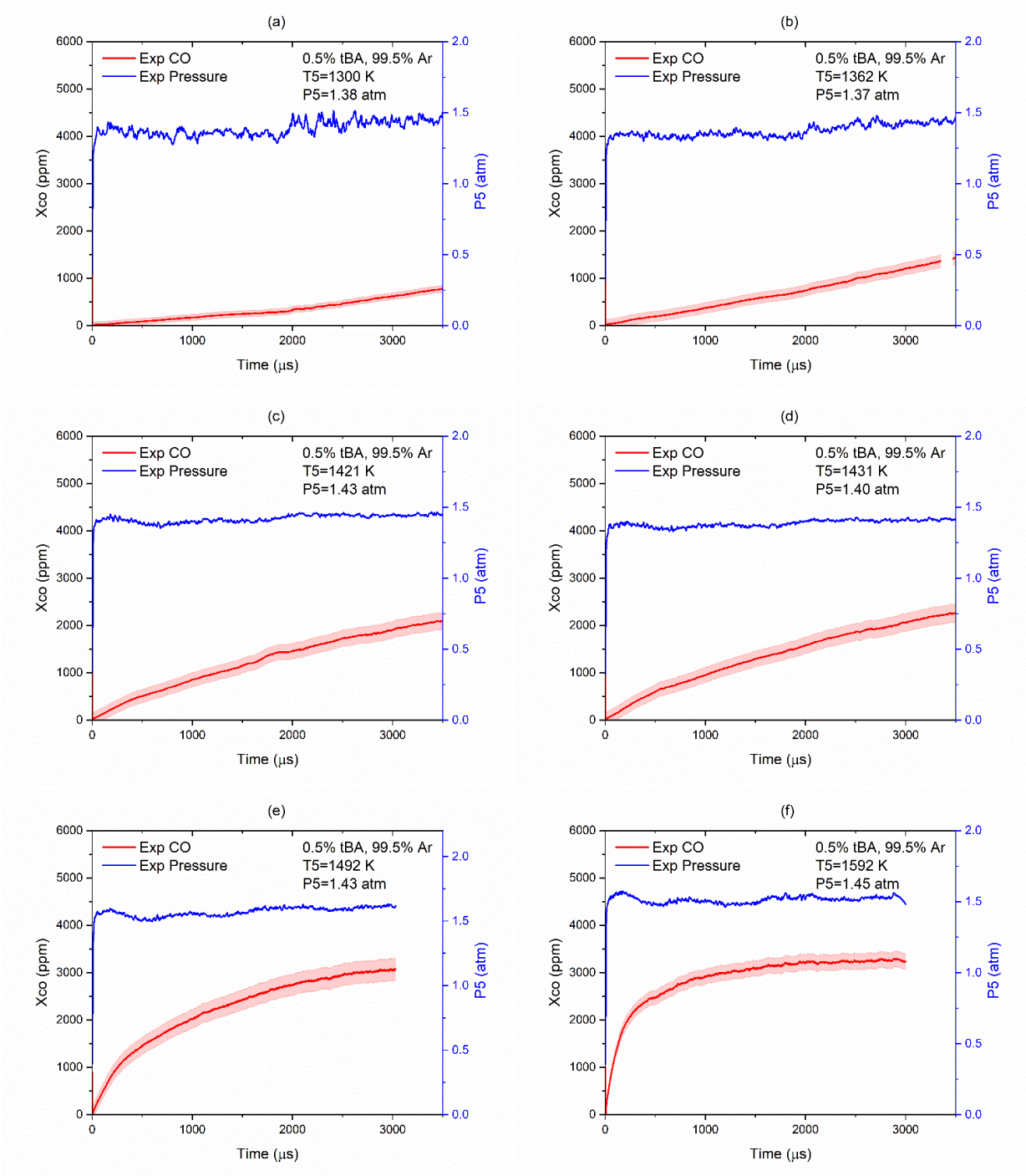

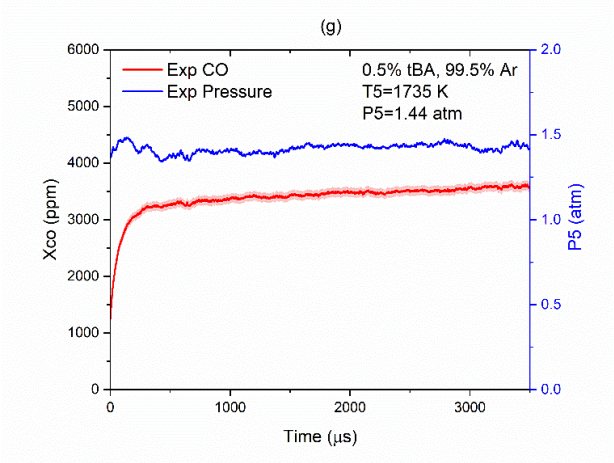

Figure S38. Pressure (blue) and carbon monoxide time-histories (red) during pyrolysis of 0.5% tBA in Ar bath at different reflected shock conditions (a-g).

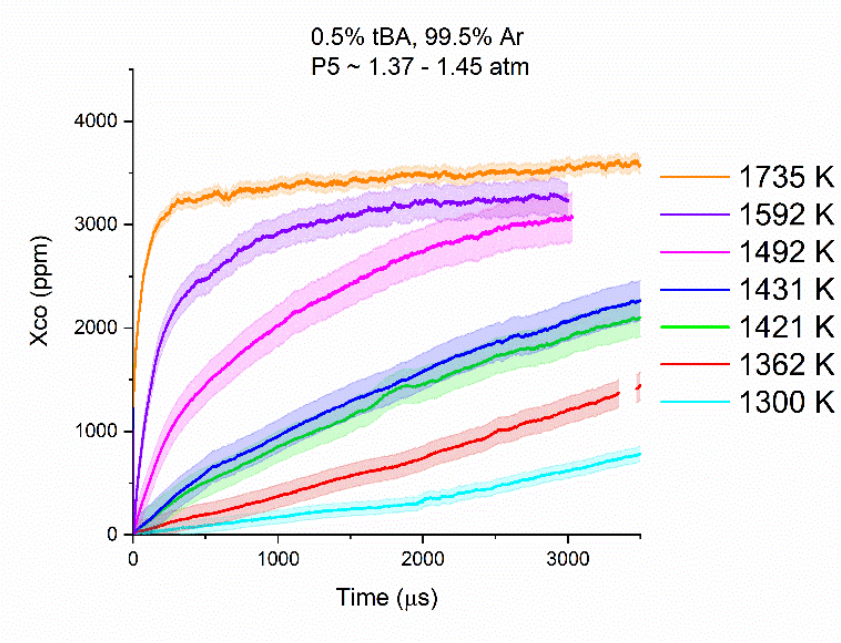

Figure S39. Comparison of CO time-histories during sBA pyrolysis at different temperatures.

8 Pyrolysis sensitivity

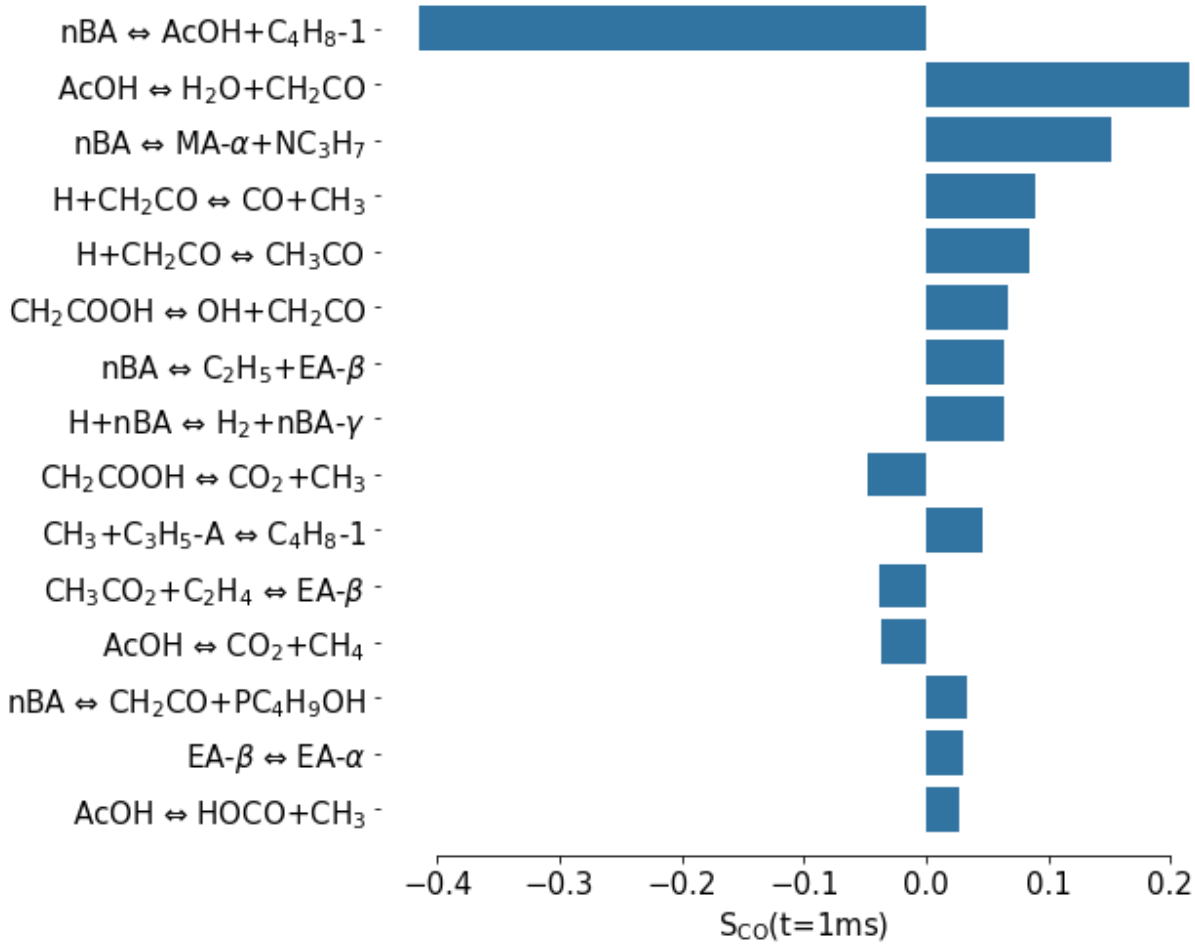

Figure S40. CO sensitivity of nBA pyrolysis in a closed, isochoric, and adiabatic reactor at 1533 K, 1.36 atm, 1 ms, and 0.5% initial mole fraction diluted by Ar. Species are renamed for better readability.

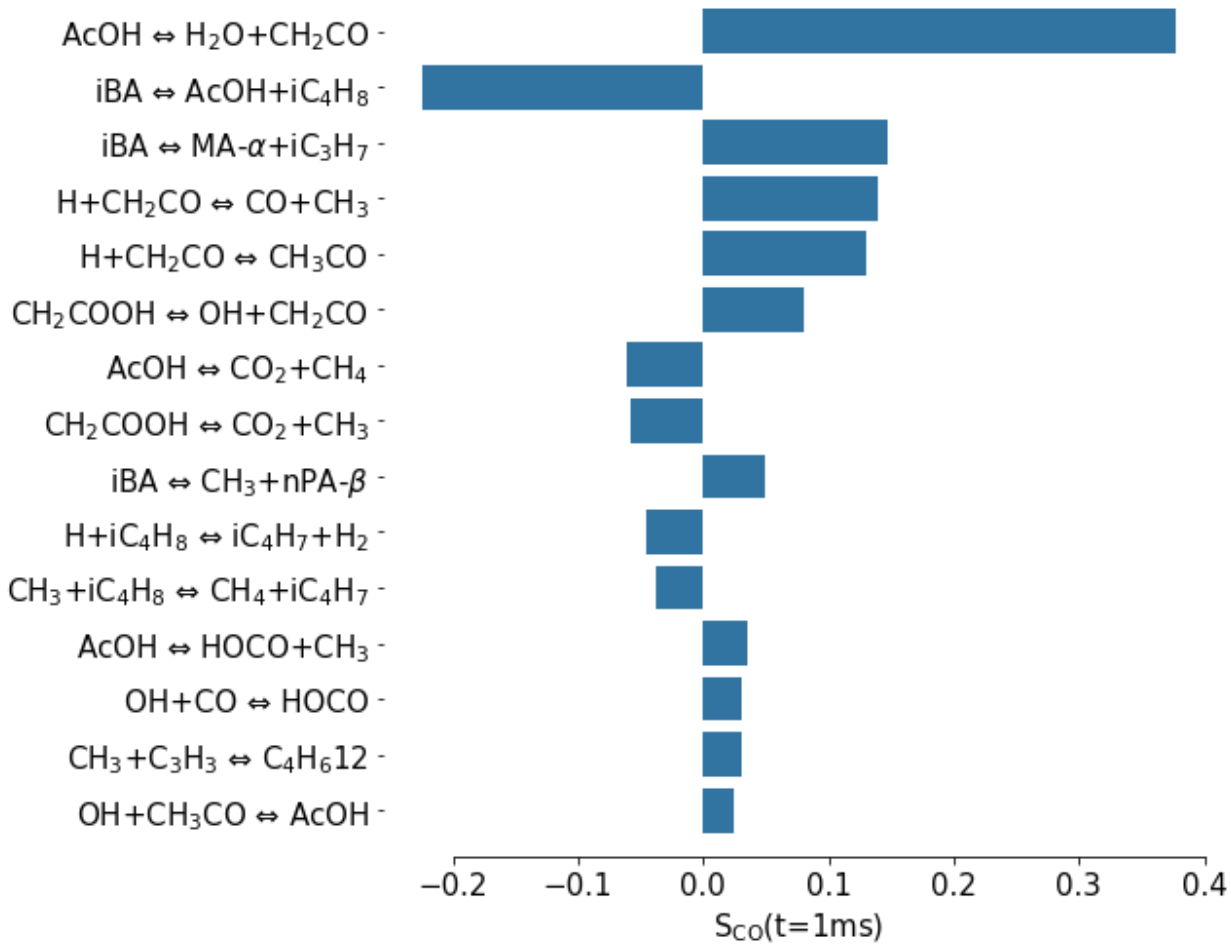

Figure S41. CO sensitivity of iBA pyrolysis in a closed, isochoric, and adiabatic reactor at 1518 K, 1.41 atm, 1 ms, and 0.5% initial mole fraction diluted by Ar. Species are renamed for better readability.

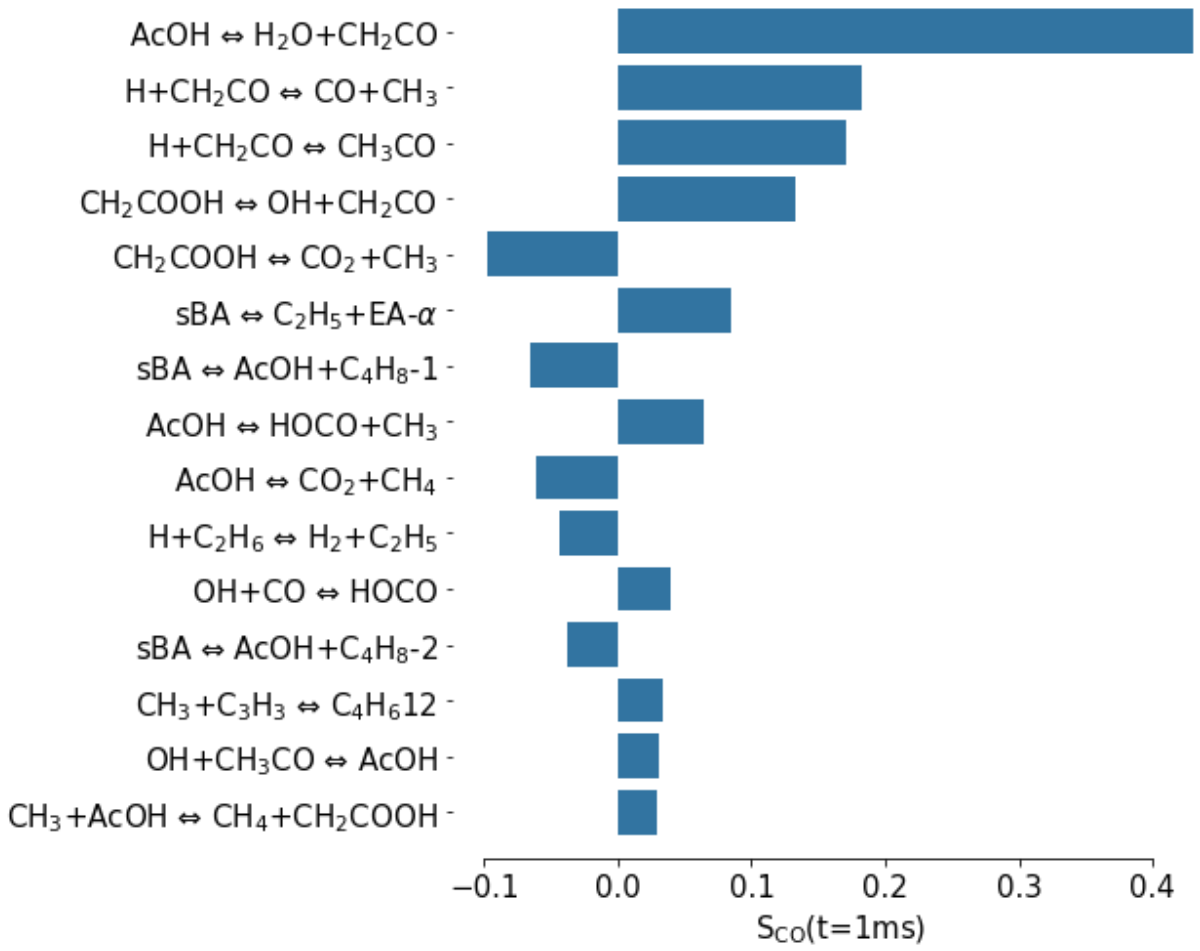

Figure S42. CO sensitivity of sBA pyrolysis in a closed, isochoric, and adiabatic reactor at 1528 K, 1.36 atm, 1 ms, and 0.5% initial mole fraction diluted by Ar. Species are renamed for better readability.

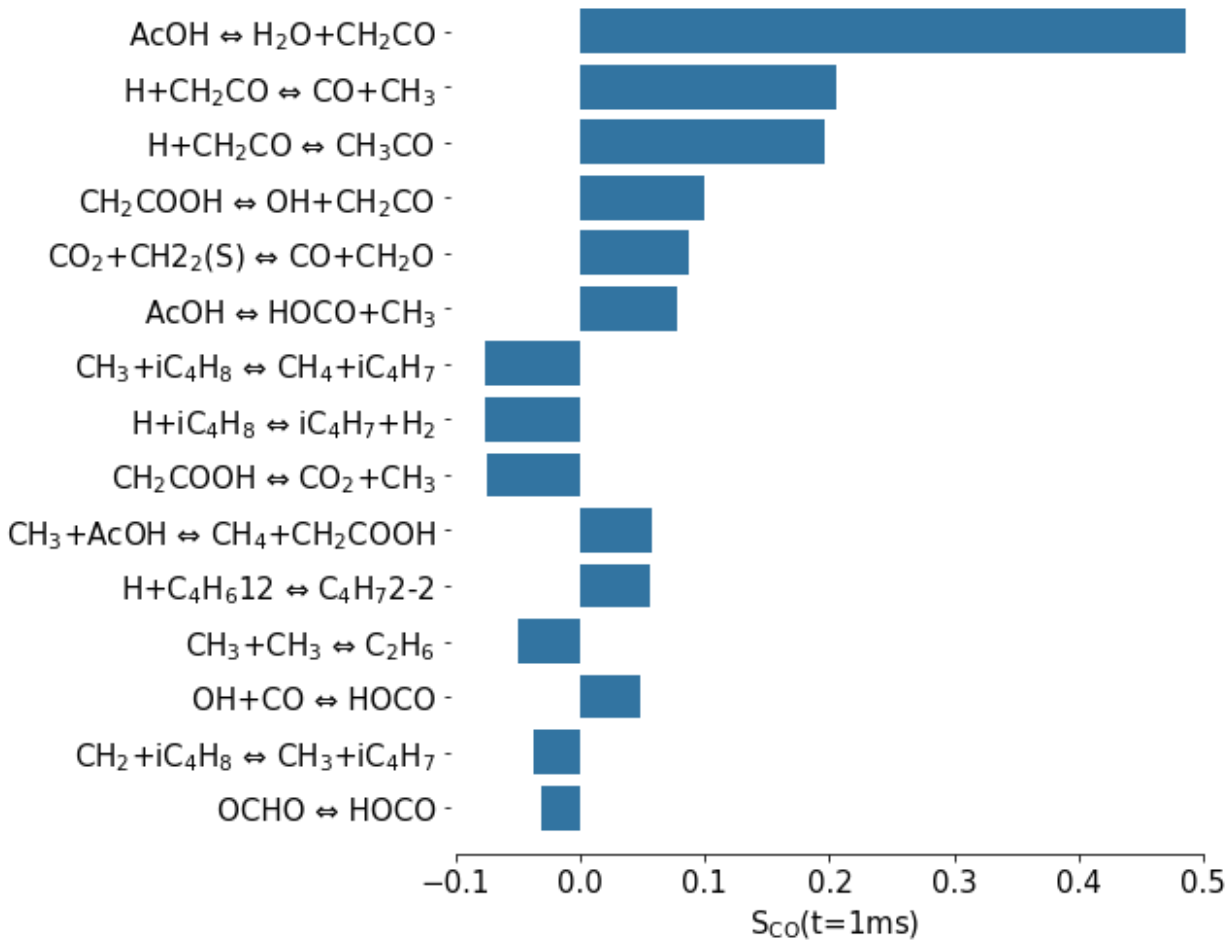

Figure S43. CO sensitivity of tBA pyrolysis in a closed, isochoric, and adiabatic reactor at 1528 K, 1.36 atm, 1 ms, and 0.5% initial mole fraction diluted by Ar. Species are renamed for better readability.

Table S2. Source of sensitive reactions in the pyrolysis system

Reaction	Source	Temperature range	Type
AcOH chemistry			
$AcOH = H_2O + CH_2CO$	Cavallotti et al.	700 - 2100 K	PLOG
$AcOH = CO_2 + CH_4$	Cavallotti et al.	700 - 2100 K	PLOG
$AcOH = HOCO + CH_3$	Cavallotti et al.	700 - 2100 K	PLOG
$CH_2COOH=OH+CH_2CO$	Cavallotti et al.	700 - 2100 K	PLOG
$CH_2COOH=CO_2+CH_3$	Cavallotti et al.	700 - 2100 K	PLOG
$H+AcOH=H_2+CH_2COOH$	Cavallotti et al.	500 - 2500 K	Arrhenius
$CH_3+AcOH=CH_4+CH_2COOH$	Cavallotti et al.	500 - 2500 K	Arrhenius
$AcOH = CH_3CO+OH$	RMG rate rules	300 - 1500 K	Arrhenius
C1-C2 chemistry			
$OH+CO=HOCO$	Klippenstein_Glarborg2016; Senosiain et al.	80 - 2000 K	PLOG
$H+C_2H_6=H_2+C_2H_5$	Klippenstein_Glarborg2016; Sivaramakrishnan et al.	300 - 2000 K	Bi-Arrhenius
$HOCO=H+CO_2$	Klippenstein_Glarborg2016;		Arrhenius
Alkene chemistry			
$H+C_3H_4\text{-}P=C_3H_5\text{-}S$	RMG rate rules; From group additivity value	300 - 1500 K	Arrhenius
$CH_3+C_3H_5\text{-}A=C_4H_8\text{-}1$	RMG rate rules; Tsang et al.	300 - 2500 K	Arrhenius
$CH_3+C_3H_3=C_4H_612$	RMG rate rules;	300 - 1500 K	Arrhenius
$H+iC_4H_8=iC_4H_7+H_2$	Power et al.	298 - 2000 K	Arrhenius
$CH_3+iC_4H_8=CH_4+iC_4H_7$	RMG rate rules; Van Geem et al.	300 - 2000 K	Arrhenius
Ester chemistry			
$nBA=AcOH+C_4H_8\text{-}1$	This work	300 - 2000 K	Arrhenius
$nBA=MA\text{-}\alpha+NC_3H_7$	RMG rate rules	300 - 1500 K	Arrhenius
$nBA=C_2H_5+EA\text{-}\beta$	RMG rate rules	300 - 1500 K	Arrhenius
$H+nBA=H_2+nBA\text{-}\gamma$	RMG rate rules	300 - 2000 K	Arrhenius
$nBA=CH_2CO+PC_4H_9OH$	RMG rate rules	300 - 1500 K	Arrhenius
$CH_3CO_2+C_2H_4=EA\text{-}\beta$	RMG rate rules	300 - 1500 K	Arrhenius
$EA\text{-}\beta = EA\text{-}\alpha$	RMG rate rules	300 - 1500 K	Arrhenius
$iBA=AcOH+iC_4H_8$	This work	300 - 2000 K	Arrhenius
$iBA=MA\text{-}\alpha+iC_3H_7$	RMG rate rules	300 - 1500 K	Arrhenius
$iBA=CH_3+nPA\text{-}\beta$	RMG rate rules	300 - 1500 K	Arrhenius
$sBA=C_2H_5+EA\text{-}\alpha$	RMG rate rules	300 - 1500 K	Arrhenius
$sBA=AcOH+C_4H_8\text{-}1$	This work	300 - 2000 K	Arrhenius
$sBA=AcOH+C_4H_8\text{-}2$	This work	300 - 2000 K	Bi-Arrhenius

Reference

(1) M. J. Frisch, G. W. Trucks, H. B. Schlegel, G. E. Scuseria, M. A. Robb, J. R. Cheeseman, G. Scalmani, V. Barone, B. Mennucci, G. A. Petersson, H. Nakatsuji, M. Caricato, X. Li, H. P. Hratchian, A. F. Izmaylov, J. Bloino, G. Zheng, J. L. Sonnenberg, M. Had, and D. J. F.; Frisch, M. J.; Trucks, G. W.; Schlegel, H. B.; Scuseria, G. E.; Robb, M. A.; Cheeseman, J. R.; Scalmani, G.; Barone, V.; Mennucci, B.; et al. Gaussian 09, Revision D.01. *Gaussian Inc., Wallingford*. Wallingford, CT 2013, p Wallingford CT. http://www.gaussian.com/index.htm.

(2) M. J. Frisch, G. W. Trucks, H. B. Schlegel, G. E. S.; M. A. Robb, J. R. Cheeseman, G. Scalmani, V. B.; G. A. Petersson, H. Nakatsuji, X. Li, M. Caricato, A. V. M.; J. Bloino, B. G. Janesko, R. Gomperts, B. Mennucci, H. P. H.; J. V. Ortiz, A. F. Izmaylov, J. L. Sonnenberg, D. W.-Y.; F. Ding, F. Lipparini, F. Egidi, J. Goings, B. Peng, A. P.; T. Henderson, D. Ranasinghe, V. G. Zakrzewski, J. Gao, N. R.; G. Zheng, W. Liang, M. Hada, M. Ehara, K. Toyota, R. F.; J. Hasegawa, M. Ishida, T. Nakajima, Y. Honda, O. Kitao, H. N.; T. Vreven, K. Throssell, J. A. Montgomery, Jr., J. E. P.; et al. Gaussian 16, Revision C. 01. *Gaussian, Inc., Wallingford CT*. Wallingford, CT 2016. https://gaussian.com/citation/%0Ahttp://gaussian.com/citation/.

(3) Grinberg Dana, A.; Ranasinghe, D.; Wu, O. H.; Grambow, C.; Dong, X.; Johnson, M. S.; Goldman, M.; Liu, M.; Green, W. H. ARC - Automated Rate Calculator. Cambridge, MA, US. https://github.com/ReactionMechanismGenerator/ARC. DOI:10.5281/zenodo.3356849 (accessed 2019-10-01).

(4) Dana, A. G.; Johnson, M.; Allen, J.; Sharma, S.; Raman, S.; Liu, M.; Gao, C.; Grambow, C.; Goldman, M.; Ranasinghe, D.; et al. Automated Reaction Kinetics and Network Exploration (Arkane): A Statistical Mechanics, Thermodynamics, Transition State Theory, and Master Equation Software. *ChemRxiv* **2022**. DOI:10.26434/CHEMRXIV-2022-4KLSM.

(5) Liu, M.; Grinberg Dana, A.; Johnson, M. S.; Goldman, M. J.; Jocher, A.; Payne, A. M.; Grambow, C. A.; Han, K.; Yee, N. W.; Mazeau, E. J.; et al. Reaction Mechanism Generator v3.0: Advances in Automatic Mechanism Generation. *J. Chem. Inf. Model.* **2021**, *61* (6), 2686–2696. DOI:10.1021/acs.jcim.0c01480.

(6) Gao, C. W.; Allen, J. W.; Green, W. H.; West, R. H. Reaction Mechanism Generator: Automatic Construction of Chemical Kinetic Mechanisms. *Comput. Phys. Commun.* **2016**, *203*, 212–225. DOI:10.1016/j.cpc.2016.02.013.

(7) Johnson, M. S.; Dong, X.; Grinberg Dana, A.; Chung, Y.; Farina, D.; Gillis, R. J.; Liu, M.; Yee, N. W.; Blondal, K.; Mazeau, E.; et al. RMG Database for Chemical Property Prediction. *J. Chem. Inf. Model.* **2022**, *62* (20), 4906–4915. DOI:10.1021/acs.jcim.2c00965.

(8) Hashemi, H.; Christensen, J. M.; Gersen, S.; Levinsky, H.; Klippenstein, S. J.; Glarborg, P. High-Pressure Oxidation of Methane. *Combust. Flame* **2016**, *172*, 349–364. DOI:10.1016/j.combustflame.2016.07.016.

(9) Li, X.; Jasper, A. W.; Zádor, J.; Miller, J. A.; Klippenstein, S. J. Theoretical Kinetics of O + C2H4. *Proc. Combust. Inst.* **2017**, *36* (1), 219–227. DOI:10.1016/j.proci.2016.06.053.

(10) Goldsmith, C. F.; Magoon, G. R.; Green, W. H. Database of Small Molecule Thermochemistry for Combustion. *J. Phys. Chem. A* **2012**, *116* (36), 9033–9047. DOI:10.1021/jp303819e.

(11) Yaws, C. L. *Yaws' Critical Property Data for Chemical Engineers and Chemists*; Knovel,

2014.
(12) Smith, G. P.; Tao, Y.; Wang, H. *Foundational Fuel Chemistry Model Version 1.0 (FFCM-1), https://web.stanford.edu/group/haiwanglab/FFCM1*. ChemRxiv. http://nanoenergy.stanford.edu/ffcm1 (accessed 2021-09-03).
(13) Burke, M. P.; Chaos, M.; Ju, Y.; Dryer, F. L.; Klippenstein, S. J. Comprehensive H 2/O 2 Kinetic Model for High-Pressure Combustion. *Int. J. Chem. Kinet.* **2012**, *44* (7), 444–474. DOI:10.1002/kin.20603.
(14) *RMG User's Guide*. http://reactionmechanismgenerator.github.io/RMG-Py/users/rmg/input.html (accessed 2022-10-01).
(15) Kee, R. J.; Rupley, F. M.; Miller, J. A.; Coltrin, M. E.; Grcar, J. F.; Meeks, E.; Moffat, H. K.; Lutz, A. E.; Dixon-Lewis, G.; Smooke, M. D.; et al. CHEMKIN-Pro. Reaction Design: San Diego 2020.
(16) Goodwin, D. G.; Speth, R. L.; Moffat, H. K.; Weber, B. W. Cantera: An Object-Oriented Software Toolkit for Chemical Kinetics, Thermodynamics, and Transport Processes. 2018. http://www.cantera.org. DOI:10.5281/zenodo.45206 (accessed 2020-03-10).
(17) Johnson, M. S.; Pang, H.; Payne, A.; Green, W. H. RMS - Reaction Mechanism Simulator. Cambridge 2022. https://github.com/ReactionMechanismGenerator/ReactionMechanismSimulator.jl (accessed 2021-10-15).
(18) Mendes, J.; Zhou, C. W.; Curran, H. J. Theoretical Study of the Rate Constants for the Hydrogen Atom Abstraction Reactions of Esters with ȮH Radicals. *J. Phys. Chem. A* **2014**, *118* (27), 4889–4899. DOI:10.1021/jp5029596.
(19) Ahmed, A.; Pitz, W. J.; Cavallotti, C.; Mehl, M.; Lokachari, N.; Nilsson, E. J. K.; Wang, J. Y.; Konnov, A. A.; Wagnon, S. W.; Chen, B.; et al. Small Ester Combustion Chemistry: Computational Kinetics and Experimental Study of Methyl Acetate and Ethyl Acetate. *Proc. Combust. Inst.* **2019**, *37* (1), 419–428. DOI:10.1016/j.proci.2018.06.178.
(20) Morsch, P.; Döntgen, M.; Heufer, K. A. Kinetic Investigations on the High- and Low-Temperature Chemistry of Ethyl Acetate. *Combust. Flame* **2022**, *243*, 111995. DOI:10.1016/j.combustflame.2022.111995.
(21) Penyazkov, O. G.; Sevrouk, K. L.; Tangirala, V.; Joshi, N. High-Pressure Ethylene Oxidation behind Reflected Shock Waves. *Proc. Combust. Inst.* **2009**, *32 II* (2), 2421–2428. DOI:10.1016/j.proci.2008.06.194.
(22) Wan, Z.; Zheng, Z.; Wang, Y.; Zhang, D.; Li, P.; Zhang, C. A Shock Tube Study of Ethylene/Air Ignition Characteristics over a Wide Temperature Range. *Combust. Sci. Technol.* **2020**, *192* (12), 2297–2305. DOI:10.1080/00102202.2019.1643333.
(23) Kopp, M. M.; Donato, N. S.; Petersen, E. L.; Metcalfe, W. K.; Burke, S. M.; Curran, H. J. Oxidation of Ethylene-Air Mixtures at Elevated Pressures, Part 1: Experimental Results. *J. Propuls. Power* **2014**, *30* (3), 790–798. DOI:10.2514/1.B34890.
(24) Li, Y.; Zhou, C. W.; Curran, H. J. An Extensive Experimental and Modeling Study of 1-Butene Oxidation. *Combust. Flame* **2017**, *181*, 198–213. DOI:10.1016/j.combustflame.2017.03.023.
(25) Li, Y.; Zhou, C. W.; Somers, K. P.; Zhang, K.; Curran, H. J. The Oxidation of 2-Butene: A High Pressure Ignition Delay, Kinetic Modeling Study and Reactivity Comparison with Isobutene and 1-Butene. *Proc. Combust. Inst.* **2017**, *36* (1), 403–411. DOI:10.1016/j.proci.2016.05.052.
(26) Zhou, C.-W. W.; Li, Y.; O'Connor, E.; Somers, K. P.; Thion, S.; Keesee, C.; Mathieu, O.;

Petersen, E. L.; DeVerter, T. A.; Oehlschlaeger, M. A.; et al. A Comprehensive Experimental and Modeling Study of Isobutene Oxidation. *Combust. Flame* **2016**, *167*, 353–379. DOI:10.1016/j.combustflame.2016.01.021.